学位論文

Laser-field-free and field-free orientation of state-selected molecules

(状態選別した分子のレーザー電場のない条件下、
及び完全に外場のない条件下での配向制御)

平成２６年１２月博士（理学）申請
東京大学大学院理学系研究科
物理学専攻
文　堤會

Abstract

Controlling rotational motion of gas phase molecules have been an attracting field of research in recent years. Our experimental and theoretical studies on molecular alignment and orientation are summarized in the present thesis. Three main themes of the present study are laser-field-free of orientation of asymmetric top molecules, numerical studies on rotational dynamics of asymmetric top molecules, and completely field-free orientation of linear molecules.

First of all, we demonstrate accomplishment of laser-field-free orientation of state-selected asymmetric top molecules. One necessary condition for molecular alignment and orientation of a gas phase molecule is making a rotational superposition of free-rotational states; furthermore, the generated wave packet must be in a good coherent condition for the alignment and orientation. Recently, for laser-field-free alignment of linear molecules, the alignment technique using a linearly polarized non-resonant ultra-short laser pulse has become a broadly-adopted basic technique for experiments with gas phase molecules. In contrast, making a good coherent wave-packet for field-free, strong alignment and orientation of asymmetric top molecule is a much more difficult subject compared to that of molecules with simpler structures like linear and symmetric top molecules because of the relatively complicated rotational spectrum of asymmetric top molecules.

For achievement of laser-field-free strong orientation of asymmetric top molecules, we have employed plasma shutter technique for shaping a laser pulse. With the plasma shutter, a special laser pulse with a slow turn on and a rapid turn off is shaped. Oriented or/and aligned states of molecules with a slow turn on of the laser field can remain for a few picosecond (in our experiment) after the rapid turn off; therefore, the shaped pulse works as a tool for achieving strong molecular orientation or/and alignment of molecules in the laser-field-free condition.

When we notice achievable degree of orientation, our method based on the shaped laser pulse has another strong advantage. The achievable degrees of orientation for initial single rotational state are maximized, when the external fields are applied slowly so that the interaction time scale is close to the adiabatic limit, while the achievable degrees of alignment do not critically depend on the interaction time scale. The oriented rotational states created by the slow turn on can be transferred into laser-field-free states by the rapid turn off.

Moreover, for further improvement of the degrees of orientation, we have employed a molecular sample which is rotational-state-selected by a molecular deflector. Since some of rotational states irradiated with external field(s) are oriented one way and the others are oriented the other way, the degree of orientation that we get from a group of molecules is much lower than that from a certain rotational state. Therefore, we have employed molecules rotational-state-selected by the home-built molecular deflector. When molecules pass through a spatially inhomogeneous strong electrostatic field, they experience force depending on Stark energy shifts of individual rotational states. Accordingly, the inhomogeneous electrostatic field generated in the molecular deflector can be used for the state-selection of molecules. By using the state-selected molecules as a sample, we have improved degrees of orientation than that achieved from a thermal ensemble of molecules.

With the combination of the two techniques of the plasma shutter and the rotational-state selection, a state-of-the-art orientation technique has been established. This experimental achievement is given in Chapter 5.

While the experimental research on laser-field-free orientation of asymmetric top molecules progresses numerical studies on asymmetric top molecules have been accompanied to understand their complex rotational dynamics. Looking at the obtained experimental results from the asymmetric top molecules, we have observed persistent alignment and orientation for 5-10 ps after the rapid turn off of the laser field by plasma shutter. Such a remarkably slow dephasing of coherent wave-packet has never been observed, which motivated us to the underlying physics by numerical simulations. We have numerically found that, even though a laser pulse whose pulse width is much longer than the rotational period of the molecule, a nonadiabatic effect plays an important role in determining the rotational dynamics of molecules in usually conceivable experimental conditions. Numerical studies associated with the laser-field-free orientation of asymmetric top molecules are given in Chapter 6.

For numerical studies on rotational dynamics of molecules, we have developed a "time-dependent unitary transformation method". Chapter 3 is dedicated for the explanation of the numerical method. With this numerical method, almost of the simulations pertaining to the rotational dynamics of molecules have become possible with a single numerical package. Especially, we can describe nonadiabatic effect caused in the regime where the time scale of interaction between molecules and external field is much longer than rotational period of the molecule but not long enough to ensure pure adia-

batic process. We can also study the dynamics of not only linear molecules but also asymmetric top molecules. The numerical results for reproducing experimental observations are described in corresponding parts.

Another main theme of the present thesis is"completely field-free orientation of state-selected (linear) molecules," which is given in Chapter 7. Even for linear molecules which have the simplest structure, techniques for orientation in the field-free condition is not well established yet. Thus, after the laser-field-free orientation technique in the presence of a weak electro-static field (Chapter 5) has been developed, we have tried to accomplish completely field-free orientation to make an oriented molecular sample available even without an electrostatic field. Instead of a one-color laser pulse and an electrostatic field, we have employed a two-color laser pulse with a slow turn on and a rapid turn off, for the field-free molecular orientation. Furthermore, we have employed OCS molecules state-selected by the molecular deflector for achieving strong degrees of orientation.

However, we have found experimentally and theoretically several difficulties associated with our orientation techniques that had never been recognized. First, the orientation process on the slow turn on of the laser pulse is not close to adiabatic, because of the difference in the pulse width between the fundamental and the second-harmonic laser pulses. Thus, degree of orientation expected to be achieved by adiabatic orientation can not be achieved this time.

Besides, during the plasma shutter operation, relative phase ϕ between the ω and 2ω is temporally unstable. Since the degrees of orientation achieved by the two-color laser field critically depend on the ϕ, temporally unstable degrees of orientation are observed.

In spite of such difficulties associated with the orientation technique, the state-selection technique and the plasma shutter technique have contributed to the field-free strong alignment of OCS molecules. Also, we have made clear next challenges for the field-free orientation, by comparing our experimentally observed data with output of numerical simulation.

Acknowledgements

The group leader, professor Sakai, gave me an invaluable opportunity to focus on my research of molecular science for the last 5 years. I remember that he always have tried to listen student's opinions thoughtfully and communicated with us. I appreciate all of his supports.

I would like to thank Professor Minemoto. I do not think I could do experiments without his technical support and advices. Improvement of my experimental skills for the last five years is owing to his help.

I am grateful to Professor Yamanouchi, another advisor through the ALPS (Advanced Leading Graduate Course for Photon Science) program for the last three years, for his warm encouragement and priceless advices.

I am grateful to the group members Dr. Kato, Mr. Sakemi, Mr. Takei and Mr. Nakagawa for various supports. They have supported my stable laboratory life. I could keep good physical and mental health owing to their support.

I also thank Mr. Suzuki and Mr. Hoshino, previous group members who had graduated Master course in 2011, Dr. Yamashiro, Dr. Matsukuma, and the other students who had belonged to our group for their preceding researches.

I thank professor Rosario Gonzáles and Dr. Yuan-Pin Chang for fruitful advices and discussions for my numerical studies.

My research for the last 3 years has been supported by ALPS of MEXT. Not only for the support for the last 3 years, I am also deeply appreciating Japanese-government's providing me the opportunity to study in Japan. I could first come to Japan in 2005 thanks to the support from Korea-Japan Joint Government Scholarship Program.

Finally, I would like to thank my family in Korea for supporting me.

The chronological order of my works

In 2010, when I first joined the Prof. Hirofumi Sakai's group as a student of master's course, I cooperated with two senior students Midai Suzuki and Tetsuro Hoshino, who had been engaged in developing apparatuses for quantum-state-selection, hexapole focuser and molecular deflector respectively.

From the middle of 2011, we have started laser-based experiments of controlling angular distribution of the molecules state-selected by the molecular deflector which we had successfully developed. We have achieved strong alignment and orientation in the (nearly) adiabatic regime, owing to employing the advanced experimental equipments like pulsed valve for low initial temperature of molecular sample and the home-built molecular deflector.

For two years, from 2012 to 2013, with the several solutions for technical issues, we have achieved laser-field-free orientation of asymmetric top molecules in the presence of a weak electro-static field. For laser-field-free molecular orientation we have applied plasma-shutter technique. The strong laser-field-free 3D molecular orientations of state-selected asymmetric top molecules have been achieved too.

In Octobor of 2013, with the financial support from ALPS program, I have visited DESY for two weeks to discuss my problem about a numerical simulation, with which I had been confronting for a long time. After I have gotten back to Japan, owing to the fruitful and kind advices they gave me even after I had come back from DESY, I could develop original numerical method for calculating rotational dynamics of asymmetric top molecules.

From January to December of 2014, the last year of my graduate student life, we have tried to develop the most ideal technique for the field-free orientation. We have applied plasma shutter technique to the combined fundamental and second-harmonic laser pulses. Even though several issues have never been recognized are found, we have achieved completely field-free orientation of OCS molecules with a moderate degree of orientation even with lower pump pulse intensity.

Contents

1 Introduction **9**

1.1 Need for developing techniques for controlling rotational motion of molecules 9

1.2 History of controlling rotational motions of molecules 10

1.3 Topic 1 : Laser-field-free alignment and orientation of large asymmetric top molecules 13

1.4 Topic 2 : Completely field-free orientation of linear molecules . 14

1.5 Outline of this thesis 19

2 Theoretical background of the quantum description of a rigid rotor exposed to external fields **21**

2.1 Hamiltonians 24

2.1.1 Field-free Hamiltonian and its eigenstates 24

2.1.2 Interaction Hamiltonians 26

2.2 Symmetry configurations of Hamiltonians and their eigenstates 30

2.2.1 Field-free condition 30

2.2.2 Parallel field condition 33

2.2.3 Tilted field condition 35

2.3 Adiabatic versus Impulsive regime 35

2.3.1 Overview 35

2.3.2 Adiabatic regime 36

2.3.3 Impulsive regime 37

3 Time-dependent unitary transformation method **38**

3.1 Overview : intermediate regime and a numerical method . . . 38

3.1.1 Example 1 : Impulsive orientation 39

3.1.2 Example 2 : Pure adiabatic orientation followed by rapid turn off of the laser field 43

3.1.3 Example 3 : Non-pure adiabatic orientation with a slow turning on of laser field 46
3.1.4 Advantages of the numerical method 46

4 Experimental setup and techniques 48
4.1 Setup of the vacuum chamber 49
4.1.1 Overview 49
4.1.2 Monte-Carlo simulation for trajectories of molecules . 51
4.1.3 Result of the state-selection 53
4.2 Optical arrangement 58
4.2.1 Overview 58
4.2.2 Shaping a laser pulse with a slow turn on and a rapid turn off 59
4.2.3 Spatial overlapping of the pump and the probe pulses . 63
4.2.4 Controlling the relative phase of the two-color laser pulse 65

5 Results and discussions 1 : Laser-field-free orientation of asymmetric top molecules 68
5.1 Quasi-adiabatic orientation of state-selected asymmetric top molecules by combined electrostatic and one-color laser fields . 68
5.2 Laser-field-free orientation of state-selected asymmetric top molecules 74

6 Results and discussions 2 : Rotational dynamics of asymmetric top molecules exposed to a laser pulse with a slow turn on and a rapid turn off 78
6.1 Rotational dynamics of asymmetric top molecules exposed to a laser pulse with a slow turn on and a rapid turn off, in the presence of a weak electrostatic field. 79
6.1.1 Dephasing dynamics 80
6.1.2 Revival structure 80
6.2 Loss of adiabaticity and its effect on rotational dynamics of asymmetric top molecules 87
6.2.1 Avoided crossings and loss of adiabaticity 89
6.2.2 Rotational dynamics of molecules in thermal ensemble 93
6.2.3 Conclusion 95

7 Results and discussions 3 : Completely field-free orientation of state-selected molecules **98**
7.1 Molecular Orientation by two-color laser field 99
7.1.1 OCS molecule 99
7.1.2 Iodobenzene molecule 102
7.2 Completely field-free orientation of OCS molecules 103

8 Summay and outlook **108**
8.1 Laser-field-free orientation of state-selected asymmetric top molecules 108
8.2 Numerical study on rotational spectrum and dynamics of asymmetric top molecules 109
8.3 Completely field-free orientation of molecules 111

9 Appendix **113**
9.1 Matrix elements of Hamiltonians 113
9.1.1 Linear molecule 113
9.1.2 Asymmetric top molecule 114
9.2 Effect of the residual laser field 117

Chapter 1

Introduction

1.1 Need for developing techniques for controlling rotational motion of molecules

Always, molecule has been an attracting research subject for scientists. One of the reasons is that there are interesting phenomena related to anisotropic structure of molecules. On the other hand, observables that we get in conceivable experiments are obtained as an averaged value over a group of molecules. Furthermore, even a single rotational state in the field-free condition has not completely but nearly isotropic angular distribution in the laboratory-fixed frame. Because of these reasons we can not explicitly observe interesting phenomena pertaining to the anisotropic structure of molecules, which is the first reason why we need to control rotational motion of molecules. Another advantage of controlling the rotational motion is that the controlling techniques can work as tools for investigating structures and properties of molecules experimentally since the techniques are deeply related with rotational spectroscopy of molecules.

The control and manipulation of the directional features of molecules, even though a long history of it, is still very promising research area. A lot of studies on molecular alignment and orientation have been reported[1]. It is a truth that one of the most widely adopted technique in various experi-

[1]A molecule asymmetric upon reflection is considered to be oriented when their direction is synchronized respect to a Laboratory-fixed frame, while it is considered to be aligned if this angular confinement along a laboratory-fixed axis is symmetric upon the inversion of the axis.

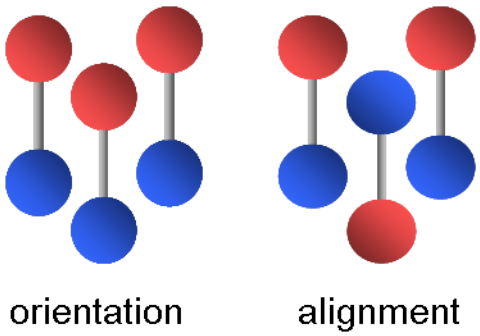

Figure 1.1: Molecular alignment and orientation

ments with gas phase molecules is"impulsive alignment" [2] technique. When molecules are irradiated with a linearly polarized impulsive laser field, the angular distribution of the molecules is synchronized along the laser field. On the other hand, while the molecular alignment technique have matured to a state with a number of associated studies, development of a robust orientation technique is still an important subject of research and many scientists around the world have been developing it.

1.2 History of controlling rotational motions of molecules

The first approach to preparing a sample of oriented molecules is based on electrostatic fields. Two techniques using electrostatic field have been utilized for orientation of molecules. The first method developed was based on rotational state selection by an inhomogeneous electro-static field. In a hexapole focuser, the inhomogeneous electrostatic hexapole field is used to select a single rotational state of molecule. The method is based on the first-order interaction between the inhomogeneous external field and a permanent dipole moment of the molecule. Researchers have utilized this technique for investigating the anisotropic effects of symmetric top molecules experimentally because a single quantum eigenstate is generally anisotropic [1, 2]. As an alternative method, the brute-force orientation using a very strong elec-

[2]In the present thesis, we represent interaction between molecules and ultra-short laser pulses as impulsive rather than nonadiabatic.

trostatic field was proposed [3]. The interaction energy of permanent dipole which is stronger than the field-free rotational energy allows the molecules to be oriented along the direction of electrostatic field. However, this method has an obvious disadvantage. Typically on the order of 100 kV/cm, which is not easily accessible experimentally, is required for the brute-force orientation.

The other approach has been reported is based on the application of optical fields to orient molecules. When randomly oriented molecules are irradiated with polarized light resonant with a transition of the electronic states, the excitation probability depends on the angle between the transition dipole vector and the polarization vector [4, 5]. The excitation to a dissociative state makes it possible to obtain oriented molecules. Weakness of this method is that only a small fraction of molecules from the original sample remains.

On the other hand, there have been theoretical [6, 7, 8] and experimental [9, 10] demonstrations of alignment with an intense non-resonant laser field. Instead of the static electric field in the brute force orientation, the strong nonresonant laser-field that interacts with polarizability of molecules can align molecules. Because this method utilizes the interaction between a nonresonant laser field and a laser-induced dipole moment stemming from anisotropic polarizability of molecule, it is applicable to any molecule irrespective of its specific characteristics.

In the adiabatic regime [6, 7], where the laser pulse is long compared to the rotational period of the molecule, molecules are aligned while the laser pulse is present, and the molecules return to their initial free-rotor states after the laser pulse. In contrast to this, in the impulsive (non-adiabatic) regime [11, 12, 13, 14, 15, 16], ultrashort laser pulse irradiated to the molecule contributes to the formation of a broad rotational wave packet via Raman mechanism. That makes molecule to be aligned in the field-free regime. In fact, the impulsive alignment technique has broadened the scope of spatially aligned molecules from the original focus on chemical reaction dynamics to new applications such as optimal control of multiphoton ionization [17] and molecular imaging based on high harmonics generation [18, 19, 20, 21, 22, 23]

In spite of the usefulness of the impulsive alignment technique, since the interaction induced by linearly polarized non-resonant laser field has inversion symmetry, the orientation is not attained in the same way with the alignment. In order to accomplish not only the alignment but also the orientation, an additional interaction breaking the symmetry have been applied by DC field,

which is much weaker than that used in the brute-force method, interacting with the molecular permanent dipole. Based on the theoretical studies by Friedrich and Herschbach [24, 25], the one-dimensional orientation technique using combined electrostatic and linearly polarized non-resonant laser fields is demonstrated[26, 27]. Also, the combined field technique have been employed for three dimensional orientation of asymmetric top molecules by using elliptically-polarized laser field instead of the linearly-polarized field[28]. Moreover, orientation by nonresonant phase-locked two-color laser field was proposed [29] and demonstrated [30].

On the other hand, when we consider the alignment, well aligned states in the field-free condition are achievable by an intense impulsive laser field. However, in the case of the orientation, the achievable degrees of orientation can be significantly enhanced only when the induced interaction time scale is close to the adiabatic limit. There have been researches pointing out the advantage of adiabatic orientation [31, 32, 33]. In the earlier study [31], it has been considered that initial field-free states can tunnel from the swallower potential wall to the deeper one when the applied external field for orientation turns on very slowly, typically on the order of ns. However, the nanosecond laser pulse orient molecules only in the presence of the laser field. A breakthrough to achieve high degrees of orientation in the laser-field-free condition is the usage of a laser pulse with an adiabatic turn on and a rapid turn off. Motivated by researches about rapidly turned off laser field [31, 35, 34], the usefulness of this method for molecular orientation have been confirmed experimentally [36].

Nevertheless of a number of the studies on the molecular orientation, the experimentally obtained degrees of molecular orientation have been still modest. That was due to the presence of many different rotational states in the initial sample. When a field for molecular orientation is applied to sample molecules, some of rotational states are oriented one way and the other states are oriented the other way, which makes the degree of orientation of the molecular sample much lower than that of certain one rotational state.

In 2009, in order to achieve strong degrees of orientation, rotational-state-selection techniques have been employed. State-selected NO molecules by a hexapole focuser have been oriented with a combination of electrostatic and impulsive laser fields [37]. While the hexapole focuser can be employed for symmetric top molecules, a molecular deflector generating "two wire field" have been used for the state-selection of large asymmetric top molecules [38, 39]. They have oriented state-selected iodobenzene molecules prepared with

the molecular deflector and demonstrated the usefulness of the state-selection technique for a high degree of orientation.

In recent years, on the other hand, with the advance of the THz laser pulse techniques, molecular orientation techniques using THz laser pulses also have been demonstrated. [40, 41].

1.3 Topic 1 : Laser-field-free alignment and orientation of large asymmetric top molecules

We have achieved laser-field-free orientation of iodobenzene molecules state-selected by a molecular deflector, and we have numerically explored their rotational dynamics. Not only the small linear molecules but also much larger molecules, which are often asymmetric top molecules, have been an active subject of research. The alignment and orientation of asymmetric top molecules are relatively not easy to achieve in the (laser-) field-free condition than other molecules with much simpler structures like linear and symmetric top molecules, which is attributed to the complex rotational spectrum of the asymmetric top molecules. Thus, the experimental achievements have been accompanied by theoretical efforts to estimate and understand their unique rotational spectrum and dynamics.

A lot of studies of field-free molecular alignment and orientation are restricted on the molecules with simpler structures. On the other hand, when we focus our attention to large asymmetric top molecules, there has been a long history of the associated studies. It have been reported that the rotational dynamics of asymmetric top molecules irradiated with impulsive laser pulse are qualitatively different with that of other simpler molecules [42, 43]. They have shown experimentally and theoretically that the rotational dynamics of asymmetric molecules sensitively depend both on intensity and fluence of laser pulses applied. On the other hand, three dimensional alignment of asymmetric top molecules have been reported by using a train of short laser pulses [44]. Also, there have been other studies on theory of field-free three dimensional alignment [45, 46].

However, samples of oriented asymmetric top molecules are mainly created in the presence of laser-field. A combination of a laser pulse and a weak static electric field method have been demonstrated for the orientation of asymmetric top molecules in the presence of the combined field [38, 39]. For

three dimensional alignment in the presence of a linearly polarized laser field, a method of using long and short pulses are reported [47, 48].

Even though the availability of the controlled asymmetric top molecules in the presence of the laser field have allowed experiments such as spectroscopy [49], photoelectron angular distribution [50, 51], we can expect that development of the field-free orientation technique of asymmetric top molecules can fuel the progress of research area such as photoelectron angular distribution and high-harmonic generation.

One of purposes of the present thesis is to demonstrate an experimental technique to achieve laser-field-free orientation of large molecules. We have employed plasma shutter technique to achieve strong degree of orientation of iodobeozene molecules in the laser-field-free condition. At least, we can expect the experimentally achievable the highest degrees of alignment and orientation in the field-free condition are accomplished by using the plasma shutter technique. Molecules controlled by slow turn on of laser field can be kept in the laser-field-free condition just after the rapid turn off of the laser field, as it is shown in Chapter 5.

Furthermore, since we have experimentally found that the generated wave-packets of iodobenzene molecules show unique temporal dynamics, we have explored the plentiful underlying physics with numerical studies in Chapter 6.

1.4 Topic 2 : Completely field-free orientation of linear molecules

Recently, many studies on field-free molecular orientation of linear molecules have reported. This section is dedicated for a brief review of several promising methods of field-free molecular orientation of linear molecules, and we compare them with our method.

In order to orient polar molecules, external potential must be asymmetric upon the inversion. For making the driving field for field-free orientation, two techniques based on all optical approaches have been proposed. One approach of field-free orientation is usage of two-color pulses [29, 55]. Two laser pulses whose optical frequencies are ω and 2ω can generate an asymmetric potential for the molecular orientation, if the relative phase between the ω and the 2ω is appropriately controlled. And another approach is based on

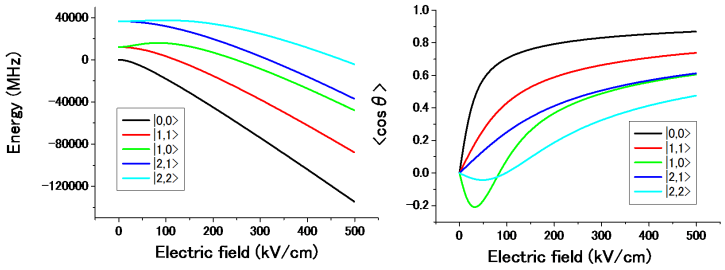

Figure 1.2: Energy shifts (left) and degrees of orientation (right) of several low-lying rotational states of OCS molecule exposed to an electrostatic field.

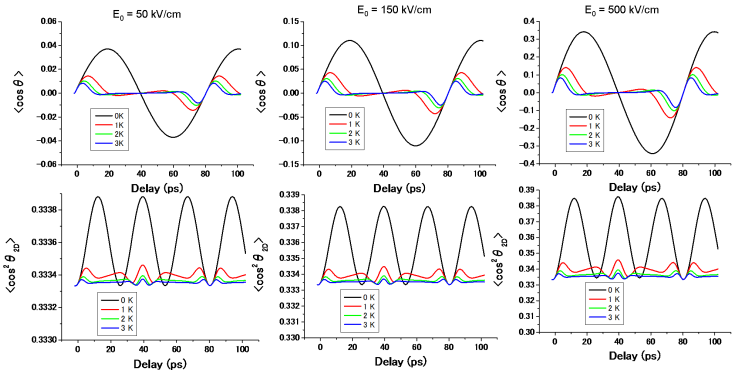

Figure 1.3: Numerically calculated time evolutions of $< \cos\theta >$ (upper panels) and $< \cos^2\theta >$ (lower panels) of OCS molecules. A half cycle pulse applied at each panels is given by equation 1.1.

THz pulses. Since single or half-cycle terahertz pulse have non-zero dipole interaction over the optical cycle, molecular orientation techniques based on interaction between electric field of THz pulse and dipole of of the molecule have been studied [40, 41].

On the other hand, nevertheless the progress of the orientation techniques, there has been a crucial problem. Since some of rotational states irradiated with external field(s) are oriented one way and the others are oriented the other way, the degrees of orientation that we get from a group of molecules are much lower than those from a certain rotational state.

This problem can be overcome by several approaches. Under a remarkably strong electric field typically much stronger than 100kV/cm, it is possible to

orient most of low lying rotational quantum states in the same direction. Fig. 1.2 shows shifted rotational energies and degrees of orientation of OCS molecules exposed to an electrostatic field as a function of the applied electric field. As it is shown in the Fig. 1.2, the two most low-lying quantum states, $|0,0>$ and $|1,0>$, are oriented oppositely when the electric field is not strong enough, while they are oriented along the same direction when the field is stronger than 100kV/cm[3]. Therefore, the orientation technique based on the THz laser pulses could be a robust breakthrough to orient most of low-lying quantum states involved in a molecular sample [60], provided the available intensity of THz pulses is further improved. In Fig. 1.3, we summarize numerical results of time evolutions of alignment and orientation of OCS molecules exposed to a half cycle THz laser pulse, whose temporal shape is given by 1.1. The obtained degree of alignments is still lower than 0.4 in the numerical results, since the intensities of THz laser pulses are much weaker than that of ultra-short laser pulses available nowadays. However, the fact that almost of low-lying quantum states are orientated same direction gives rise to the achieved considerable degree of orientation, 0.05∼0.1, even when the rotational temperature is moderately high.

$$\mu E(t) = \begin{cases} \mu E_0 \sin^2(\pi t) \ (0 < t < 1\text{ps}) \\ 0, \ (\text{otherwise}) \end{cases} \tag{1.1}$$

As another way to overcome the problem associated with initial state dependence of molecular orientation, recently, a theoretical proposal to control the rotational wave packet and to enhance the achievable degrees orientation have been reported. [52]. They have shown that the degree of orientation can be significantly enhanced by using a combination of one-color and two-color laser pulses. Following the theoretical proposal, molecular sample even with a high rotational temperature have been strongly oriented compared to when it is oriented by only an ultrashort two-color laser field. [58, 59].

While the two methods described above provides opportunities to perform various experiment with the oriented molecular sample, the reported degrees of orientation are still far from the maximum degree of orientation value that we can expect from an ideal experimental condition. While an achievable degree of orientation in an ideal condition is more than 0.9 ($< \cos\theta >$), the recently reported degrees of orientation are still much lower.

[3]The orientation based on strong electrostatic field on the order of 100 kV/cm is the brute force orientation technique.

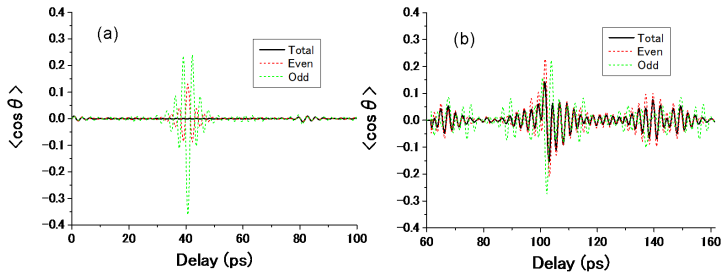

Figure 1.4: Numerically calculated time evolutions of $< \cos\theta >$ of OCS molecules. (a) is a result observed when only a two-color laser pulse is applied at 0 ps . (b) is a result with both one-color and the two-color pulses are applied at 0 ps and 61.5, respectively. For the results shown in each panels, the total intensity of two-color laser pulse is $5.2 \times 10^{13}\mathrm{W/cm}^2$, the pulse width 70 fs (FWHM) and the ω-to-2ω intensity ratio three. The intensity of the one-color laser pulse is $4.2 \times 10^{13}\mathrm{W/cm}^2$ and the pulse width is 85 fs (FWHM). The results are calculated under 3 K of rotational temperature.

As a method to accomplish the strongest degree of molecular orientation in the field-free condition, we describe a method, which is another main theme of the present thesis. Our recipe for the orientation is applying two-color laser pulse shaped by plasma shutter to state-selected molecules. When we consider a molecule in a single rotational-quantum state, the achievable maximum degree of orientation is achieved when the interaction is purely adiabatic, while the achievable degrees of alignment do not critically depend on the interaction time scale. However, the oriented molecules by a laser pulse with a long duration exist as field-dressed states. To make field-free, strong molecular orientation of a single rotational-quantum-state, we apply plasma shutter technique for making a two-color laser pulse with a slow turn on and a rapid turn off. The field-dressed rotational states which is oriented with an extremely high degree of orientation can be transferred into field-free condition by the rapid turn off. In our recipe, problem associated with the initial rotational state dependence of orientation is overcome by using state-selected molecules.

Let us compare our method with the other one using combination of one-color and two-color ultra-short laser pulses. In Fig. 1.4, we show a set of numerical results illustrating the significant enhancement of degree

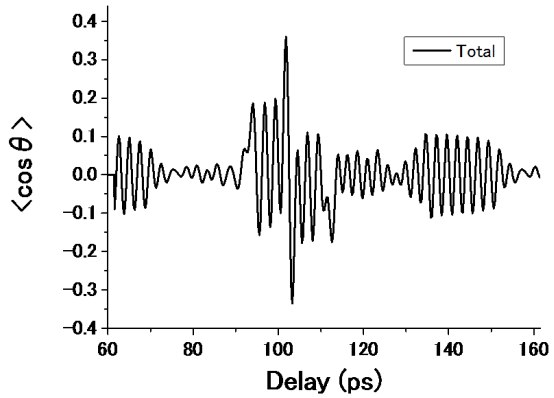

Figure 1.5: Numerically calculated time evolutions of $< \cos\theta >$ of OCS molecules. The same with the Fig. 1.4 (b) but the the rotational temperature is 0 K.

of orientation accomplished by the combination of an one-color and a two-color laser pulses. When only two-color laser pulse is irradiated Fig. 1.4(a), near the half of the rotational period of the molecule 41 ps the isolated contributions from the odd- and even-J initial states to the orientation are strong. However, since phase of the two contributions does not match, the total degree of orientation at the half-revival 41 ps is nearly zero. In contrast, when the two-color pulse irradiation is preceded by one-color irradiation with a delay of 3/4 of the rotational period, the contribution from the odd-J states is suppressed, which give rise to a pronounced total orientation [52]. This approach has opened up the experimental opportunities to use well oriented molecular sample in the field-free condition.

On the other hand, further strong degrees of orientation can be expected if molecular sample includes only a single or several initial rotational states and they are oriented adiabatically by a long laser pulse rather than impulsively by ultra-short laser pulses. In Fig 1.6, we show numerical result of field-free orientation obtained by two-color laser pulse with a slow turn-on and a rapid turn off. Our method based on a laser pulse shaped to be slowly turned on and rapidly turned off gives rise to much higher degrees of orientation when the initial rotational temperature is low. This is because in the orientation process, non-adiabatic transition between a pair of states which oriented oppositely results in the decrease of accomplished degree orientation. As

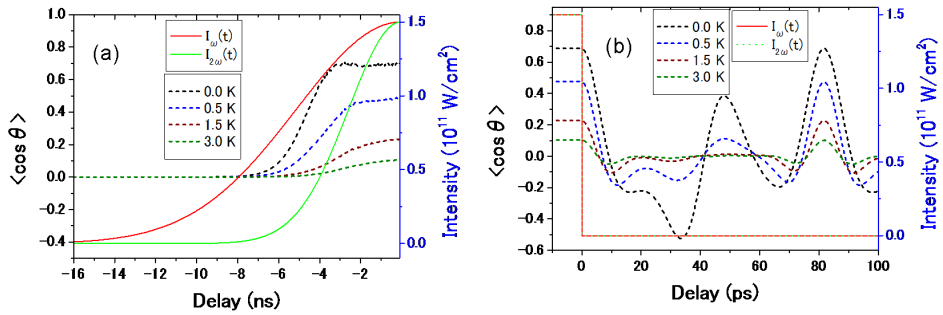

Figure 1.6: Numerically calculated time evolutions of $< \cos\theta >$ of OCS molecules exposed to a two-color laser pulse with a slow turn on and a rapid turn off. (a) shows the time evolution on the rising part of the laser field, while (b) shows that after the rapid turn off of the laser field. The peak intensities of the ω and 2ω is same as 1.5×10^{11}W/cm^2. The pulse widths (HWHM) on the rising part are 6 ns and 3 ns for the ω and 2ω, respectively. The degrees of orientation are averaged over thermal ensembles with several differnet rotation temperatures.

that is shown in Fig. 1.5, the achievable degree of orientation with the orientation technique based on the ultra-short laser pulse does not give rise to a very pronounced degree of orientation for a single rotational state. Thus, the method with the shaped two-color laser pulse works as an unique tool for accomplishing the strongest orientation of molecules if it is applied to a molecular sample including one or several rotational quantum states, while the method based on the combination of a one-color and a two-color pulses is advantageous in that it can be used for molecular sample with relatively high-rotational temperature.

Our achievement of field-free orientation of OCS molecules is given in Chapter 7.

1.5 Outline of this thesis

This thesis consists of 9 chapters. The present Chapter is dedicated for the introduction.

In Chapter 2, theoretical background of molecules, ranging from the simplest linear molecule to the most general asymmetric top molecule, and their

interactions with external fields are reviewed.

Chapter 3 is dedicated for describing "time-dependent unitary transformation method" that is employed for our numerical studies.

In Chapter 4, we describe all about the experimental set-ups and used methods.

Chapter 5 presents the most notable results including laser-field-free orientation of state-selected asymmetric top molecules. In Chapter 6, with the time-dependent unitary transformation method, we mainly explore rotational dynamics of asymmetric top molecules exposed to a combination of electrostatic field and laser field with a slow turn on and a rapid turn off.

In Chapter 7, we describe our experimental results of field-free orientation and discuss the results with numerical demonstrations.

In Chapter 8, we summarize the present studies and discuss the outlook.

Chapter 9 is dedicated for Appendix.

Chapter 2

Theoretical background of the quantum description of a rigid rotor exposed to external fields

In this chapter, we describe the theoretical background of a rigid-rotor model for understanding rotational dynamics of molecules. The theoretical description of this chapter is restricted within the Born-Oppenheimer approximation and we focus our attention on the nuclear dynamics of molecule since the applied external fields we consider are not so strong to cause the ionization of molecules. Furthermore, for simplicity we assume that vibrational and rotational motions can be adiabatically separated even though the rovibrational coupling by an external field is also an interesting field of research.[1] The rovibrational coupling, however, is not so crucial when we consider molecular sample cold enough. Through the present chapter, we confine the attention to a rigid-rotor model which allows us to explore the angular distributions of molecules adequately. The rigid-rotor model can well reproduce a lot of experimental results of molecular alignment and orientation.

Parameterization of rotations by Euler angles

First, the way to define any finite rotation must be reviewed to be self-contained. Any finite rotation can be uniquely specified by giving three

[1]The coupling of vibrational and rotational motion of heteronuclear diatomic molecule exposed to an external homogeneous and static electric field have been studied [53, 54].

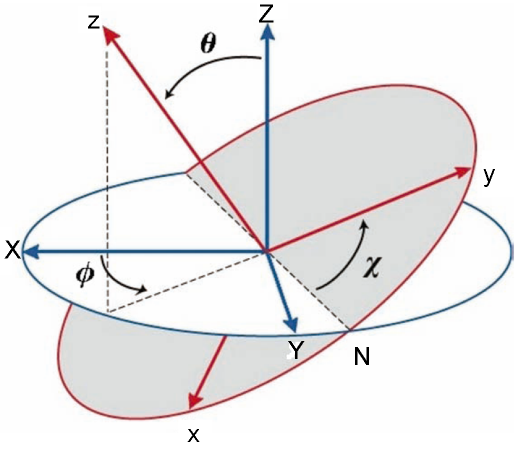

Figure 2.1: Euler angles ϕ, θ, and χ relating the two different coordinate systems

parameters. A useful and general description is achieved by introducing the three Euler angles ϕ, θ, and χ shown in figure 2.1. The Euler angles should be regarded as defining a prescription whereby a coordinate system $F = XYZ$ can be made to coincide with another coordinate system $g = xyz$ by three successive finite rotations [76].

1. A counterclockwise rotation ϕ about Z, the vertical axis. This carries the Y axis into the line of nodes N.

2. A counterclockwise rotation θ about the line of nodes N. This carries the Z axis into the z axis (the figure axis of the coordinate system g).

3. A counterclockwise rotation χ about z, the figure axis. This carries the line of nodes N into the y axis.

In the quantum mechanics, an operator for arbitrary rotation of system about $\hat{n}$ by an angle a can be expressed as

$$R_n(a) = \exp(-iaJ \cdot \hat{n}), \tag{2.1}$$

where J is an angular momentum operator. Thus, the above prescription specified by the three Euler angles express

$$R(\phi, \theta, \chi) = \exp(-i\chi J \cdot \hat{n}_\chi) \exp(-i\theta J \cdot \hat{n}_\theta) \exp(-i\phi J \cdot \hat{n}_\phi)$$

$$= \exp(-i\chi J_z)\exp(-i\theta J_N)\exp(-i\phi J_Z). \tag{2.2}$$

A unitary transformation U carries an operator Q into UQU^{-1}. Hence

$$\exp(-i\theta J_N) = \exp(-i\phi J_Z)\exp(-i\theta J_Y)\exp(-i\phi J_Z),$$

$$\exp(-i\chi J_z) = \exp(-i\theta J_N)\exp(-i\chi J_Z)\exp(-i\theta J_N). \tag{2.3}$$

By substituting Eq.(2.3) and Eq.(2.3) into Eq.(2.2), $R(\phi,\theta,\chi)$ can be described with angular momentum operators only referred to the F coordinate system.

$$R(\phi,\theta,\chi) = \exp(-i\phi J_Z)\exp(-i\theta J_Y)\exp(-i\chi J_Z) \tag{2.4}$$

Any rotational transformation of coordinate in the three dimensional space, thus, can be expressed by the Eq.(2.2) or (2.3). We note that this Unitary transformation can be expressed as a matrix. Let an arbitrary vector have the Cartensian component (X,Y,Z) in the space-fixed frame and the Cartesian component (x,y,z) in the molecule-fixed frame. Following the prescription for making a coordinate transformation described and considering the geometric interpretation, the three steps$-\exp(-i\phi J_Z)$, $\exp(-i\theta J_N)$, $\exp(-i\chi J_z)$- are denoted by following matrices.

$$\begin{pmatrix} x' \\ y' \\ z' \end{pmatrix} = -\exp(-i\phi J_Z)\begin{pmatrix} X \\ Y \\ Z \end{pmatrix} = \begin{pmatrix} \cos\phi & \sin\phi & 0 \\ -\sin\phi & \cos\phi & 0 \\ 0 & 0 & 1 \end{pmatrix}\begin{pmatrix} X \\ Y \\ Z \end{pmatrix}$$

$$\begin{pmatrix} x'' \\ y'' \\ z'' \end{pmatrix} = -\exp(-i\theta J_N)\begin{pmatrix} x' \\ y' \\ z' \end{pmatrix} = \begin{pmatrix} \cos\theta & 0 & -\sin\theta \\ 0 & 1 & 0 \\ \sin\theta & 0 & \cos\theta \end{pmatrix}\begin{pmatrix} x' \\ y' \\ z' \end{pmatrix}$$

$$\begin{pmatrix} x \\ y \\ z \end{pmatrix} = -\exp(-i\chi J_z)\begin{pmatrix} x'' \\ y'' \\ z'' \end{pmatrix} = \begin{pmatrix} \cos\chi & \sin\chi & 0 \\ -\sin\chi & \cos\chi & 0 \\ 0 & 0 & 1 \end{pmatrix}\begin{pmatrix} x'' \\ y'' \\ z'' \end{pmatrix} \tag{2.5}$$

The above coordinate frames (x',y',z'), (x'',y'',z'') and (x,y,z) are represent the coordinate frames after the rotations $\exp(-i\phi J_Z)$, $\exp(-i\theta J_N)$, and $\exp(-i\chi J_z)$ respectively. Therefore, the molecule-fixed (x,y,z) and the space-fixed (X,Y,Z) frames are connected by the relations shown below.

$$\begin{pmatrix} x \\ y \\ z \end{pmatrix} = \begin{pmatrix} \mathrm{c}\phi\ \mathrm{c}\theta\ \mathrm{c}\chi - \mathrm{s}\phi\ \mathrm{s}\chi & \mathrm{s}\phi\ \mathrm{c}\theta\ \mathrm{c}\chi + \mathrm{c}\phi\ \mathrm{s}\chi & -\mathrm{s}\theta\ \mathrm{c}\chi \\ -\mathrm{c}\phi\ \mathrm{c}\theta\ \mathrm{s}\chi - \mathrm{s}\phi\ \mathrm{c}\chi & -\mathrm{s}\phi\ \mathrm{c}\theta\ \mathrm{s}\chi + \mathrm{c}\phi\ \mathrm{c}\chi & \mathrm{s}\theta\ \mathrm{s}\chi \\ \mathrm{c}\phi\ \mathrm{s}\theta & \mathrm{s}\phi\ \mathrm{s}\theta & \mathrm{c}\theta \end{pmatrix} \begin{pmatrix} X \\ Y \\ Z \end{pmatrix} \tag{2.6}$$

and

$$\begin{pmatrix} X \\ Y \\ Z \end{pmatrix} = \begin{pmatrix} \mathrm{c}\phi\ \mathrm{c}\theta\ \mathrm{c}\chi - \mathrm{s}\phi\ \mathrm{s}\chi & -\mathrm{c}\phi\ \mathrm{c}\theta\ \mathrm{s}\chi - \mathrm{s}\phi\ \mathrm{c}\chi & \mathrm{c}\phi\ \mathrm{s}\theta \\ \mathrm{s}\phi\ \mathrm{c}\theta\ \mathrm{c}\chi + \mathrm{c}\phi\ \mathrm{s}\chi & -\mathrm{s}\phi\ \mathrm{c}\theta\ \mathrm{s}\chi + \mathrm{c}\phi\ \mathrm{c}\chi & \mathrm{s}\phi\ \mathrm{s}\theta \\ -\mathrm{s}\theta\ \mathrm{c}\chi & \mathrm{s}\theta\ \mathrm{s}\chi & \mathrm{c}\theta \end{pmatrix} \begin{pmatrix} x \\ y \\ z \end{pmatrix}, \tag{2.7}$$

where c and s stand for cos and sin, respectively. These relations of the two coordinate frames are utilized for deriving interaction Hamiltonians discussed in the following section.

2.1 Hamiltonians

In this section, we overview interaction Hamiltonians for molecular alignment and orientation with our attention focused on the rigid-rotor model.

2.1.1 Field-free Hamiltonian and its eigenstates

The Hamiltonian for the rotational motion of a free rigid rotor is

$$H_{rot} = AJ_a^2 + BJ_b^2 + CJ_c^2, \tag{2.8}$$

where a,b,and c are the molecular-fixed axes and A, B, and C are the corresponding rotational constants ($A \geq B \geq C$). In the case of an oblate symmetric top ($A = B > C$) molecule and a prolate symmetric top ($A > B = C$) molecule,

$$H_{rot} = AJ^2 + (C - A)J_z^2 \tag{2.9}$$

and

$$H_{rot} = CJ^2 + (A - C)J_z^2, \tag{2.10}$$

respectively. For a linear molecule the field-free Hamiltonian is written with only one rotational constant B,

$$H_{rot} = BJ^2. \tag{2.11}$$

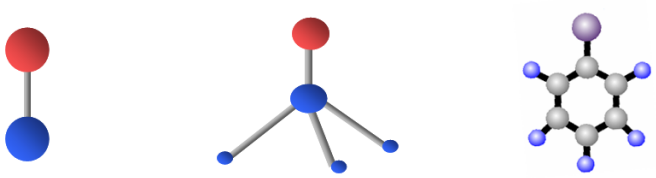

(a) Linear molecule

(b) Symmetric top molecule

(c) Asymmetric top molecule

Figure 2.2:

In the case of the linear molecule illustrated in figure 2.2 (a), the total rotational energy is proportional to the square of total angular momentum $\hat{J}^2$. Thus, Spherical harmonics $|J, M>$, the eigenstates of the operator $\hat{J}^2$ are eigenstates of the free rotational states of a linear rigid rotor.

On the other hand, eigenstates of an asymmetric top (figure 2.2 (c)) molecule is a linear combination of elements of Wigner-D-matrix, which are eigenstates of symmetric top (figure 2.2 (b)) molecule. We look to the description of the rotational wave function of an asymmetric and a symmetric top molecule [76].

ψ_{JM} is an eigenfunction of the field-free Hamiltonian H_{rot} with the eigenvalue E_{JM}, the square of the total angular momentum operator J^2 with an eigenvalue $J(J+1)$, and the the component of a space-fixed axis of the total angular momentum J_Z with an eigenvalue M.

When a rotation $R_1 = (\phi_1, \theta_1, \chi_1)$ is applied to the system, ψ_{JM} will be transformed into ψ'_{JM} according to

$$\psi'_{JM} = \psi_{JM}(\phi - \phi_1, \theta - \theta_1, \chi - \chi_1)$$

$$= R_1\psi_{JM}(\phi, \theta, \chi) = \sum_{M'} D^J_{M'M}(\phi_1, \theta_1, \chi_1)\psi_{JM'}(\phi, \theta, \chi), \tag{2.12}$$

where $D^J_{M'M}$ is the rotation matrix which corresponds to the rotation R_1. By setting $\phi_1 = \phi$, $\theta_1 = \theta$, and $\chi_1 = \chi$, Eq. (2.12) reads

$$\psi_{JM}(0,0,0) = \sum_{M'} D^{J}_{M'M}(\phi,\theta,\chi)\psi_{JM'}(\phi,\theta,\chi). \tag{2.13}$$

Then we multiply both sides of this equation by $D^{J^*}_{M''M}(\phi,\theta,\chi)$ and sum over the index M. From the unitarity of the rotation matrices, we find

$$\begin{aligned}
&\sum_{M} D^{J^*}_{M''M}(\phi,\theta,\chi)\psi_{JM}(0,0,0) \\
&= \sum_{M}\sum_{M'} D^{J^*}_{M''M}(\phi,\theta,\chi)D^{J}_{M'M}(\phi,\theta,\chi)\psi_{JM'}(\phi,\theta,\chi) \\
&= \sum_{M'} \delta_{M'M''}\psi_{JM'}(\phi,\theta,\chi) \\
&= \psi_{JM''}(\phi,\theta,\chi)
\end{aligned} \tag{2.14}$$

Changing M'' to M and M to K, we obtain

$$\psi_{JM}(\phi,\theta,\chi) = \sum_{K} D^{J^*}_{MK}(\phi,\theta,\chi)\psi_{JK}(0,0,0). \tag{2.15}$$

Therefore, the general wave function for an asymmetric top rigid rotor (Fig. 2.2 (c)) is a linear combination of rotational matrices (Wigner-D-matrix). Besides, when the rigid rotor has an axis of symmetry (Fig. 2.2 (b)), an arbitrary rotation about this axis must leave the probability amplitude $|\psi_{JM}|$ unchanged. Hence, we require $\psi_{JM}(\phi,\theta,\chi)$ to be the same up to a phase factor for a rotation about the axis z through the angle χ. On the other hand, the rotation matrix $D^{J^*}_{MK}$ is proportinal to $e^{iK\chi}$. This means a wave function having a symmetric axis must proportional to a rotation matrix. Thus the wave function of a symmetric top(Fig. 2.2 (b)) is proportional to a rotation matrix,

$$D^{J^*}_{MK} \equiv < J,K|\exp(-i\phi J_Z)\exp(-i\theta J_Y)\exp(-i\chi J_Z)|J,M> . \tag{2.16}$$

2.1.2 Interaction Hamiltonians

Generally speaking, the field-free rotational quantum states are not isotropic. However, a group of molecules in the field-free condition is isotropic. For

molecular alignment and orientation, a formation of broad rotational superposition over the field-free states with different J values is a necessary condition. The interaction Hamiltonians for making the molecular alignment and orientation are reviewed in this subsection.

Considering the systems where molecules exposed to both an electrostatic field and a nonresonant laser field, the interaction Hamiltonian stemming from the external fields can be written by

$$H_{\text{interaction}} = -\sum_{I} \mu_I E^I(t) - \frac{1}{2!}\sum_{IJ} \alpha_{IJ} E^I(t) E^J(t) - \frac{1}{3!}\sum_{IJK} \beta_{IJK} E^I(t) E^J(t) E^K(t) - \ldots, \tag{2.17}$$

where μ is a permanent dipole moment tensor, α a component of a polarizability tensor and β a hyperpoarizability tensor. I, J, K denote the space-fixed coordinates X, Y, Z. Here, the electric field, $E^I(t)$, is a sum of electrostatic field E^I_{static} and laser field $E^I_\omega(t)$.

The interaction Hamiltonian that plays a crucial role in a laser-field-induced molecular alignment is the second term of 2.17. However, because the term $\mathrm{H}_{\text{alignment}}$ has the inversion symmetry along the polarization of the one-color laser field, the "head versus tail" order confinement, referred as orientation, does not come true in the same way as alignment. When the one-color field alignment interaction and a weak permanent dipole interaction are simultaneously applied to molecules, molecular orientation much stronger than that induced only from an electrostatic field is achieved [24, 25]. In contrast, without the electrostatic field, owing to the interaction by hyperpolarizability, molecular orientation is achieved when a two-color field is applied [29]. The oriented state of molecules can be made also by irradiating laser pulse whose optical frequency is much lower than the inverse of rotational period of molecule [56]. The first term in 2.17, which is much larger than the other terms in this case, contributes to both alignment and orientation.

Interaction of the permanent dipole

The permanent dipole interaction $V_\mu = -\mu_I E^I(t)$ is composed by an nonzero term, $\mu_I E^I_{\text{static}}$, and the component $\mu_I E^I_\omega(t)$ which vanishes when it is averaged over the optical cycle if the oscillation frequency ω is far removed from any molecular resonance and much higher than the rotational frequency of the

molecule. When the molecule has a pair of electronic states resonant with the frequency ω, the laser-field attributes to the formation of a broad coherent-rotational-wave-packet constituting molecular alignment via the dipole interaction.

The components of the permanent dipole in the laboratory-fixed frame μ_I are related to its molecule-fixed components μ_i through the relation of 2.7. We set the electrostatic field to be involved in the laboratory-fixed XZ plane and tilted from the Z axis by the angle β. Assuming the permanent dipole of molecule has only molecule-fixed z component, the interaction term is denoted as

$$\sum_I \mu_I E^I(t) = |E|(t)(\cos\beta\cos\theta + \sin\beta\cos\phi\sin\theta)\mu_z. \tag{2.18}$$

Interaction of the polarizability

On the other hand, the interaction Hamiltonian with the polarizablity, the second term of 2.17, can be written in the molecule-fixed frame by,

$$H_{\text{alignment}} = -\frac{1}{2}\sum_{ij}\alpha_{ij}E^i_\omega(t)E^j_\omega(t). \tag{2.19}$$

The other terms multiplied by E_{static} in (2.17) is not denoted since they are negligible because the laser-field is much stronger than the electrostatic field in conceivable experimental conditions. When we consider a molecule whose permanent dipole moment is parallel to the molecule-fixed z-axis, the polarizability tensor in the molecule-fixed frame α_{ij} must be a diagonal matrix to satisfy the plus-minus inversion symmetries over the x and y coordinates.

Let us consider a laser-field linearly polarized along the laboratory-fixed Z axis $(0, 0, E(t)\cos\omega t)$. The molecule-fixed components of the laser field, E_i in Eq. (2.19), are related to its laboratory-fixed components E_I by the realtion of 2.6. Then, the Hamiltonian is given by

$$H_{\text{alignment}} = -\frac{1}{4}E(t)^2(\alpha_{xx}\sin^2\theta\cos^2\chi + \alpha_{yy}\sin^2\theta\sin^2\chi + \alpha_{zz}\cos^2\theta) \tag{2.20}$$

$$= \frac{1}{4}E(t)^2(\alpha^{zx}\cos^2\theta + \alpha^{yx}\sin^2\theta\sin^2\chi + \alpha_{xx}), \tag{2.21}$$

where $\alpha^{ij} \equiv \alpha_{ii} - \alpha_{jj}$. The rapidly oscillating terms are averaged over the optical cycles. The constant term α_{xx} is omitted in a lot of papers since

it just introduce an energy shift to the system. When we consider a linear and a symmetric top molecule, the Hamiltonian is χ independent since the polarizabilities satisfy $\alpha_{xx} = \alpha_{yy}$. Then the Hamiltonian is given by

$$\frac{1}{4}E(t)^2((\alpha_{\parallel} - \alpha_{\perp})\cos^2\theta), \tag{2.22}$$

with $\alpha_{\parallel}$ and $\alpha_{\perp}$ are the polarizability components parallel and perpendicular to the molecular axis respectively.

With a laser-field circularly polarized in the laboratory-fixed XY plane $E = (E(t)\cos\omega t, E(t)\sin\omega t, 0)$, the Hamiltonian is written as

$$-\frac{1}{8}E(t)^2(\alpha_{xx}(\cos^2\theta\cos^2\chi + \sin^2\chi) + \alpha_{yy}(\cos^2\theta\sin^2\chi + \cos^2\chi) + \alpha_{zz}\sin^2\theta) \tag{2.23}$$

$$= \frac{1}{8}E(t)^2(\alpha^{zx}\cos^2\theta + \alpha^{yx}\sin^2\theta\sin^2\chi - \alpha_{yy} - \alpha_{zz}). \tag{2.24}$$

When we confine our attention to a linear or a symmetric top molecule, the term is reduced in a simple form denoted below.

$$H_{\text{alignment}} = \frac{1}{8}E(t)^2(\alpha_{\parallel} - \alpha_{\perp})\cos^2\theta. \tag{2.25}$$

Similarly with the case of linear polarization to the Z axis, circular polarization induces a alignment to the molecule. The χ dependent term included in the linear and circular polarization cases indicates the confinement of rotation around the molecule-fixed Z axis, even though the motion in χ can not be controlled independently to the θ.

Interaction of the hyperpolarizablilty

When a laser field and its second harmonic field are simultaneously applied, the third order interaction term contributes to molecular orientation [29]. A molecule symmetric upon the plus-minus inversions along the molecule-fixed x and y axises has β_{ijk}, the hyper polarizability tensor of the molecule which follows the same symmetry condition. To satisfy the inversion symmetry, the elements of β must be zero if the subscripts have odd number of x or y. Let us consider the electric field of two-color laser field, $(0, 0, E_{\omega}(t)\cos\omega t + E_{2\omega}(t)\cos(\omega t + \phi))$, linearly polarized along the laboratory-fixed Z axis with the relative phase ϕ. By focusing our attention on linear and symmetric top

molecules, the interaction Hamiltonian by the two-color laser field is given by

$$H_{\mathrm{two-color}} = \tag{2.26}$$

$$-\frac{1}{4}[E_\omega(t)^2 + E_{2\omega}(t)^2](\alpha_\parallel - \alpha_\perp)\cos^2\theta \tag{2.27}$$

$$-\frac{1}{8}[\cos\phi E_\omega(t)^2 E_{2\omega}(t)][(\beta_\parallel - 3\beta_\perp)\cos^3\theta + 3\beta_\perp\cos\theta], \tag{2.28}$$

where $\beta_\parallel$ is β_{zzz} and $\beta_\perp$ represents all other nonzero components.

2.2 Symmetry configurations of Hamiltonians and their eigenstates

When we solve a Schrödinger equation, the symmetry of the Hamiltonian imposes some limitations to the wavefunction they must obey to. Dividing the Hamiltonian into independent subsystems possessing different symmetry conditions is advantageous in that we can reduce the calculation costs and distinguish quantum states explicitely. In a lot of numerical calculations for a relatively complicated system of molecules, symmetry properties play a crucial role. In this section, we denote symmetry of an asymmetric top molecule in various field conditions.

2.2.1 Field-free condition

While linear and symmetric top molecules have trivial eigenstates which are spherical harmornics and Wigner D-matrix respectively, a wave function of an asymmetric top molecule, which is a linear superposition of eigenstates of a symmetric top molecule, can not be obtained analitically. To obtain eigenstates of an asymmetric top molecule with a computational method, it is convenient to take into account symmetry of the Hamiltonian.

The rotational Hamiltonian obviously has the property that a rotation by 180° about a, b, c axes leaves the Hamiltonian unchanged. Then, expressing this condition in a language of the group theory, any wave function of the system belongs to the point group $V(a, b, c)$. In other words, the operations denoted by C_2^a, C_2^b, C_2^c, and the identity E commute with the rotational

symmetry	E	C_2^a	C_2^b	C_2^c
A	1	1	1	1
B_a	1	1	-1	-1
B_b	1	-1	-1	-1
B_c	1	-1	-1	1

Table 2.1: Character table of the Four-group $V(a, b, c)$. [76]

Hamiltonian[2]. Therefore, the eigenstates of the Hamiltonian can be chosen as eigenstates of the symmetry operations. Since states possessing different eigenvalues of the symmetry operations are not mixed with each other, we can divide a full basis set into several subgroups according to their eigenvalues of the symmetry operations.

A character table of the four-group operators is given in table 2.1. Wave functions that belong to symmetry species A are symmetric under all four operations. Symmetry species B_a corresponds to wave functions that are symmetric with respect to rotation by 180° about the a-axis and antisymmetric with respect to rotations about b and c. Likewise, wave functions belonging to $B_b(B_c)$ are symmetric with respect to rotations about $b(c)$ and antisymmetric with respect to the rotations about the other two principal axes. Owing to the symmetry of the system, we can deal with each group independently by selecting an appropriate basis set.

Instead of $|JKM>$, we employ an asymmetry basis set constructed from linear combinations of $|J \pm KM>$ that can be expressed as $|JKMs>$, which is defined for $K \neq 0$ as

$$|JKMs>= \frac{1}{\sqrt{2}}[|JKM> +(-1)^s|J-KM>], \tag{2.29}$$

where we may take $s = 0$ or 1, and for $K = 0$

$$|J0Ms>= (-1)^s|J0M>= |J0M> . \tag{2.30}$$

This basis set, Wang basis, is invariant under the four-symmetry operations, whereas the Wigner D matrix is not, as shown below,

[2]In the present thesis, we assign the molecule fixed frame (x, y, z) to (a, b, c), followng a general way for expressing prolate-like asymmetric top molecule. For expressing oblate-like asymmetric top or oblate top molecule, the molecule fixed frame (x, y, z) is assigned to (b, c, a) in general.

	Transformations		
Operation	ϕ	θ	χ
C_2^z	$\phi \to \phi$	$\theta \to \theta$	$\chi \to \chi - \pi$
C_2^y	$\phi \to \phi - \pi$	$\theta \to \pi - \theta$	$\chi \to -\chi$
C_2^x	$\phi \to \phi - \pi$	$\theta \to \pi - \theta$	$\chi \to \pi - \chi$
σ_{XZ}	$\phi \to 2\pi - \phi$	$\theta \to \theta$	$\chi \to 2\pi - \chi$
$C_X(\pi)$	$\phi \to 2\pi - \phi$	$\theta \to \pi - \theta$	$\chi \to \pi + \chi$
$C_{\perp 2}^{\alpha}(\pi)$	$\phi \to 2\alpha - \phi$	$\theta \to \pi - \theta$	$\chi \to \chi + \pi$
$C_Z\delta$	$\phi \to \phi + \delta$	$\theta \to \theta$	$\chi \to \chi$

Table 2.2: Action of the symmetry operations on the Euler angles [86]. Euler angles ϕ, θ and χ relate the space-fixed (X, Y, Z) and the molecule-fixed (x, y, z) frames [76].

$$\begin{aligned} C_2^x|J,K,M> &= (-1)^{J+K}|J,-K,M> \\ C_2^y|J,K,M> &= (-1)^{J}|J,-K,M> \\ C_2^z|J,K,M> &= (-1)^{K}|J,K,M> \end{aligned} \tag{2.31}$$

$$\begin{aligned} C_2^x|J,K,M,s>^w &= (-1)^{J+K+s}|J,K,M,s> \\ C_2^y|J,K,M,s>^w &= (-1)^{J+s}|J,K,M,s> \\ C_2^z|J,K,M,s>^w &= (-1)^{K}|J,K,M,s> . \end{aligned} \tag{2.32}$$

These characteristics can be verified by operating each Four-group operators, denoted in Table 2.2, to the rotational matrix . Using the Wang states as a basis set, we can divide the field-free rotational Hamiltonian into four sub-matrices that contain only wave functions of the same symmetry according to the parity of K and s.

$$H_{rot}^{Wang} := \tilde{X} H_{rot} X = E^+ + O^+ + E^- + O^- = H_A + H_{B_a} + H_{B_b} + H_{B_c}. \tag{2.33}$$

Generally, the eigenstates are labeled by J_{K_{-1},K_1}, where K_{-1} is the value of $|K|$ in the limit of a prolate top ($A > B = C$) and K_1 is the value of

$|K|$ in the limit of an oblate top ($A = B > C$). K_{-1} is associated with a rotation about the a axis and K_1, the c axis. Then the four symmetry group designations may be identified with the (even, odd) parity of the $K_{-1}K_1$ pair. The relations between the parity and the symmetry group is shown 2.34.

Since we assign the molecule fixed frame (x, y, z) to (a, b, c) in the present thesis, for a given quantum number J the quasi quantum number K_{-1} represents the strength of rotational motion around the molecule-fixed z(a) axis. And $\tau \equiv K_{-1} - K_1$ represents the energy order of the states with a same J value[3]. Some rotational energies of asymmetric top molecules with various rotational constants are shown in Fig. 2.3.

$$\begin{aligned} A &\longleftrightarrow ee \\ B_a &\longleftrightarrow oe \\ B_b &\longleftrightarrow oo \\ B_c &\longleftrightarrow eo \end{aligned} \tag{2.34}$$

As a reference, calculated rotational energies of iodobenzene molecule, whose $A = 5669, B = 750.4$ and $C = 662.6$(MHz) are given in appendix of the master's thesis [66]. Because of its small rotational constants B and C, rotational cooling down to 1 K still leaves the molecular ensemble of iodobenzene distributed over a considerable number of states.

2.2.2 Parallel field condition

We described in the section 2.1 that the symmetry of the field-free Hamiltonian of an asymmetric top rotor consists of three two-fold rotation around the principle axis of the molecule, which denotes the field-free Hamiltonian commutes with the operators of C_2^x, C_2^y, C_2^z- expressed in Table 2.2.

For an asymmetric top molecule subject to an electrostatic field along the space-fixed Z axis, or both the electrostatic and linearly polarized laser fields parallel to the same space-fixed Z axis, there are three symmetry operators which commute with the field-dressed Hamiltonian excepting the identity operator. Those are two-fold rotation around the molecule-fixed z-axis C_z^2, the rotation around the space-fixed Z axis $C_Z(\delta)$, and the reflection in any plane including the Z axis $C_{\perp 2}^{\alpha}(\pi)$ [86]. Here we consider a symmetry operation, the reflection in the XZ plane σ_{ZX}, as a representative of the reflection

[3]It is possible to label the energy levels by $\tau \equiv K_{-1} - K_1$ [76].

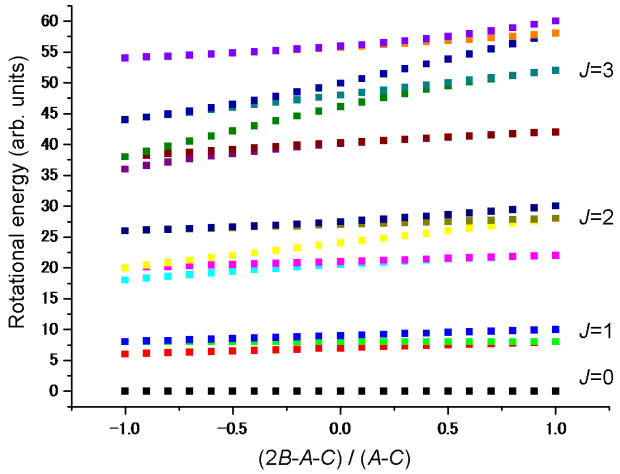

Figure 2.3: Rotational energies of asymmetric top molecule. A and C are fixed as $A = 5$, $C = 3$. $\frac{(2B-A-C)}{(A-C)}$ ranges between -1 for a prolate top ($B = C$) and +1 for oblate top ($A = B$)

operation $C^{\alpha}_{\perp 2}(\pi)$, because the system in the parallel fields along the Z axis is cylindrically symmetric around the Z axis. The symmetry operations onto the Wigner D-matrix elements are summarized below.

$$\begin{aligned} C_2^z|J,K,M> &= (-1)^K|J,K,M> \\ \sigma_{XZ}|J,K,M> &= (-1)^{M+K}|J,-K,-M> . \end{aligned} \tag{2.35}$$

Both the quantum numbers M and K change their parity by the reflection σ_{XZ}. Then, we use an expanded Wang basis set instead of the Wang basis set because the latter is not a good basis set in the parallel field condition. The definition of the expanded Wang basis set for our calculation and the result of the symmetry operations onto the elements of the basis set are summarized

below.

$$
\begin{aligned}
&|J,K,M,s,p>\equiv \\
&\frac{1}{\sqrt{2}}|J,K,M,s>^{w}+(-1)^{p}\frac{1}{\sqrt{2}}|J,K,-M,s>^{w},(M>0 \text{ and p}=0,1) \\
&|J,K,M,s>^{w},(M=0 \text{ and p}=0)
\end{aligned}
$$

$$
\begin{aligned}
C_2^z|J,K,M,s,p>&=(-1)^K|J,K,M,s,p> \\
\sigma_{XZ}|J,K,M,s,p>&=(-1)^{M+K+p+s}|J,K,M,s,p>
\end{aligned}
\tag{2.36}
$$

The results illustrate that the Hamiltonian can be divided into four sub-blocks according to the parity of $p+s$ and K. Thus, the states with M=0, whose p=0 by definition, can be divided into four blocks according to the parity of K and s. The quantum states with $M \neq 0$, whose quantum number $p+s$ is odd or even, have two representations characterized by the parity of K.

2.2.3 Tilted field condition

When the electrostatic field is not parallel to the Z axis along which the laser field is polarized, the symmetries of the Hamiltonian are reduced much more. Then, not only J but also M cease to be good quantum numbers. The Hamiltonian commutes with the C_2^z and the reflection σ_{XZ}. Again, the expanded Wang-basis set (2.36) can be utilized as a basis-set. The wave function can be divided into four subgroups according to the quantum numbers K and $M+p+s$.

2.3 Adiabatic versus Impulsive regime

2.3.1 Overview

A time scale of an interaction is need to be considered appropriately in order to describe a system effectively. A quantum-mechanical system in an eigenstate of initial Hamiltonian $\hat{H}(t_0)$ reaches to a final state followed by temporal change of the Hamiltonian. Then the modification to the final state depends on the time during which the change takes place. Provided

the time derivative of the Hamiltonian is always much smaller than that of the energy gaps of eigenstates of the Hamiltonian, the process is considered adiabatic. In that case, the modified system is characterized by eigenstate of the corresponding time-independent Hamiltonian.

Regarding a rotational quantum state exposed to an external potential, it is required that the temporal variation is much slower than the rotational period of molecule for the adiabatic regime. Since gas phase molecules rotate in periods of the pico second scale, a laser pulse with a few nano seconds of pulse-width provides quasi-adiabatic interaction for controlling the rotational motion. Interaction induced by static field to molecules in a supersonic molecular beam is another example of the adiabatic process.

On the other hand, when the interaction time scale is much shorter than the rotational period of molecule, the interaction is considered as impulsive, and the time evolution of the initial quantum state is determined by the temporally integrated strength of interaction rather than the detailed temporal shape of the interaction. There are several reported method to describe the time evolution of the rotational wave-packet without directly solving the time-dependent Shrödinger equation [13, 16].

The middle of the adiabatic and the impulsive regime also frequently takes place in actual experiments [33, 32]. In this case, solving the time dependent Shrödinger equation sometimes takes too much of calculating cost. An effective method developed originally for successfully describing the intermediate regime is described in Chapter 3.

2.3.2 Adiabatic regime

If the interaction is fully adiabatic, the wave functions are the corresponding eigenstates of the time-dependent Hamiltonian at any moment. One can completely describe the wave function by solving the time-independent Schrödinger equation (TISE).

The adiabatic regime has been numerically explored in many researches. Theoretical studies of the rotational spectrum of linear molecule in the presence of adiabatically applied combined electrostatic and non-resonant laser fields have been reported in earlier time [24, 25]. In recent years, the detailed studies on rotational spectrum of symmetric-top and asymmetric-top molecules exposed to the combined electrostatic and nonresonant radiative fields are reported [88, 86]. In their studies of symmetric and asymmetric top molecules, the time-independent Schrödinger equations are solved by

considering the symmetry properties. .

2.3.3 Impulsive regime

In 1999, the early period of researches on molecular alignment, it had been reported that impulsively applied strong-field-interaction can generate a rotational wave packets after the impulsive interaction, which allows molecular alignment in the field-free conditions [11, 16]. The impulsive nature of the excitation is brought when that the pulse is much shorter than the rotational period of the molecule. The impulsive "kick" transfers angular momentum to the molecules sets them into angular motions in the direction of the "kick" once field-free. Many theoretical descriptions to successfully deal with this regime have been reported.

One important fact we notice from many theoretical description is that the detailed shape of an applied short laser pulse is not important for entire dynamics of molecules. Only the temporally integrated value of interaction $\int f(t)dt$, the action, determine the rotational dynamics of the molecules rather than the detailed shape of the $f(t)$, which ensures the "time-dependent unitary transformation method" described in Chapter 3.

Chapter 3

Time-dependent unitary transformation method

We explain a useful numerical method in this chapter. Traditionally, rotational motion of molecule constrained by laser pulse with a few nanosecond of pulse width is considered adiabatic. However, in actual experimental conditions, purely adiabatic process does not take place and sometimes nonadiabatic effect plays important roles in determining the rotational dynamics of molecules [33, 32]. In order to appropriately describe such cases where interaction is neither impulsive nor purely adiabatic, we describe a numerical method based on time-dependent unitary transformation. With the method, we could significantly reduce calculation cost taking place when someone calculates rotational dynamics of molecules over a few nanoseconds or an even longer time.

3.1 Overview : intermediate regime and a numerical method

In many conceivable experimental conditions, even though an interaction induced by a few nanoseconds of laser pulse is close to the adiabatic regime, non-adiabatic effect can play a crucial role for the dynamics of molecules. For example, when the electrostatic field and the several nanoseconds of laser field linearly polarized and tilted with the electrostatic field are applied to the molecules, non-adiabatic transitions between eigenstates corresponding to the time-independent Hamiltonian significantly take place [33]. As a

result of the transitions, the experimental results are not successfully reproduced by the calculation assuming the adiabatic condition. Furthermore, in the molecular orientation by a two-color laser field, the non-adiabatic transitions between a pendular doublet - the pair of oppositely oriented and nearly degenerated states- take place[1]. Thus, to understand the rotational dynamics, an appropriate numerical method for describing the intermediate regime is required. It is the recent years that the intermediate regime, where the interaction is long compared to the rotational period of molecule but still not enough to ensure fully adibatic interaction, start to be studied [33, 87, 32]. Here we introduce our effective and successful method to obtain a numerical solution for the intermediate regime.

Our approach have been motivated from the several previous numerical results illustrating that in the impulsive regime where pulse width of laser field is much shorter than rotational period of molecule, energy fluence of laser pulse rather than the detailed shape of the pulse is an important quantity in determining rotational motion of molecules. Accordingly, we can flexibly transform the shape of the pulse into a shape in order to deal with the regime more straightforwardly. We approximate a shape of impulsive laser pulse as a "square shaped laser pulse". Time dependent schrödinger equation for rotational motion of molecule exposed to "square shaped laser pulses", even though which is not a realistic form, can be accurately calculated by solving time-independent Shrödinger equation. For concrete descriptions, we give several examples.

3.1.1 Example 1 : Impulsive orientation

First, we start the discussion from the impulsive regime. Let us consider a linear molecule irradiated with a linearly polarized HCP (Half Cycle Pulse). The TDSE for the rotational motion of the rigid rotor is given by,

$$i\hbar\frac{d}{dt}\psi(t) = [B\hat{J}^2 - \mu E(t)\cos\theta]\psi(t). \tag{3.1}$$

Here, we use the impulsive interaction Hamiltonian whose temporal changes are expressed by instantaneous jumping as it is shown in figure 3.1 and equation 3.2.

[1]This subject is discussed in Chapter 7.

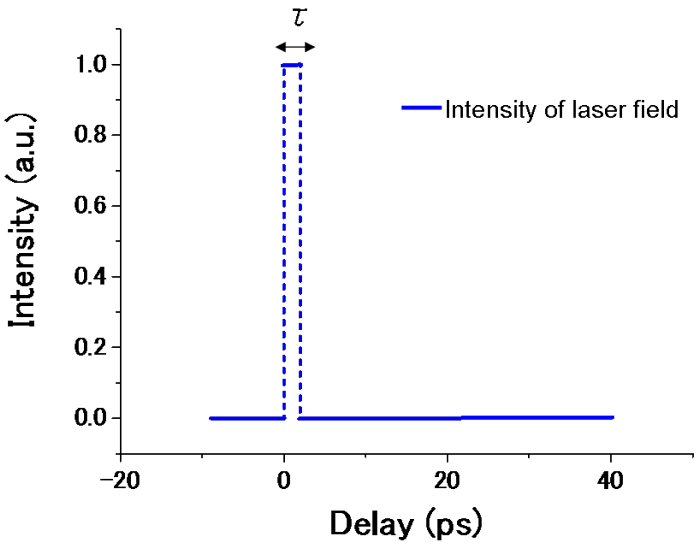

Figure 3.1: The temporal shape of an impulsive HCP laser pulse used in the calculation.

$$\mu E(t) = \begin{cases} \mu E_0, \ (0 < t < \tau) \\ 0, \ (\text{otherwise}) \end{cases} \tag{3.2}$$

The analytic solution of equation 3.1 for a wave function $\psi(t)$ is obvious.

$$\psi(t) = \begin{cases} \exp(\frac{-i}{\hbar}(B\hat{J}^2)(t-t_0)) \cdot \psi(t_0) \\ , (t <= 0) \\ \exp(\frac{-i}{\hbar}(B\hat{J}^2 - \mu E_0 \cos\theta)(t)) \cdot \psi(0) \\ , (0 <= t <= \tau) \\ \exp(\frac{-i}{\hbar}(B\hat{J}^2)(t-\tau)) \cdot \psi(\tau) \\ , (t >= \tau). \end{cases} \tag{3.3}$$

When $t < 0$, the initial field-free state is preserved since it is a eigenstate of the field-free Hamiltonian. The absolute phase factor is not important here. The coherent wave-packet generated by the field-induced interaction can be expressed as $\exp(\frac{-i}{\hbar}(B\hat{J}^2 - \mu E_0 \cos\theta)(t)) \cdot \psi(0)$ and $\exp(\frac{-i}{\hbar}(B\hat{J}^2)(t-\tau)) \cdot \psi(\tau)$, when the field is being applied $(0 < t < \tau)$ and after the field has been applied

($\tau < t$), respectively. Since the Hamiltonian H is time-dependent only by the instantaneous jumping, the time dependent equation come to a set of time-independent equations associated to each other, which allows us to express the temporal rotational state of a molecule by

$$\psi(t) = \begin{cases} U \cdot \exp(\frac{-i}{\hbar} \cdot H_{\text{diagonal}} \cdot (t))\hat{U}^{+} \cdot \psi(0) \\ (0 <= t <= \tau) \\ \exp(\frac{-i}{\hbar}(B\hat{J}^2)(t-\tau))\psi(\tau) \\ (t >= \tau). \end{cases} \tag{3.4}$$

In the (5), U is the unitary matrix diagonalizing the field-dressed Hamiltonian, and the corresponding diagonalized matrix is $H_{\text{diagonal}} \equiv \hat{U}^{+} \cdot (B\hat{J}^2 - \mu E_0 \cos\theta) \cdot \hat{U}$ whose elements are eigenenergies of the field-dressed Hamiltonian.

When the external field is applied instantaneously at $t = 0$, initial field-free state is expanded by eigenstates of field-dressed Hamiltonian, then, the each eigenstates experience phase-shifts according to the eigenenergies of the field-dressed Hamiltonian. Finally, the phase-shift attributes to a formation of wave-packet after it is transformed back into the field-free basis by operating the U^{+} at $t = \tau$.

When the interaction time scale characterized by τ is short enough compared to the rotational period molecule, the field-free rotational term $B\hat{J}^2$ involved in the field-dressed Hamiltonian could be neglected. Then the solution has the same form attained from the impulsive model.

Here we introduce results obtained by our approach to compare it with that from the impulsive model 3.2. Obviously, our result is consistent with that from the previously reported study [56]. As we describe in the subsection "impulsive limit" in Chapter 2, the fluence of a laser pulse is an important parameter rather than the shape of laser pulse if the pulse width is much shorter than the rotational period of molecule.

By contrast, it is a different point between the two models that, while the operator at the impulsive model [56] does not involve rotational term during the field-molecule interaction, present approach takes into account the phase-shift from not only interaction term but also free rotational term during the interaction, which allows us to apply our model for the case where much longer laser pulse are used.

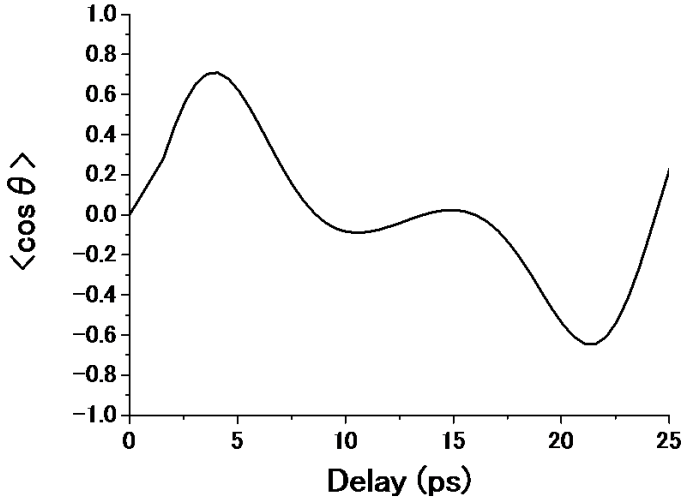

Figure 3.2: $< \cos\theta >$ as a function of time for rotational ground state of $^{7}Li^{35}Cl$ molecule who irradiated with the square shaped laser pulse. The $E_0 = 150$kV/cm and $\tau = \pi/2$ ps. Other constants used in the calculation like the permanent dipole and the rotational constant of the molecule are from Ref. [13].

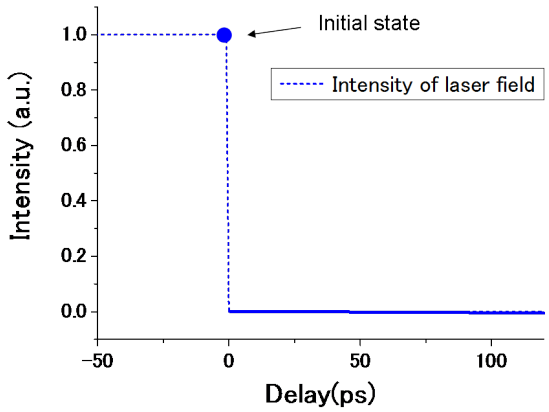

Figure 3.3: Scheme of a model for numerical simulations. The eigenstates of field-dressed Hamiltonian at t=0 are employed as initial quantum states. We analize the time evolution of the initial state after the rapid falling of the laser field in the presenece of electrostatic field.

3.1.2 Example 2 : Pure adiabatic orientation followed by rapid turn off of the laser field

To demonstrate the validity of our method, as an example we introduce another set of results of calculations. Lets consider a molecule exposed to parallel electrostatic field and laser field tunred on slowly and turned off suddenly. The two basis sets representing eigenstates of the Hamiltonians right before the sudden change and after that are obtained by diagonalizing the corresponding Hamiltonians described below, where the two regimes are labeled as (a) and (b), respectively.

$$\begin{aligned} \hat{H}_a \psi_{a,i} &= E_{a,i} \psi_{a,i} \\ \hat{H}_b \psi_{b,i} &= E_{b,i} \psi_{b,i} \end{aligned} \tag{3.5}$$

By assumming that the molecule is controlled with a pure adiabatic process by the slow turn on (figure 3.3), the time evolutions after the sudden change of Hamiltonian from (a) to (b) of an initial eigenstate denoted by (i) can be described as

$$\psi_{a,i}\big(t_0+t\big)=\sum_m(<\psi_{b,m}||\psi_{a,i}>)\psi_{b,m}e^{-iE_{b,m}t}, \tag{3.6}$$

where t_0 represents the time of the rapid change. The field-dressed states, the eigenstates of the Hamiltonian (b), are used as a basis set for expanding the initial quantum state. Time evolution after the instantaneous change of the external field is determined by the phase relation between the field-dressed states.

Now, the above quantum state is expressed as a superposition of an appropriate basis set so that the expectation values of $\cos\theta$ and $\cos^2\theta$ can be calculated analytically.

$$\begin{aligned}\psi_{a,i}\big(t_0+t\big)&=\sum_m(<\psi_{b,m}||\psi_{a,i}>)\psi_{b,m}e^{-\mathrm{iE_{b,m}t}}\\&=\sum_{m,h,k,n}(<h|b_{m,h}a_{i,k}|k>)b_{m,n}|n>e^{-\mathrm{iE_{b,m}t}}\\&=\sum_{m,h,n}(b_{m,h}a_{i,h})b_{m,n}|n>e^{-\mathrm{iE_{b,m}t}}\\&=\sum_{m,n}(U_aU_b^T)_{i,m}b_{m,n}|n>e^{-\mathrm{iE_{b,m}t}}\end{aligned}$$

Here $|n>$ is an element vector of certain basis set such as Spherical harmonics. Then, the expectation value of an operator $\hat{O}$ and other operators such as $\cos\theta$ and $\cos^2\theta>$ are also calculated as a function of time as follows,

$$\begin{aligned}&<\hat{O}>(t)\\&=\sum_{m,m',n,n'}(U_a{U_b}^T)_{i,m}(U_a{U_b}^T)_{i,m'}b_{m,n}b_{m',n'}\\&\qquad<n|\hat{O}|n'>e^{+\mathrm{iE_{b,m}t}}e^{-\mathrm{iE_{b,m'}t}}\end{aligned} \tag{3.7}$$

As another way to solve the regime, we can directly solve the TDSE. A TDSE shown below has been solved with Runge-Kutta Method and the results are compared 3.4. In the direct TDSE shown below, an initial condition

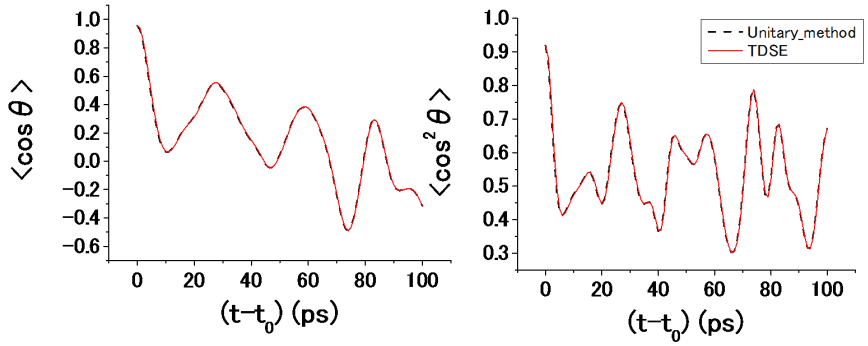

Figure 3.4: The temporal evolutions of $< \cos\theta >$(left) and $< \cos^2\theta >$(right) after the sudden change of Hamiltonian. The black lines and red lines show the results from the direct time dependent shrödinger equation and the method based on Unitary transformation, respectively. Initial state is a ground state of OCS molecule adiabatically controlled by 2×2^{12}W/cm^2 of laser field and 800V/cm of electrostatic field. The electrostatic field and 5percent of the initial field intensity are kept applied after the rapid truncation.

is employed as the eigenstate of the Hamiltonian just before the truncation. The falling time scale is set as 176.6 fs with half width at half maximum (HWHM). It have been confirmed that the results from the two different methods are consistent, which means that the 176.6 fs of finite falling time is short enough to do not affect the time evolution of the wave-packet generated from the sufficiently long interaction [34, 36] and our numerical model can be employed for the simulation. In other words, the 176.6 fs of impulsive half Gaussian pulse is too weak to influence the rotational dynamics of initial field-dressed eigenstates. On the other hand, this 176.6fs of impulsive interaction could not be neglected if we consider initial field-free states.

$$\psi_{a,i}(t_0+t) = \sum_n a_{i,n}|n>$$
$$i\hbar\dot{a}_{i,m}(t_0+t) =< m|\hat{H}_b|n > a_{i,n}(t_0+t) \tag{3.8}$$

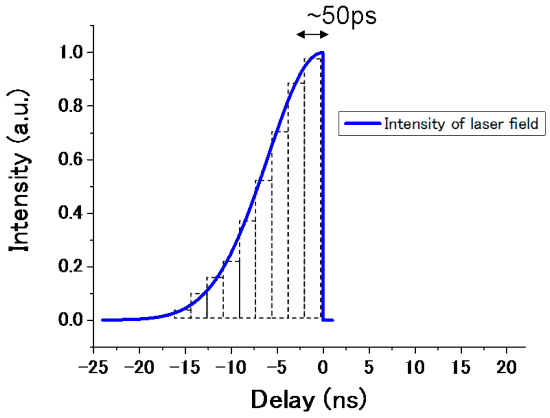

Figure 3.5: Scheme of a model for numerical simulations. We calculated TDSE by asumming that a long laser pulse is composed by sequentially lined square shaped short laser pulses.

3.1.3 Example 3 : Non-pure adiabatic orientation with a slow turning on of laser field

When we slove the intermediate regime with taking into account non-adiabatic effect, we assume that the applied nano second laser pulse is composed by sequentially lined impulsive pulses. The divided step width is set around 50∼100ps, which is enough to ensure accurate calculation. Because during the 50ps of time scale, the intensity of the several nano seconds of laser pulses are almost unchanged. We can successfully reproduce nonadiabatic effects reported in the references [32, 33] by this method.

3.1.4 Advantages of the numerical method

With our method, there are several advantages that we can obtain. First of all, calculation cost for solving time-dependent Schrödinger equation for rotational dynamics of molecules are significantly reduced. We solve the equation for rotational motion over a few nanosecond with a computation time 1000 times faster than that required when the equation is solved without the time-dependent unitary transformation method.

Secondly, all the interaction regimes such as the purely adiabatic, the impulsive, and the intermediate regimes can be calculated by single numerical

package. From a calculated rotational state at time t

$$\psi = \sum_{J,K,M} C_{J,K,M}(t)|J,K,M>, \tag{3.9}$$

the expectation value of an operators denoted O is given by

$$\sum_{(J,K,M)(J',K',M')} C(t)^{\star}_{J,K,M} C(t)'_{J',K',M'} < J,K,M|O|J',K',M' > . \tag{3.10}$$

The alignment parameter $< \cos^2\theta >$, the orientation parameter $< \cos\theta >$ and the other parameters can be evaluated in the same way. In the adiabatic condition, the expectation values can be obtained by following the Hellman-Feynman theorem and differentiating energy-shift by normalized strength of interaction.

Furthermore, since we can solve time-independent equations on individual steps independently to each other, parallel calculation is possible.

Author also expects that we can investigate recipe for making best field-free orientation of molecules by applying the present method to inverse problem.

Chapter 4

Experimental setup and techniques

We have used the plasma shutter technique for (laser-)field-free strong molecular orientation. The achievable degrees of orientation for an initial single rotational state are maximized when the interaction process takes place near the adiabatic limit, which motivated us to utilize the plasma-shutter technique. The shaped laser pulse to be slowly turned on and rapidly turned off by the plasma shutter allows the wave-packet (quasi-) adiabatically generated by the slow turn on to be transferred into the laser-field-free condition by the rapid turn off.

Besides, we have used molecular deflector for rotational state-selection of molecules. Considering the underlying physics of the molecular orientation, if a single rotational state is used as a molecular sample, a remarkably strong orientation is anticipated with the plasma shutter. However, in the thermal ensemble of molecules, many initial quantum-states tending to be oriented in opposite directions to each other exist together. Thus, as it had been reported earlier [38, 39], the state-selection technique by inhomogeneous electrostatic field can be utilized for the state-selection, leading to a strong molecular orientation.

This chapter is dedicated for describing the experiments and the technical methods employed. In the first section of this chapter, we describe experimental setup of the vacuum chamber including the molecular deflector for the state-selection and velocity map imaging spectrometer for observing the molecular alignment and orientation. Also, we describe a Monte-Carlo simulation for trajectories of molecules. In subsection 4.1.3, we summarize the

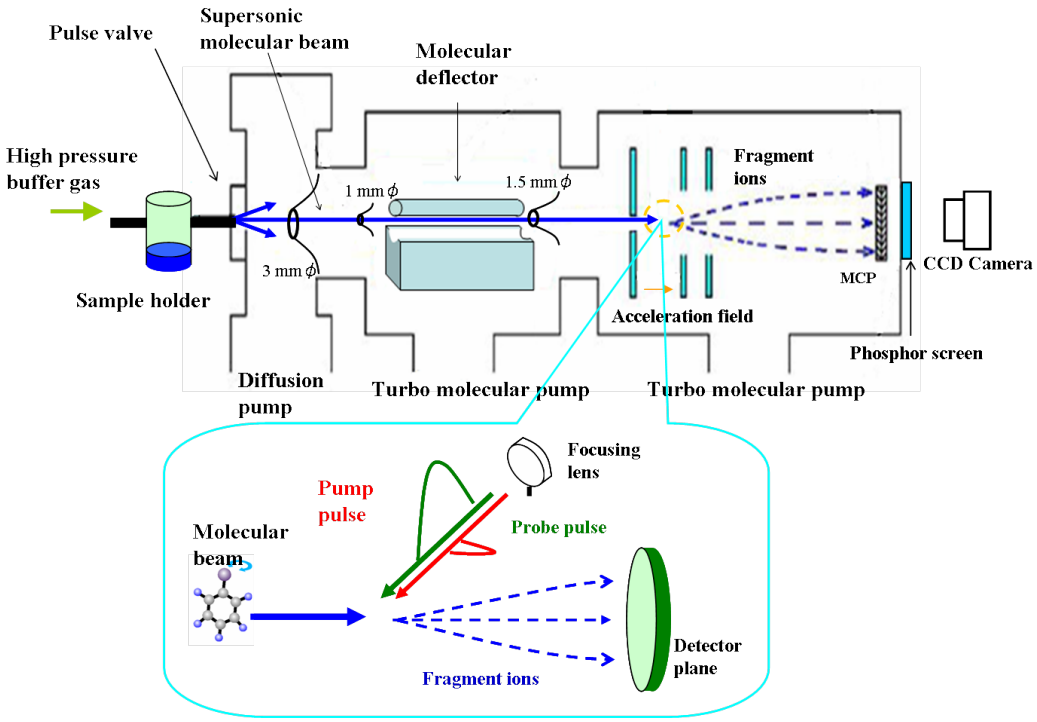

Figure 4.1: Schematic diagram of the experimental setup

results of state-selection of molecules. Experimental observations of vertical profile of OCS molecular samples are compared with the results of trajectory simulation. In the section 4.2, other important experimental setups and techniques associated with optics are given.

4.1 Setup of the vacuum chamber

4.1.1 Overview

We describe the experimental setup for preparing rotational-quantum-state-selected molecules and observing the angular confinement of the molecules. The apparatus consists of three vacuum chambers the source chamber, the deflector chamber, and the detection chamber which are pumped separately.

In the source chamber, the molecules optimally cooled by an Even-Lavie valve with a high stagnation pressure are collimated by a 3 mm-diam skim-

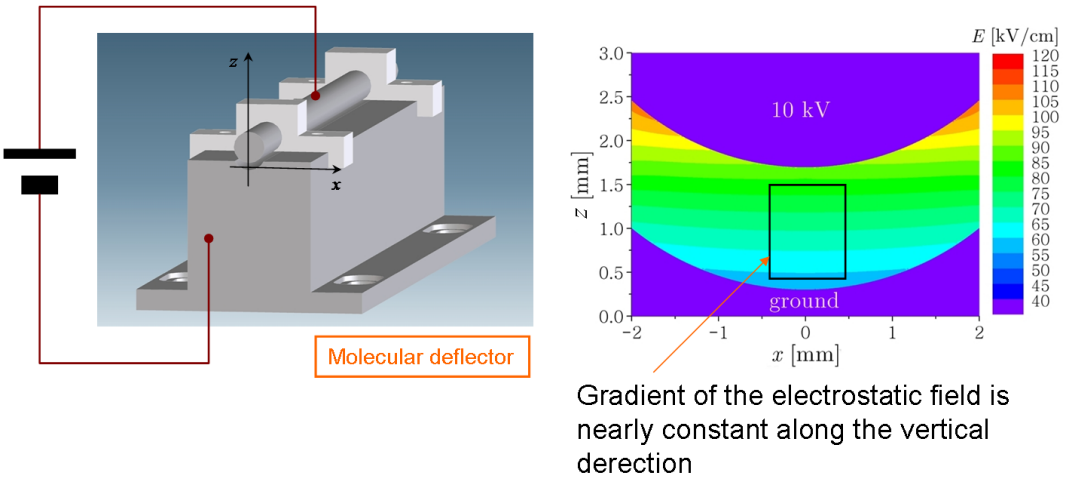

Figure 4.2: The deflector electrodes ([75])

mer located in front of the deflector chamber. Molecules escaping through the orifice of the valve collide frequently with the carrier gas, and adiabatic cooling of all degrees of freedom takes place in the expansion region [78]. By passing through the skimmer, a cold and well-collimated supersonic molecular beam is produced [77].

The supersonic molecular beam genertated in the source chamber is collimated again by a 1.0 mm-diam skimmer located near the entrance of the molecular deflector. After passing through the skimmer, molecular beam enters a strong inhomogeneous electric field created by a 15 cm-long molecular deflector. The deflector electrodes create a two-wire field [80, 81, 39, 79]. (The schematic diagram of the molecular deflector and the created two-wire field are shown in Fig.4.2 (right)). While the electric field is very homogeneous along the horizontal direction, the gradient of the electric field along the vertical direction is large and nearly constant over a large area where molecules pass through. Thus, the vertical gradient of the electrostatic field forces each rotational quantum state to be deflected vertically according to its Stark-energy-dependence on the field strength. In our setup, a high voltage is applied to the rod, while the another electrode is grounded for deflecting high-field-seeking quantum states upward. The deflected molecular beam enters a detection chamber through another 1.5 mm-diam skimmer placed near the exit of the molecular deflector.

In the detection area, the molecular beam is irradiated with pump and

probe pulses at right angles by a focusing lens with the focal length of 300 mm. The focusing lens is set on a vertical translational stage to selectively irradiate the laser pulses on a position of the deflected molecular beam. When we measure the vertical profile of molecular beam to observe its deflection, we move probe pulse to ionize the molecules and record intensities of the produced fragment ions as a function of the vertical position of the translational stage.

In the experiment of molecular orientation, the rotationally controlled molecules by the pump pulse are also ionized by the probe pulse. Some of the ionized molecules are divided into fragment ions via the Coulomb explosion process. Since the ionization and the subsequent Coulomb explosion processes take place in a very short time scale compared to that of the rotational motion of molecules, we can measure the degrees of alignment and orientation of the controlled molecules by observing the velocity distribution of the fragment ions. The velocity distributions of the fragment ions are observed by applying an appropriate set of voltages to the electrodes of the TOF mass spectrometer, which serve as the electrostatic lens for ions [83, 84]. When a particular condition is met for the extractor/repeller ratio, the fragment ions with the same initial velocity component perpendicular to the TOF axis reach the same point on the MCP, irrespective of the initial position of the fragment ions. A detection system which consists of an MCP backed by a phosphor screen and a CCD camera placed behind the phosphor screen serves as a position-sensitive detector. For selectively observing the target fragment ions, a gate voltage is applied to the MCP at the arrival time of the target ions. As an appropriate voltage ratio of the present experiment, 4 kV is applied to the extractor and 6 kV to the repeller. Figure 4.3 shows typical images of the velocity distributions of the fragment ions.

4.1.2 Monte-Carlo simulation for trajectories of molecules

As we described in the preceding subsection, polar molecule traveling through the molecular deflector experience force depending on the rotational-quantum-state and the electric field strength generated by the deflector. We performed a Monte-Carlo simulation to investigate the trajectories of individual initial quantum states and to estimate the distribution of quantum states in the spatially deflected molecular beam.

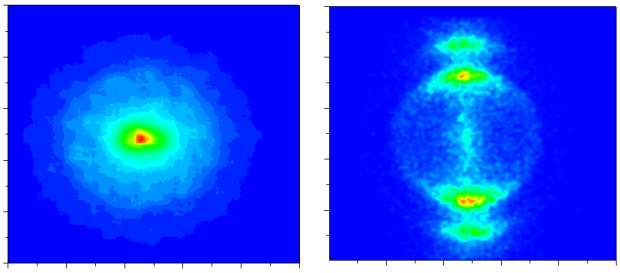

Figure 4.3: Typical images with (left) and without (right) the pump pulses.

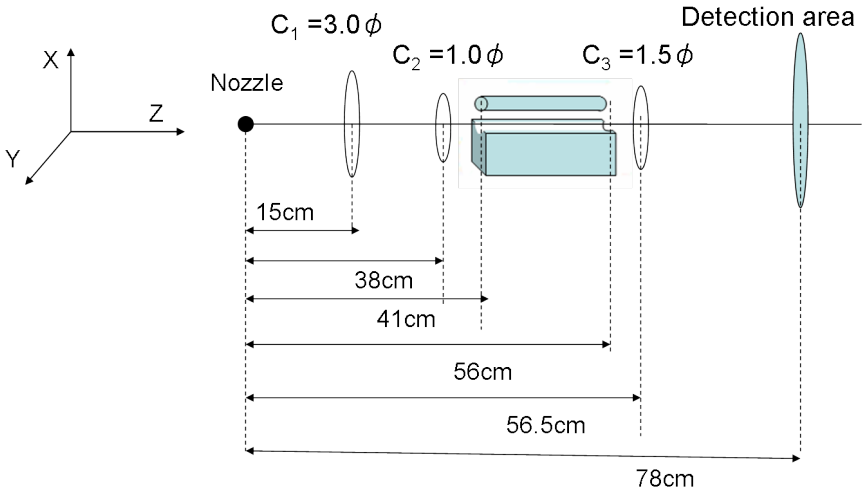

Figure 4.4: Geometry of the apparatus involved in the trajectory simulation

Initial velocities and positions of an individual rotational state following Gaussian distribution are generated by the Von Neumann's algorithm. For the mean value of the initial velocity of Z-component, we use a value estimated by our experimental observation. We set the half width at half maximums of the velocity coordinates as 1 percent and 0.1 percent of the mean velocity for Z and XY components, respectively. Then, with the three-dimensional equation of motion, a given particle (molecule) is propagated through the chamber. All mechanical apertures and electrodes of the experimental setup are included in the simulation (Fig. 4.1.2).

When the molecule is outside of the molecular deflector, there is no acceleration field, while inside the molecular deflector a force that a molecule experiences F is given by

$$F = -\nabla W_{\mathrm{Stark}} = -\frac{d}{dE} W_{\mathrm{Stark}} \sum_i \frac{\partial}{\partial x_i} E. \tag{4.1}$$

The Stark energies W_{Stark} of quantum states exposed to an electrostatic field E are obtained by solving the time-independent Schrödinger equation. Moreover, to obtain electric field strength and the its gradients as function of the XY positions, we employed the finite element method. We assume that the electric field is homogeneous along the Z coordinate.

At the detection area of the simulation, we recorded the number of particles as a function of the vertical position X. The obtained vertical profiles of individual quantum states are summed up by taking into account of the Boltzmann distribution.

Results of the trajectory simulations are summarized along with the experimental results in the next section.

4.1.3 Result of the state-selection

Isolating a single quantum state or a small set of states from other quantum states is very beneficial for a large range of experiments of molecules. For example, different conformers of a molecule that often easily be interconverted under thermal condition can be spatially separated by using inhomogeneous electric fields and the conformer-specific effects in chemical reaction can be investigated [61]. Also, the selected single rotational state of molecule provides an unique opportunity to achieve the highest degree of orientation.

In our experiment, the home-built molecular deflector is utilized for the initial rotational-quantum-state-selection of molecules. We have measured

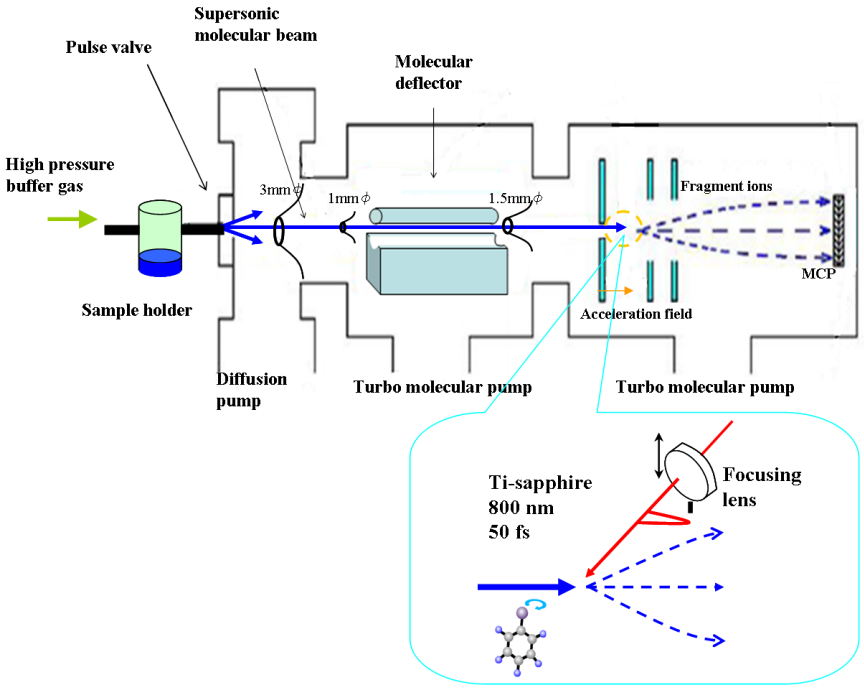

Figure 4.5: Schematic diagram of the experimental setup. We observe vertical intensity profiles of the molecular beam by recording the signal of ions generated by femtosecond probe pulse as a function of the vertical position of the laser focus.

the vertical intensity profile of the deflected molecular beams by recording intensity of the fragment ions as a function of the vertical position of the translational stage on which the focusing lens mount (Fig 4.5). Although higher applied voltages sometimes (not always) are desirable for more effective state selection, for avoiding discharge between the electrodes and other parts in the vacuum chamber, voltages up to 8 kV are applied to the electrode of the molecular deflector in our experiments. .

We show the observations of the vertical spatial profiles of the molecular beams used in our experiments and the corresponding results of trajectory simulations.

Iodobenzene molecule

As a large asymmetric top molecule, iodobenzene molecule have employed in our experiments. The vertical intensity profiles are measured by recording the signal of I^+ ions, generated by irradiating the femto second probe pulse. Fig. 4.6 shows the measured vertical profile of IB molecule buffered by 60-bar of He. The data shown in Fig. 4.6 (a) is measured in the early stage from the development of the deflector in the our laboratory, while the data shown (b) is obtained recently and we could applied much higher voltage of 7kV to the deflector owing to several trial-and-errors.

When the deflector is turned off, the molecular beam extends over 1.5mm, mainly determined by the geometry inside of the chamber. By turning on the deflector, the molecular beam profiles shift toward upper (plus) region. This indicates that most of the quantum states are high field seeking in our experimental condition. Fig. 4.7 shows the calculated Stark-energy-curves of several rotational states of IB molecule. Because the rotational states are closely distributed in energies, the Stark-energy-curves show a large number of crossings among them. Because the curves of rotational states in a same symmetry condition show avoided-crossing [86], the energy order of the initial states in the same symmetry are preserved. Consequently, low-lying quantum states tend to be high field seeking states, and the ground state experience the strongest acceleration by the electrostatic field.

According to the other group's trajectory simulation, the state-selected molecules still involve a large number of quantum states [38, 39]. Thereby, it is not practical to observe quantum-state-specific effects in the experiments. However, because the the state-selected molecular sample have a narrower state distribution and mainly consists of the lower-lying quantum states, we

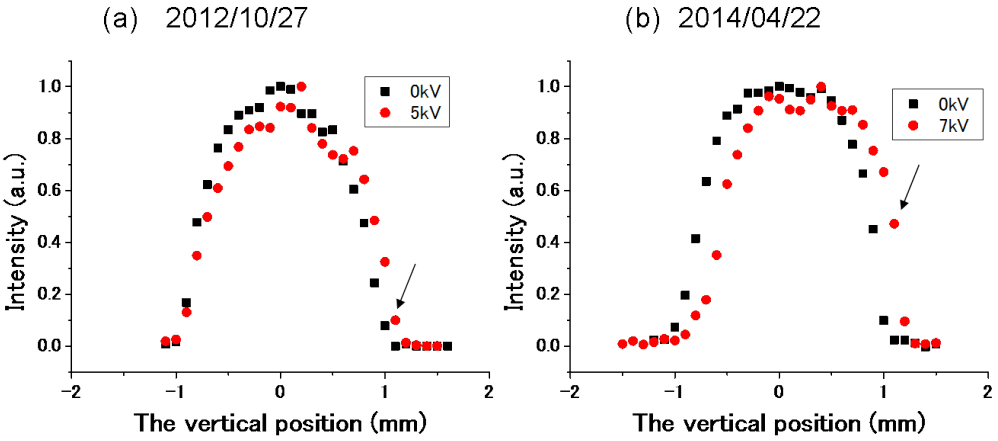

Figure 4.6: The vertical profiles of the molecular beam. The experimental data are shown by black circles (deflector off) and red squares (deflector on). The molecular sample was seeded in 60 bar of He buffer gas

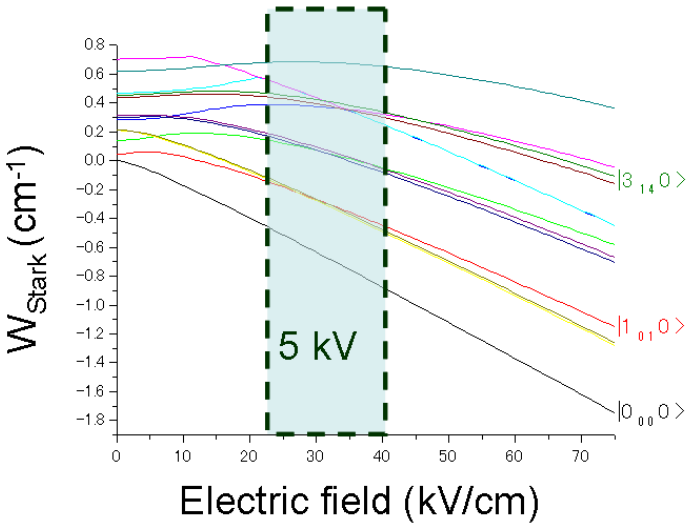

Figure 4.7: At the electrostatic field strengths present in the deflector, all low-lying quantum states are high-field seeking.

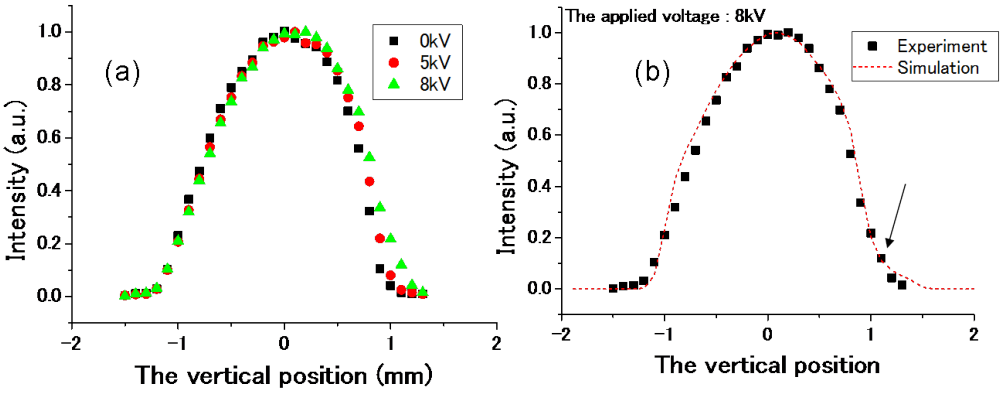

Figure 4.8: The vertical profiles of the OCS molecular beam. The experimental data are shown by black circles (deflector off) and colored squares (deflector on). The molecular sample was seeded in 50 bar of He buffer gas

can achieved higher degrees of alignment and orientation with the state-selected molecules.

We employed the molecules in the region indicated by the black arrows as rotational-state-selected samples. The state-selected sample in the figure 4.6 (a) is used in the experiment introduced in the Chapter 5 and the sample in the figure 4.6 (b) is used in the experiment of Chapter 7.

OCS molecule

OCS molecules have been state-selected by the molecular deflector. We measure the vertical profile of the OCS molecule by recording the signal of OCS^+, while we employ the S^+ fragment ions to observe the molecular alignment and orientation in the Chapter 7.

Fig. 4.8 shows the measured vertical profiles. The Fig. 4.8 (a) is the result with a sample which consists of 5mbar of OCS and 50-bar of He buffer gas. To make this molecular sample, we mixed a gas composed by 95 percent of He and 5 percent of OCS with a pure He gas appropriately. By turning on the deflector, the molecular beam profiles shift toward upper (plus) region. Similarly with the result from the IB molecule, the molecular beam extends over 1.5mm when the deflector is turned off. However, the spatial shift raised by the turning on of the deflector is much weaker than that of the IB molecule.

In order to estimate the rotational state distribution in a portion of the deflected molecular beam, we have performed the trajectory calculation that is described the former section. From the delay between the arrival of a probe pulse and the operation of the high-pressure-pulsed-valve, we estimate the central velocities of the molecular beam as 1350 m/s. The trajectory simulations are performed for each individual quantum state. And the obtained individual results are averaged according to the Boltzman distribution with a rotational temperature which is optimized to make the result consistent with the experiment. Fig. 4.8 (b) shows vertical profile obtained from the simulation with the experimental result. The rotational temperature used for the summing up is 4K. In the position upper than 1.0mm, more than 80 percent of the particles are composed by $|0,0>$ and $|1,\pm1>$ states.

There remains much uncertainty in estimating the rotational distribution from the trajectory simulation because the deflection of the molecular beam is not distinct. In fact, the estimated ratio between the two states $|0,0>$ and $|1,\pm1>$ in the state-selected molecules are considerably different depend on the precise vertical position. However, undoubtedly, the most deflected portion of the molecular beam consists of a lot of ground states as we can expect from the Stark energy curve of the OCS molecule, which is shown in figure 4.9.

The molecules in the region indicated by the black arrows in the figure are used as a rotational-state-selected sample in experiment of Chapter 7.

4.2 Optical arrangement

4.2.1 Overview

A schematic diagram of the optical arrangement is shown in figure 4.10. A femto-second laser pulse is divided into two parts, a trigger pulse which generates the plasma on the jet sheet of ethylene glycol and a probe pulse for observing the molecular orientation. The pump pulse is supplied by a 1064nm of pulse with a 6∼7 ns of HWHM. And a 532nm of the second harmonic pulse with a 3∼3.5 ns of that[1].

The plasma shutter operates in a following manner. The pump pulse are focused near the jet-sheet collinearly with the trigger pulse via an achromatic

[1]In the experiment with orientation with combined electrostatic and nonresonant laser fields, only the fundamental laser pulse is used.

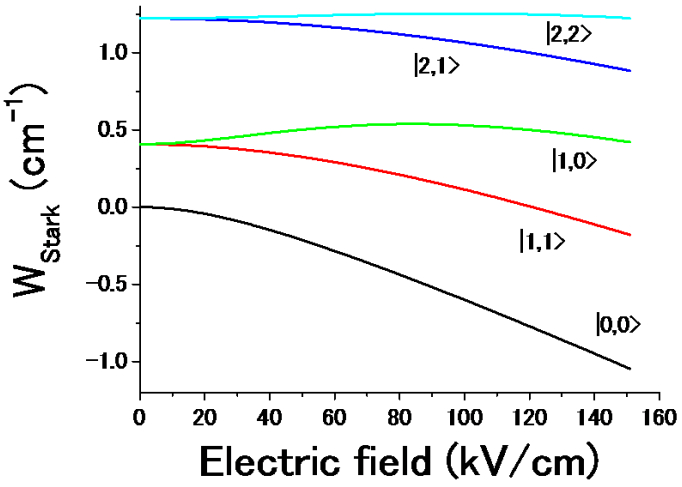

Figure 4.9: Stark-energy-curves of several low-lying rotational states of OCS molecule.

lens of f=700mm[2]. The trigger pulse is temporally synchronized to arrive at the jet sheet when the first half of the pump pulse has passed so that the second half of the pulse is truncated on the jet-sheet.

The shaped pump pulses by the plasma shutter then pass through a fused-silica which make the relative-phase between the ω and 2ω pulses variable.

A set of beam expander for optimizing the focusing point of pump pulse is preceded by a dichroic mirror on which the pump and the probe pulses are combined collinearly.

4.2.2 Shaping a laser pulse with a slow turn on and a rapid turn off

The experimental technique

The rapid truncation of the 12-ns-long laser pulses is performed with the optical arrangement shown in Fig 4.10. The 12-ns-long pulse, the target (pump) pulse, is copropagated with a portion of the femtosecond pulse, the trigger

[2]The lens of f=700mm is used for experiments with two-color laser field, while a lens of f=500 is used for the one-color laser field experiments.

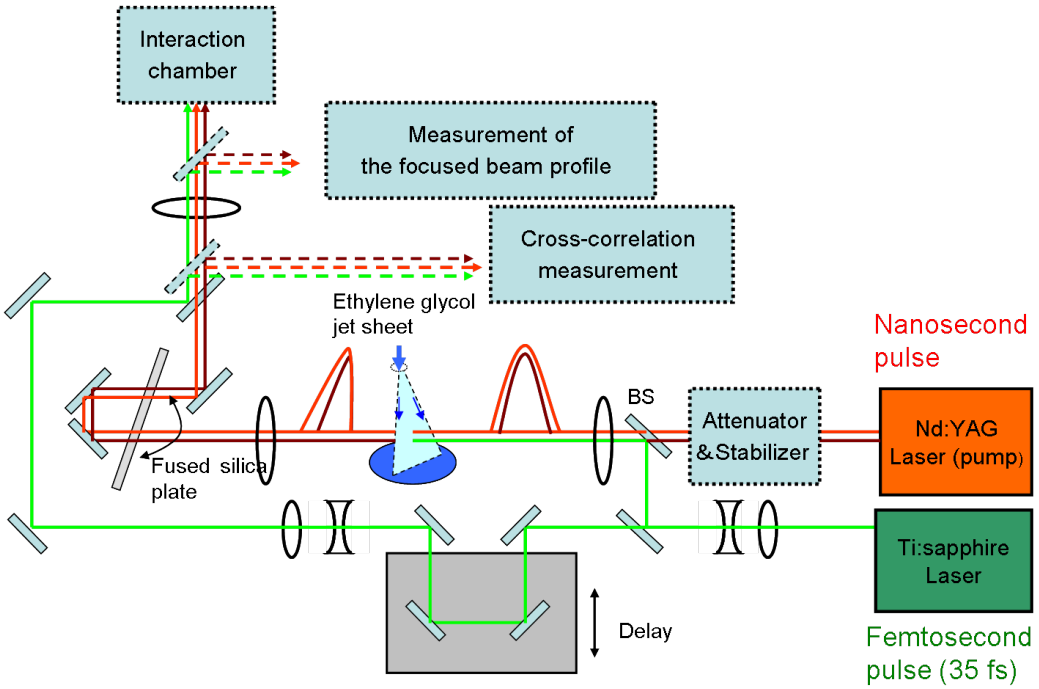

Figure 4.10: Schematic diagram of the optical arrangement

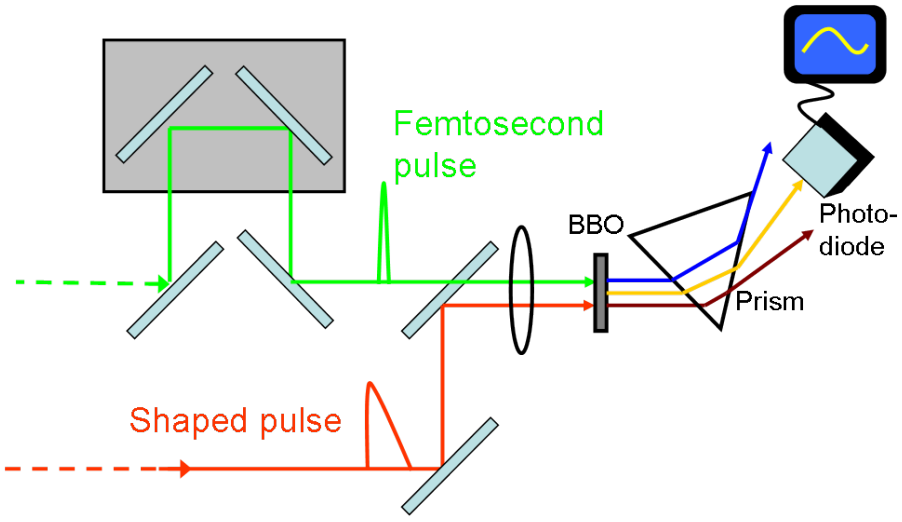

Figure 4.11: Schematic diagram of the experimental setup for the cross-correlation measurement.

pulse for the rapid plasma excitation. The peak intensity of the focused trigger pulse is kept well above the threshold of the ionization intensity of the ethylene glycol, whereas that of the target pulse is kept below the threshold. On the ethylene glycol jet sheet, the beam diameter of the trigger pulse is kept larger than the target pulse so that a lot of part of the pulse is covered by the plasma as much as possible. These two beams are temporally centered with respect to each other; thus, after the plasma excitation by the trigger pulse, second half of the target pulse is rapidly truncated.

In the our experiments of plasma shutter, energy fluences absorbed by the plasma have been much higher than that in the pioneering work reported by another group [35]. We have truncated the second half of laser pulse with 10-40mJ of energy that is larger than that of the preceding experiment by more than one order of magnitude.

To achieve such a high energy plasma shutter operation, we have appropriately optimized the focused beam diameters of the laser pulses. First, the target pulse must be tightly focused at the liquid jet sheet to provide the enough energy to the plasma as it is shown in a numerical model shown next subsection. The plasma can be kept excited due to the energy offered by the target pulse after the plasma is driven by the trigger pulse at t=0. This mechanism allows the second half of the transmission of target pulse to be kept truncated. In contrast, the target pulse, at the same time, must not be focused too tightly. Even though the intensity of the target pulse is well below the threshold of the ionization, providing too much energy fluence to the plasma causes"dirty air" around the liquid jet sheet. A lot of vapor generated with the intense plasma shutter operation interacts with other target pulses arriving on the subsequent operations. The vapor around the jet sheet frequently causes the self-break-down even without the plasma generation by the trigger pulse. Furthermore, in the case of two-color pump pulse, the relative phase between the fundamental and its second harmonic laser pulses becomes unstable because of the vapor interacting with laser pulses.

Thus, to avoid the breakdown caused by the "dirty air" and to provide enough energy to generated plasma, we investigated good experimental condition for the stable plasma shutter operation. In the one-color laser field experiment, the focusing lens with f= 500 is employed and the plasma shutter have been operated for target pulses with $10 \sim$ 50mJ of energies. In the two-color laser field experiment, the focusing lens of f=700 is used to focus the target pulse in a much loose manner.

The temporal shape of the rapidly turned-off pulse is observed by measur-

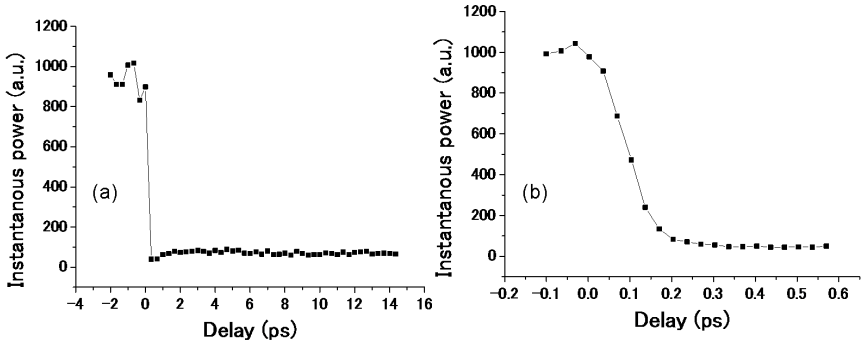

Figure 4.12: Results of the cross-correlation measurement. (a) and (b) shows the temporal shapes of the laser pulse near the rapid turn off for 15 ps and 0.5 ps, respectively.

ing the sum-frequency signals between the shaped pulse and another portion of the femto second pulse in a BBO crystal as illustrated in Fig. 4.11. Fig. 4.12 shows a result of cross-correlation. The fundamental one-color pulses are truncated with the falling time less than 200 fs. And about 5 percent of the peak power remains after the rapid truncation.

We note that while we measured the relative power (W) of the residual laser field by the cross-correlation measurement, it will not be well focused in the laser-molecule interaction region because the excited plasma also influences the focusability of the residual field. In Appendix, we show numerically that residual field intensity can be estimated by comparing numerical simulations and corresponding experimental observations of rotational dynamics of molecules.

A numerical model

Here, we show a numerical model for qualitative understanding of the plasma shutter.

In the studies on laser-induced damage in dielectrics, the number of electrons at time t is described by classical rate equation [63]. Although the condition on kinetics of electrons in the dielectrics is not the same as that in our experiment, we adopt a simplified equation for qualitative understanding of the plasma shutter operation in our experiment.

Only collision-induced ionization and the relaxation effects of free electrons are taken into account as two constants α and τ, respectively, whereas multiphoton ionization by the applied 12-ns-long laser field is neglected since intensity of the pulses are sufficiently low for the multi photon ionization.

The rate equation expressing the temporal evolution of the plasma (electron) density in the liquid jet sheet is,

$$\frac{d}{dt}N_e(t) = \alpha I(t)N_e(t) - N_e(t)/\tau, \tag{4.2}$$

where the constant $\tau \equiv$10 ps is typical average relaxation time of non-relativistic free electrons which is approximately consistent with experimental result in Fig 4.13 (b). The $\alpha = 0.009$ cm^2 ps^{-1}/GW , a coefficient proportional to the average collisional ionization rate, is determined by the balance between the electron density gain and loss rates in the calculation.

Also transmission rate is calculated with a model of driven harmonic oscillators. The refractive index is given by

$$n(t) = n_0 \times \sqrt{1 - N_e(t)/N_c}. \tag{4.3}$$

The electron density is assumed to be spatially uniform.

Although there are unresolved details on the precise mechanism of the plasma generation process [64], an initial value $N(t = 0)$ is set as a density of free electrons formated by the trigger pulse. The initial density is estimated to be 5.0×10^{21}cm^{-3}, 5 times larger than the critical density N_c, and lower than typical density of molecule in liquid.

Fig. 4.13 (a) shows the obtained the transmission rate and the density of electrons. The time evolutions of electron density are so sensitively depend on the laser intensity in the numerical model, which does not necessarily correspond to our experimental observations. However, the numerical model can reproduce the experimentally observed increase of residual field power of laser pulse. Typical experimental results are shown in the right panel of Fig. 4.13(b). By raising the energy of the applied laser field, we can make the residual field are kept truncated as it is illustrated in the Fig. 4.13 (b).

4.2.3 Spatial overlapping of the pump and the probe pulses

The pump and probe laser pulses were combined by a dichroic mirror which reflects the probe pulse and transmits the pump laser pulses, then, the pump

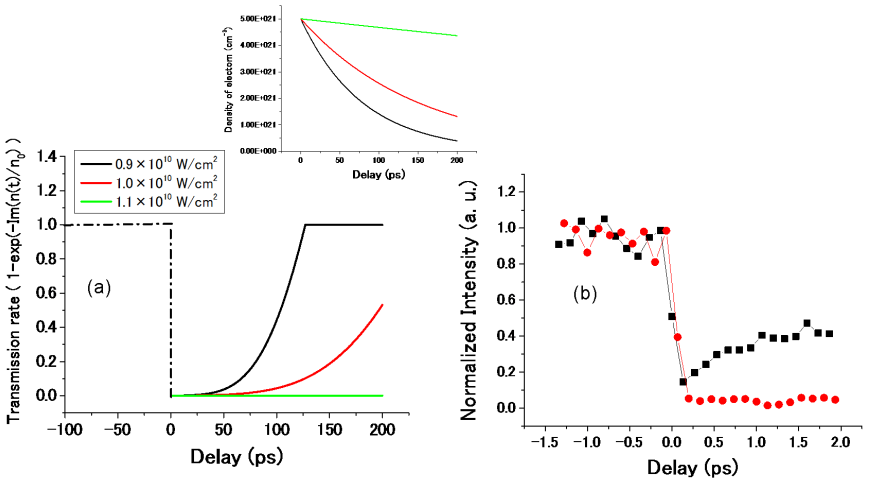

Figure 4.13: (Left) : Numerical result of transmission rates of uniform plasmas irradiated with laser pulses with different peak intensities. The inset shows the corresponding densities of electrons. (Right) : Experimental results of evolutions rate of the laser pulses. The rapid plasma excitations take place at the t=0.

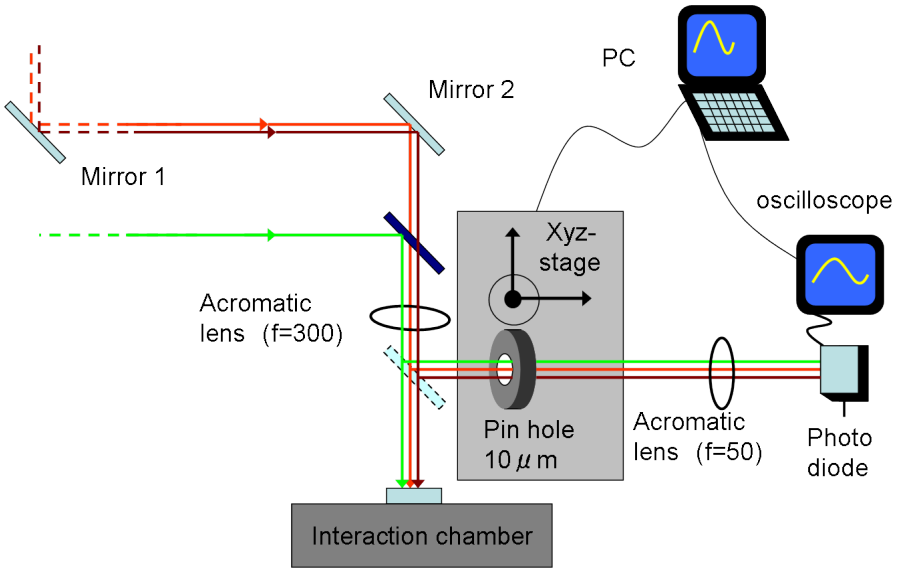

Figure 4.14: Schematic diagram of the experimental setup for the confirming the overlap between the two beams.

and the probe pulses are collinearly focused into the vacuum chamber via a achromatic lens.

We have observed the spatial overlap of the laser pulses with the set-up shown in the Fig. 4.14. We locate a 10-micron-diam pinhole mounted on a XYZ-stage to the focus of a portion of the probe pulse, which is reflected from a glass plate located before the interaction chamber. The laser pulses which passed through the pinhole are focused again into photodiode via a lens. Then, we plot the intensities of the pulses measured by the photodiode as a function of the two dimensional position of the stage.

Even though the fundamental and the second harmonic pump pulses are synchronized, we need to precisely overlap the fundamental and the second harmonic pump pulses precisely at the focus of the probe pulse. Thus, we used a normal fused silica lens instead of an achromatic lens as a later part of the beam-expander for pump pulse. Then, we optimized the position of the lens so that the two laser pulses are well overlapped. Then, the two pump and probe pulses are very precisely overlapped again at the focus of the probe pulse by adjusting two sterring mirrors for the pump pulses.

Fig. 4.15 shows a typical result of the observation of the two dimensional spatial overlap at the focus of probe pulse. We need to keep radius of pump pulses to be larger than that of probe pulse to primarily probe molecules exposed to the stronger pump laser field. To do so, we have intentionally displaced the focus of the pump pulses from that of the probe pulse by about 1mm.

4.2.4 Controlling the relative phase of the two-color laser pulse

The interaction Hamiltonian induced by the two-color laser field can be given by,

$$\begin{aligned} H_{\mathrm{two-color}} = & \\ -\frac{1}{4}[E_\omega(t)^2 + E_{2\omega}(t)^2](\alpha_\parallel - \alpha_\perp)\cos^2\theta & \\ -\frac{1}{8}[\cos\phi E_\omega(t)^2 E_{2\omega}(t)][(\beta_\parallel - 3\beta_\perp)\cos^3\theta + 3\beta_\perp\cos\theta]. & \end{aligned} \tag{4.4}$$

Since the term raising the orientation is proportional to $\cos\phi$, it is important to control the relative phase ϕ to maximize the $\cos\phi$. We locate a fused silica

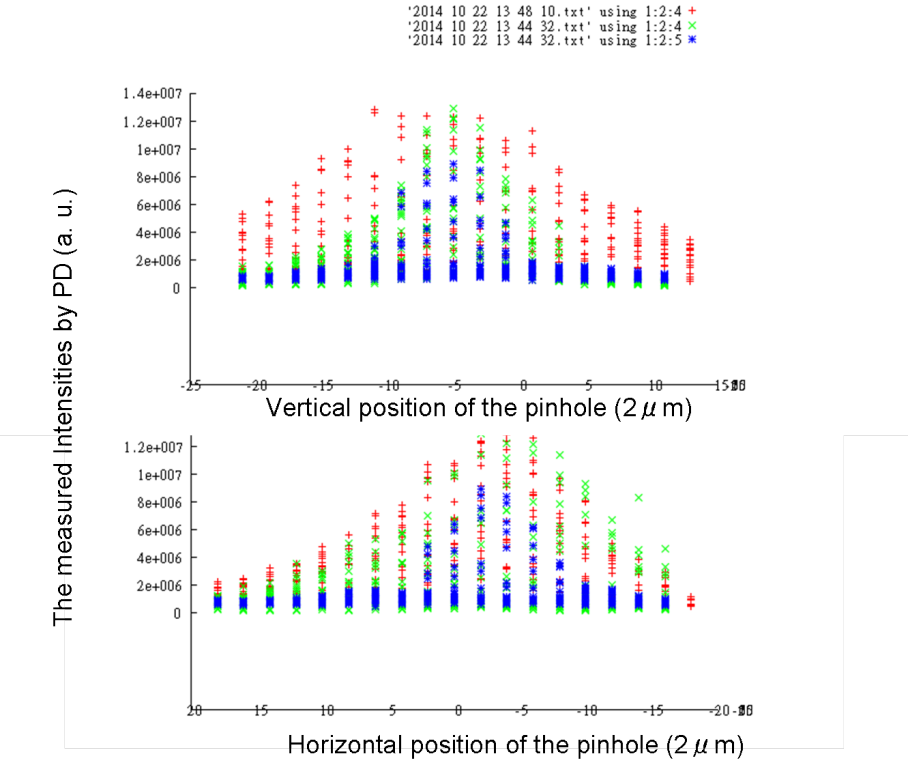

Figure 4.15: Typical result of a spatial overlap of laser pulses. Upper and lower panels, respectively, show the vertical and horizontal views of a two-dimensional state of the overlap. The red and green represent the ω and the 2ω, respectively, while the blue represents the probe laser pulse.

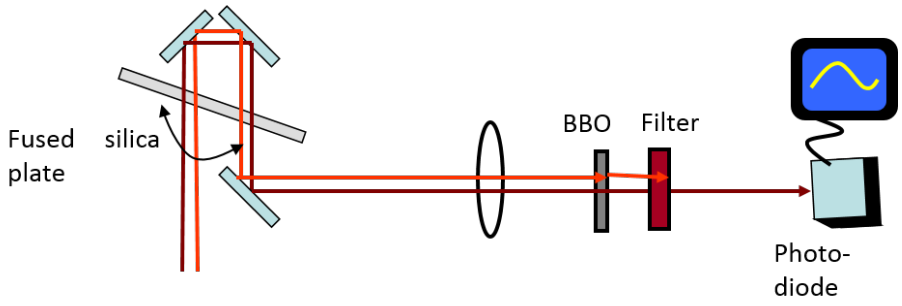

Figure 4.16: Schematic diagram of setup for observing the change of the relative phase between the ω and 2ω.

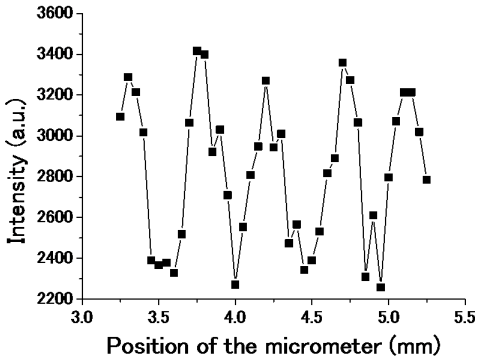

Figure 4.17: Schematic diagram of setup for observing the change of the relative phase between the ω and 2ω.

plate with 5 mm of thickness in the path of the two-color laser pulse with the 45 degrees of the incident angle. In our experiment, the glass plate is mounted on a gimbal mirror holder driven by two independent micrometers. Taking into account the displacement of path of laser pulses caused when they pass the fused silica plate, the laser pulses pass through the fused silica plate twice as shown in Fig. 4.10 and 4.16 in order to compensate the displacement. The relative phase between the two laser pulses is adjustable by rotating the fused silica plate. We measured the change of the relative phase with the setup illustrated in Fig. 4.16.

The ω and 2ω laser pulses are collinearly focused into BBO crystal in a collinear manner and we measured the intensity of the 2ω after the laser pulses passed through the crystal. The observed sum-signal of the original and the generated 2ω from the BBO crystal is plotted as a function of the position of micrometer of the holder on which the fused silica plate is mounted (Fig. 4.17). The observed modulation is used for evaluating the relative phase between the ω and the 2ω in the experiment of molecular orientation.

Chapter 5

Results and discussions 1 : Laser-field-free orientation of asymmetric top molecules

We describe experimental results of the laser-field-free orientation of asymmetric-top molecules. Aligning and orienting asymmetric top molecules in the laser-field-free condition is much more difficult subject compared to that of other simpler molecules like linear and symmetric top molecules. To accomplish laser-field-free orientation of asymmetric top molecules, we employed plasma shutter technique. Both thermal ensemble molecules and state-selected molecules by the molecular deflector are used as samples.

5.1 Quasi-adiabatic orientation of state-selected asymmetric top molecules by combined electrostatic and one-color laser fields

For a strong molecular orientation, rotationally cold iodobenzene molecules generated by the high-pressure buffer gas are deflected and used as a sample [85]. Both the rotationally cooled thermal ensemble and the further state-selected molecules are oriented by combined electrostatic and non-resonant one-color laser fields.

As shown in Fig. 5.1(a), when we observe molecular alignment, the polarizations of the pump and probe pulses are set parallel and perpendicular

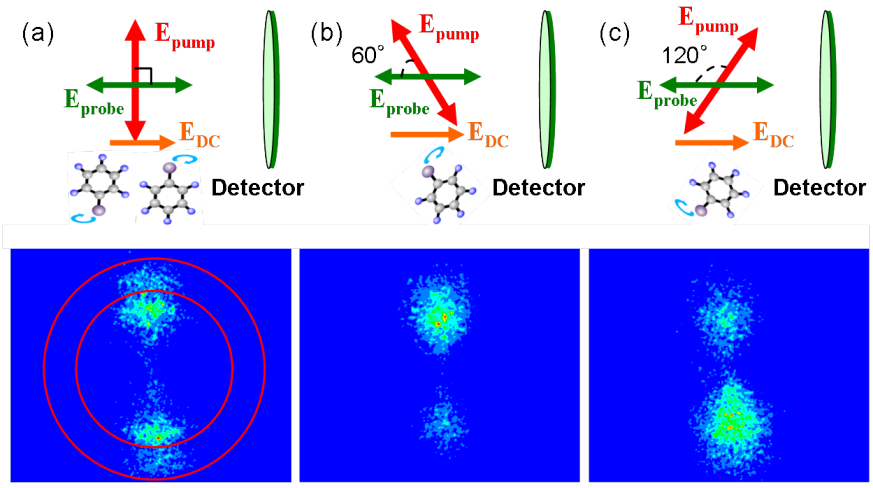

Figure 5.1: The observations of molecular alignment and orientation. (a) When observing alignment, the polarizations of the pump and probe pulses are parallel and perpendicular to the detector plane, respectively. (b) and (c) When observing orientation, the polarization of the pump pulse is tilted 60 or 120 degrees from the time of flight axis to utilize the combined effect of the electrostatic and the pump laser fields, while the probe polarization is perpendicular to the detector plane. In (a)-(c), also included are the ion images for molecular alignment and orientation observed with a sample of state-selected molecules. Reproduced from Ref.[65].

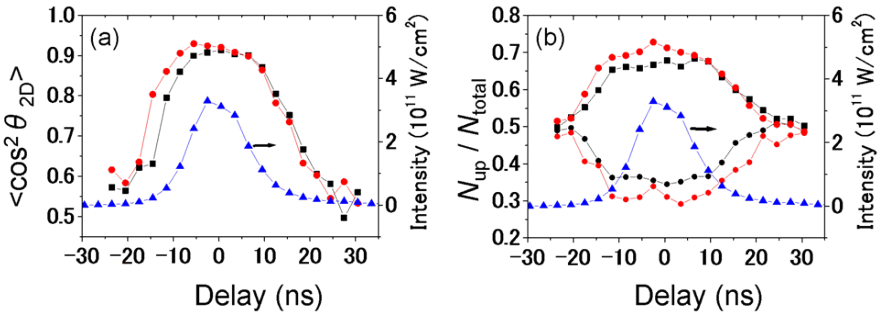

Figure 5.2: The temporal evolutions of the degrees of alignment (a) and orientation (b) for the thermal ensemble (black squares) and the state-selected molecules (red circles) during the pump pulse (blue triangles) with the peak intensity of 3.3 x 10^{11} W/cm^2. Reproduced from Ref.[65].

to the detector plane. The degree of alignment is evaluated by $<\cos^2\theta_{2D}>$, where θ_{2D} is the polar angle between the pump pulse polarization and the molecular axis projected onto the detector plane. When evaluating $<\cos^2\theta_{2D}>$, the I^+ ions observed between the concentric rings in Fig. 5.1(a), which originate from the Coulomb explosion process $C_6H_5I + N\hbar\omega \rightarrow C_6H_5I^{3+} \rightarrow C_6H_5{}^{2+} + I^+$, are used [38, 10].

As shown in Figs. 5.1(b) and 1(c), when we observe molecular orientation, the polarization of the pump pulse is tilted 60 or 120 degrees to utilize the combined effect of the electrostatic and the pump laser fields, while the probe polarization is remained perpendicular to the detector plane. The electrostatic field, which is originally the acceleration field of the velocity-map imaging spectrometer, is 2.4 kV/cm. The degree of orientation is characterized by the ratio N_{up}/N_{total}, where N_{up} is the number of the fragment ions observed in the upper half of the ion image and N_{total} is the total number of the fragment ions observed [38]. When the polarization of the pump pulse is tilted, the double-ring structure in the ion images gets blurred. We therefore employ all the I^+ ions in the images to evaluate N_{up}/N_{total}.

Figure 5.2 shows the temporal evolutions of the degrees of alignment (a) and orientation (b) for the thermal ensemble and the state-selected molecules during the pump pulse with the peak intensity of 3.3×10^{11} W/cm^2. Seemingly, they follow well the temporal profile of the pump pulse, suggesting that the laser-molecule interaction proceeds at least in the nearly adiabatic regime.

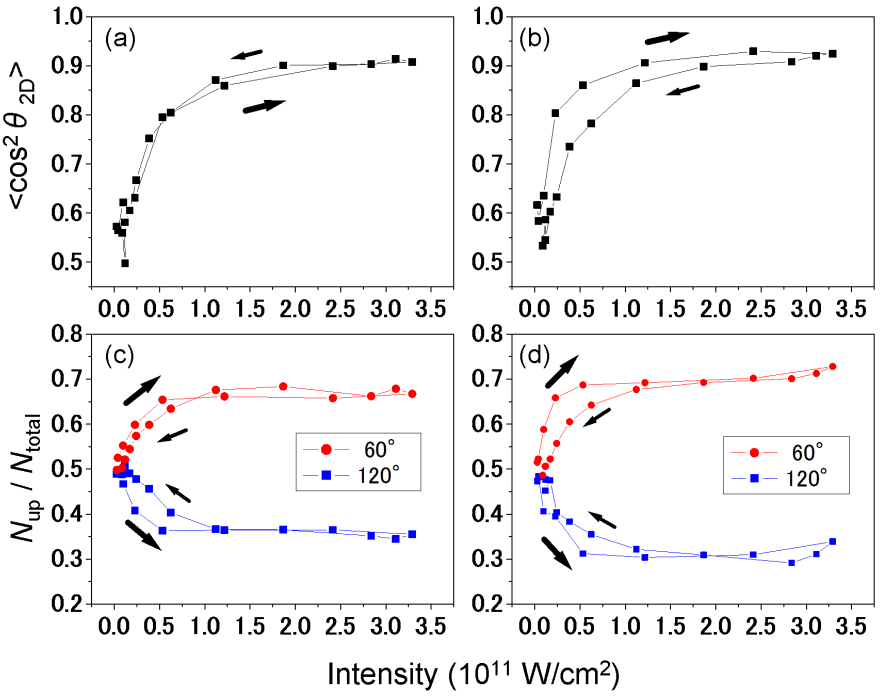

Figure 5.3: The instantaneous intensity dependence of the degrees of alignment $<\cos^2\theta_{2D}>$ for the thermal ensemble (a) and for the state-selected molecules (b). The instantaneous intensity dependence of the degrees of orientation N_{up}/N_{total} for the thermal ensemble (c) and for the state-selected molecules (d). In (a)-(d), the degrees of alignment and orientation are plotted as a function of the instantaneous intensity of the pump pulse on its rising part (thick arrows) and falling part (thin arrows), separately. Reproduced from Ref.[65].

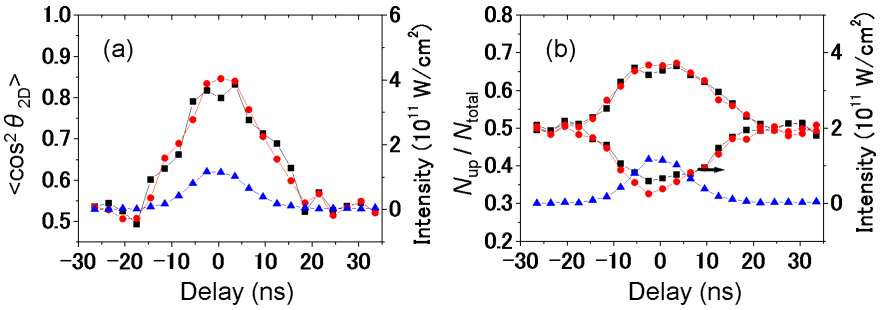

Figure 5.4: The temporal evolutions of the degrees of alignment (a) and orientation (b) for the thermal ensemble (black squares) and the state-selected molecules (red circles) during the pump pulse (blue triangles) with the peak intensity of 6.0 x 10^{10} W/cm^2.

However, here we show a replotted result with the same data of Figure 5.2. To carefully examine the temporal evolutions of the degrees of alignment and orientation, and to judge how well the laser-molecule interaction proceeds adiabatically, we plot the degrees of alignment and orientation as a function of the instantaneous intensity of the pump pulse on its rising part and falling part, separately (Figure 5.2). Significant differences between the degrees on the rising part and those on the falling part are observed. This indicates that the process is not purely adiabatic even though the rotational periods of the IB molecule, characterized by the rotational constants A, B and C, are much shorter than the pulse width of the pump pulse. The instantaneous intensity dependence of the degrees of alignment and orientation are also measured when a laser pulse much lower energy is applied. The temporal evolution of the degree of alignment and orientation are shown in Fig. 5.4, and the corresponding graph showing the intensity dependence are shown in Fig. 5.5. Both for degree of alignment and orientation does show slight differences between the degrees on the rising part and those on the falling part.

Traditionally, molecular alignment orientation have been considered adiabatic when a nanosecond laser pulse is irradiated with molecules. However, as we show in the present section, the temporal evolution of degrees of alignment and orientation does not adiabatically follow the temporal variation of the applied laser field. This nonadiabatic behavior plays an important role in determining rotational dynamics of molecules after the rapid turn off of the pump pulse as it is denoted in the next section.

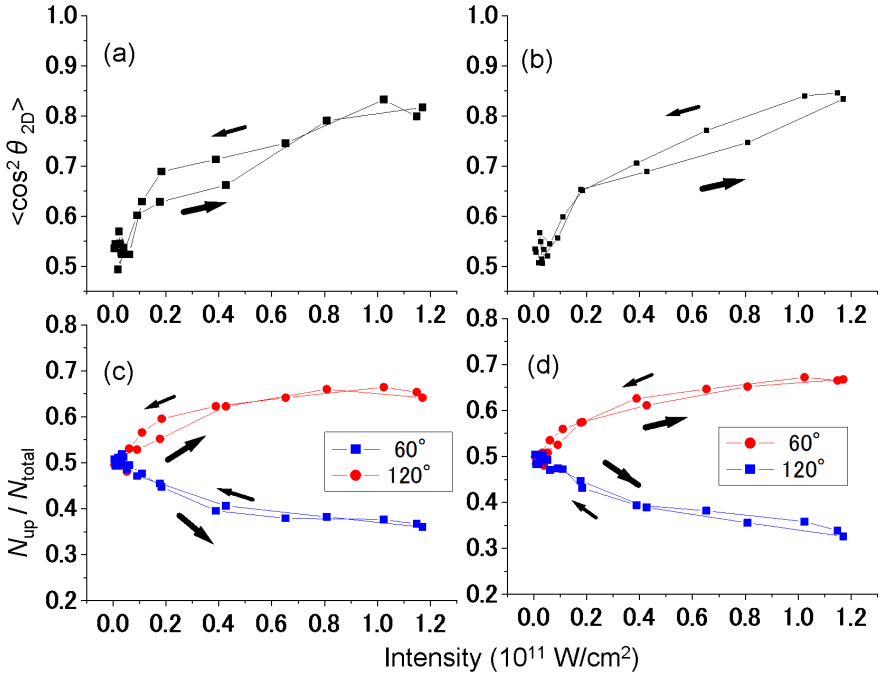

Figure 5.5: The instantaneous intensity dependence of the degrees of alignment $<\cos^2\theta_{2D}>$ for the thermal ensemble (a) and for the state-selected molecules (b). The instantaneous intensity dependence of the degrees of orientation N_{up}/N_{total} for the thermal ensemble (c) and for the state-selected molecules (d). In (a)-(d), the degrees of alignment and orientation are plotted as a function of the instantaneous intensity of the pump pulse on its rising part (thick arrows) and falling part (thin arrows), separately.

5.2 Laser-field-free orientation of state-selected asymmetric top molecules

We apply the plasma shutter technique to achieve laser-field-free alignment and orientation of (state-selected) asymmetric top molecules. Here we focus on the temporal evolutions of alignment and orientation just after the rapid turn off of the pump pulse. A cross-correlation measurement confirms that the fall time of the pump pulse is about 150 fs.

As in the case of the instantaneous intensity dependence, we first look at the temporal evolutions of alignment. Figure 5.6 shows the temporal evolutions of alignment of the thermal ensemble (a) and the state-selected molecules (b) observed with two intensities of 1.7×10^{11} W/cm^2 and 6.0×10^{10} W/cm^2. Before the rapid turn off of the pump pulse, the degrees of alignment are higher at 1.7×10^{11} W/cm^2 than at 6.0×10^{10} W/cm^2. After the rapid turn off of the pump pulse, the highest degrees of alignment before the rapid falling of the laser-field are maintained in the laser-field-free condition for 5-10 ps until the degrees of alignment start to decrease. [1]

In addition, it is confirmed that the dephasing time of degree of alignment is more rapid with 1.7×10^{11} W/cm^2 than with 6.0×10^{10} W/cm^2. This intensity dependence of the dephasing time is more distinct for the state-selected molecules than for the thermal ensemble. The more rapid dephasing with higher intensities of the pump pulse is understood by considering the rotational spectrum of the aligned rotational states. Higher intensities of the pump pulse can transfer the initial rotational state to more highly excited rotational states with broader spectrum ranges. Thus, the highly and broadly excited rotational superposition results in the more serious interferences and the rapid dephasing. The quantum state dependence of the dephasing time scale can be understood with the same manner in that the lower-lying quantum states prepared by the state selection are more sensitive to the external field strength.

Fig. 5.7 shows the temporal evolutions of orientation of the thermal ensemble (a) and the state-selected molecules (b) observed with two intensities of 1.7×10^{11} W/cm^2 and 6.0×10^{10} W/cm^2. Before the rapid turn off of the pump pulse, the degrees of orientation are almost the same for the two intensities, which reflects the strong saturation tendency of orientation. We can

[1] We will discuss this long dephasing time with results of numerical simulations in Chapter 6.

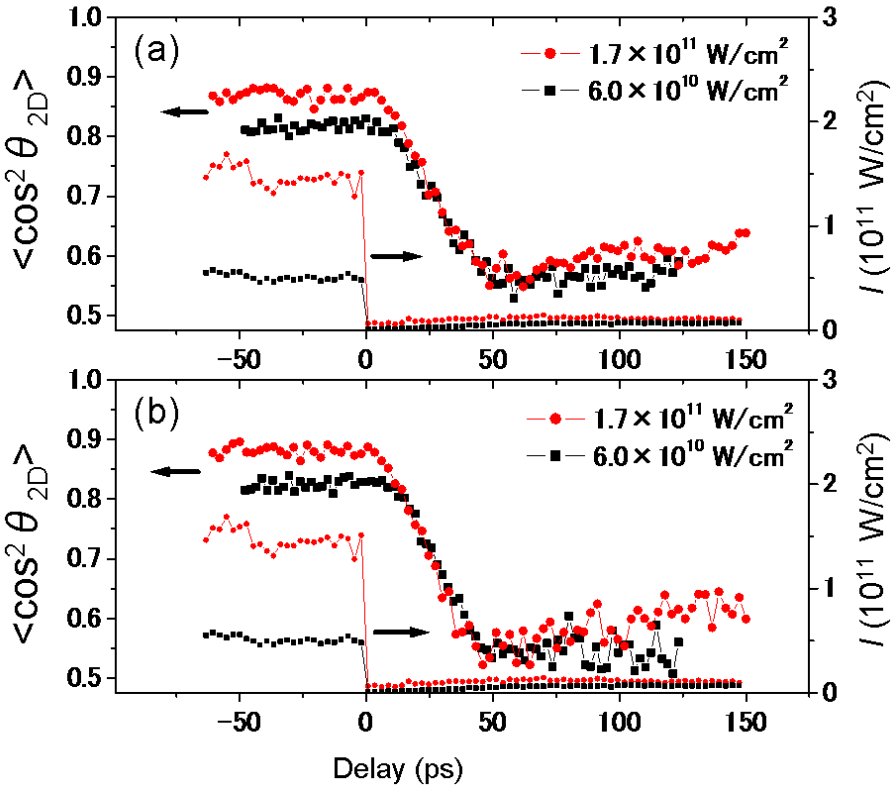

Figure 5.6: The temporal evolutions of alignment of the thermal ensemble (a) and the state-selected molecules (b) observed with two intensities of 1.7×10^{11} W/cm^2 and 6.0×10^{10} W/cm^2, for which the temporal profiles of the shaped pump pulses are also included. Reproduced from Ref.[65].

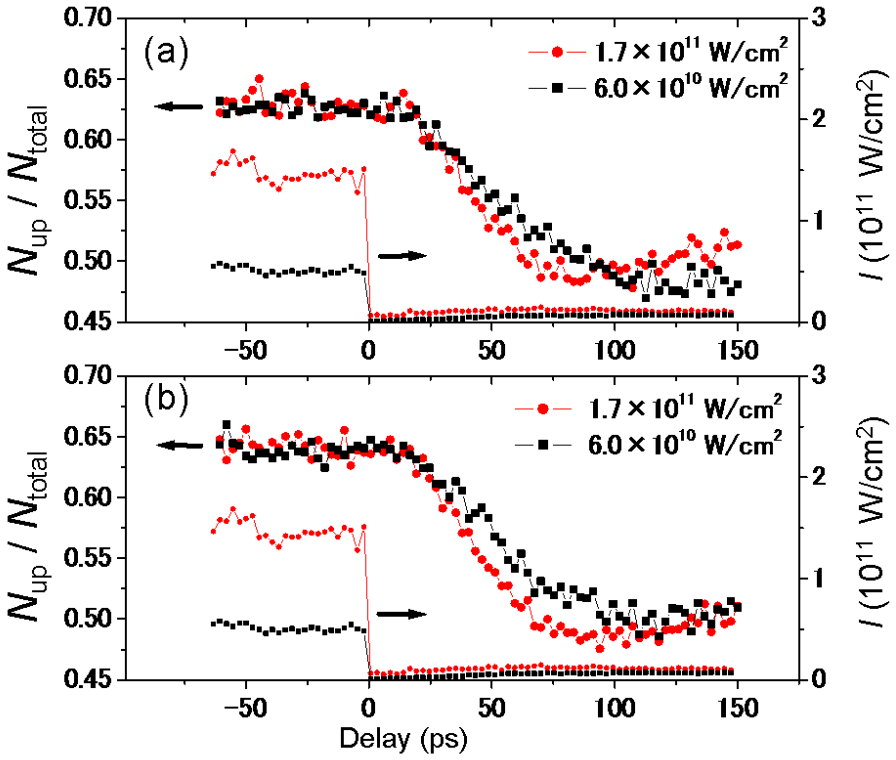

Figure 5.7: The same as in Fig. 5.6 but for orientation. Reproduced from Ref.[65].

find in the Fig. 5.7, the degrees of orientation $N_{\mathrm{up}}/N_{\mathrm{total}}$ are already reached to around a maximum value at the laser intensity of 5.0×10^{10} W/cm^2.

After the rapid turn off of the pump pulse, one can see that the highest degrees of orientation before the rapid truncation are maintained in the laser-field-free condition for ∼20 ps, which is apparently longer than the duration, during which higher degrees of alignment are maintained. The apparently longer duration of orientation comes from the fact that degree of orientation is a result of a coherent superposition of rotational quantum states with regular interval 1 of quantum number J, while the degree of alignment is attributed by rotational quantum states with regular interval 2 of quantum number J. This is same for other linear and symmetric top molecules. For a linear molecule, the selection rules associated with alignment and orientation of a rotational wave packet are summarized below. Thus, nearly two-times faster dephasing is observed from the alignment.

$$< J, M|\cos^2\theta|J', M' >= \begin{cases} \neq 0, \text{ (for J = J' } \pm 2 \text{ and M = M', J = J' and M = M')} \\ = 0, \text{ (otherwise).} \end{cases} \tag{5.1}$$

$$< J, M|\cos\theta|J', M' >= \begin{cases} \neq 0, \text{ (for J = J' } \pm 1 \text{ and M = M')} \\ = 0, \text{ (otherwise)} \end{cases} \tag{5.2}$$

The observation of the 5-10 ps of strong, laser-field-free persistent orientation has been observed for the first time. This experimental achievement ensures future prospect of diverse studies with oriented asymmetric top molecules.

We note that clear revival structures of degrees of alignment and orientation have not been observed in the experimental conditions.

Chapter 6

Results and discussions 2 : Rotational dynamics of asymmetric top molecules exposed to a laser pulse with a slow turn on and a rapid turn off

In our experiment described in Chapter 5, whereas clear revival structures of degrees of alignment and orientation after the rapid turn off have not appeared, the 5-10 ps of laser-field-free orientation have been observed after the rapid turn off of the laser field. This is a first demonstration of rotational dynamics of asymmetric top molecules exposed to a laser pulse with a slow turn on and a rapid turn off. In this section, we elucidate the underlying physics associated with the rotational dynamics of the molecules by numerical studies.

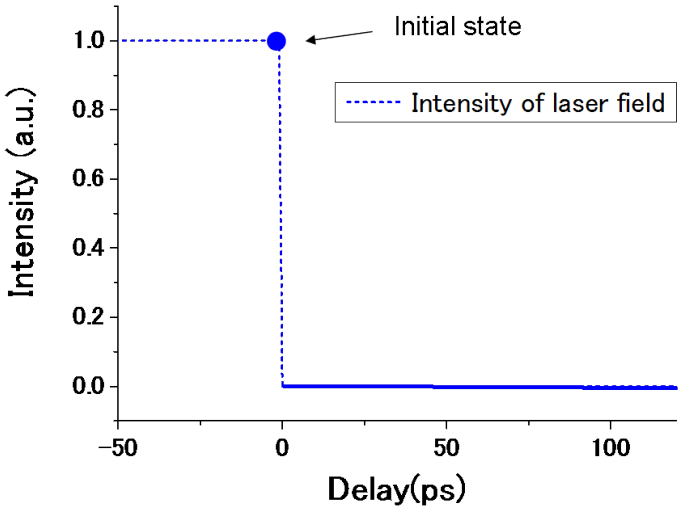

Figure 6.1: (The same for figure 3.3) Scheme of a model for numerical simulations. The eigenstates of field-dressed Hamiltonian at $t = 0$ are employed as initial quantum states. We analize the time evolution of the initial state after the rapid turn off of the laser field in the presenece of an electrostatic field.

6.1 Rotational dynamics of asymmetric top molecules exposed to a laser pulse with a slow turn on and a rapid turn off, in the presence of a weak electrostatic field.

In this section, we explore rotational dynamics of asymmetric top molecules with an assumption that the molecules are controlled with a purely adiabatic process in the slow turn on of the laser field. The rotationally excited states just before the rapid turn off of the laser field are calculated by solving the time independent Schrödinger equation (See Fig. 6.1). We also assume that the electrostatic field and laser-field are parallel to each other and the laser field is completely turned off. [1]

[1]Conceivable effects from finite intensities that possibly remains after the rapid turn off of the laser field are summarized in Appendix.

6.1.1 Dephasing dynamics

In this subsection, we show the numerically observed dephasing dynamics of iodobenzene molecules. Experimentally observed 5-10 ps of persistent molecular alignment and orientation are not obtained, and the degrees of alignment and orientation by pure adiabatic interaction start to decrease soon after the rapid truncation of the laser field as shown in the Fig 6.2 and 6.3.

Except the presence of the persistent orientation, however, a lot of points are consistent with the experiment. Let us consider a time interval between the rapid turn off and the moment when the first local minimum of the degree of alignment or orientation appears as a dephasing time to discuss the dephasing dynamics. The faster dephasing times of degrees of alignment and orientation are observed when the coherent wave-packets have broader rotational spectrum and higher rotational energies. Thus, the dephasing times become shorter when the applied laser-field is strong or the initial rotational temperatures are higher. Also, the applied laser-field dependence of the dephasing times are more distinct with a lower rotational temperature. [2]

The observed dephasing times are more than 10 ps, which is longer than that observed from other small linear molecules $\sim$ 1ps [36]. This long dephasing dynamics of iodobenzene molecules mainly comes from the long rotational period of the molecule. The rotational constants $B = 760.4$ and $C = 662.6$ MHz are crucial parameters for determining the observed one-dimensional dephasing dynamics of alignment and orientation. The rotational constant around C_2^z axis, A=5669 MHz, does not affect the dephasing time scale.

6.1.2 Revival structure

We look to the numerically observed time evolutions of molecular alignment and orientation for 900 picosecond. The degrees of alignment and orientation after the rapid turn off are shown in Fig. 6.4 and 6.5. The Fig. 6.4 and 6.5 are results for different rotational temperatures of 0.1 K and 0.5 K, respectively. For comparison, the results for an imaginary large linear rigid rotor are shown in Fig. 6.4 and 6.5 as well. The rotational constant of the linear molecule is

[2] We can consider that the molecular sample with a lower rotational temperature in the numerical simulation corresponds to a state-selected molecular sample in the experiment in that low-lying quantum states are more included.

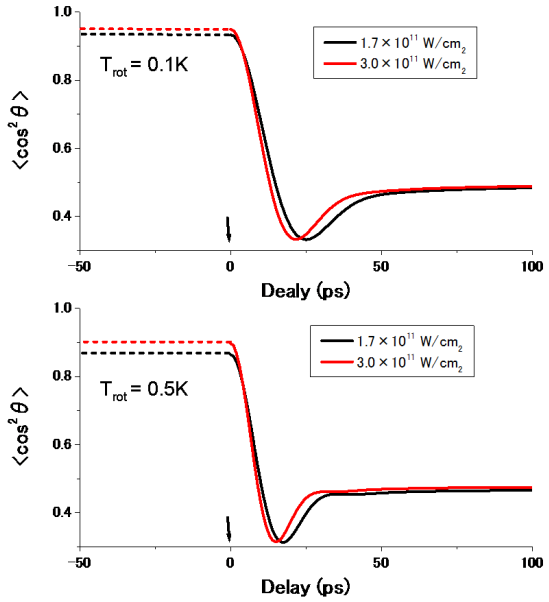

Figure 6.2: Temporal evolutions of degree of alignment of the initial field-dressed iodobenzene molecules exposed to a rapid turn off of the laser field. The molecules are in the electrostatic field of 2078 V/cm. The irradiated laser pulses, whose peak intensity are 3.0×10^{11}W/cm^2 (black) and 1.7×10^{11}W/cm^2 (red), are turned off at t=0.

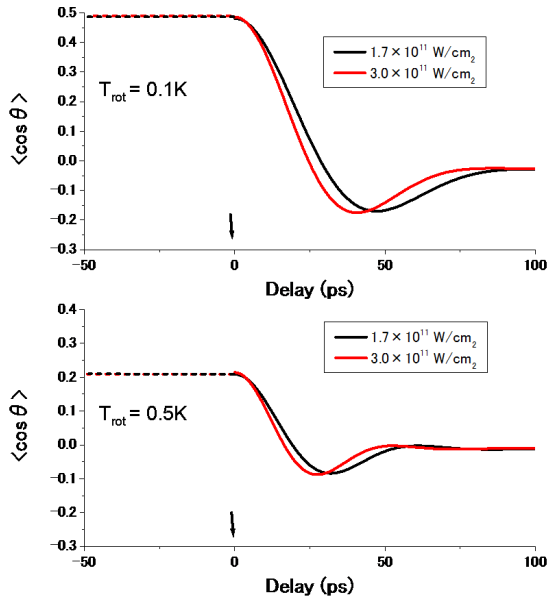

Figure 6.3: Temporal evolutions of degree of orientation of the initial field-dressed iodobenzene molecules exposed to a rapid turn off of the laser field. The molecules are in the electrostatic field of 2078 V/cm. The irradiated laser pulses, whose peak intensity are 3.0×10^{11}W/cm^2 (black) and 1.7×10^{11}W/cm^2 (red), are turned off at t=0.

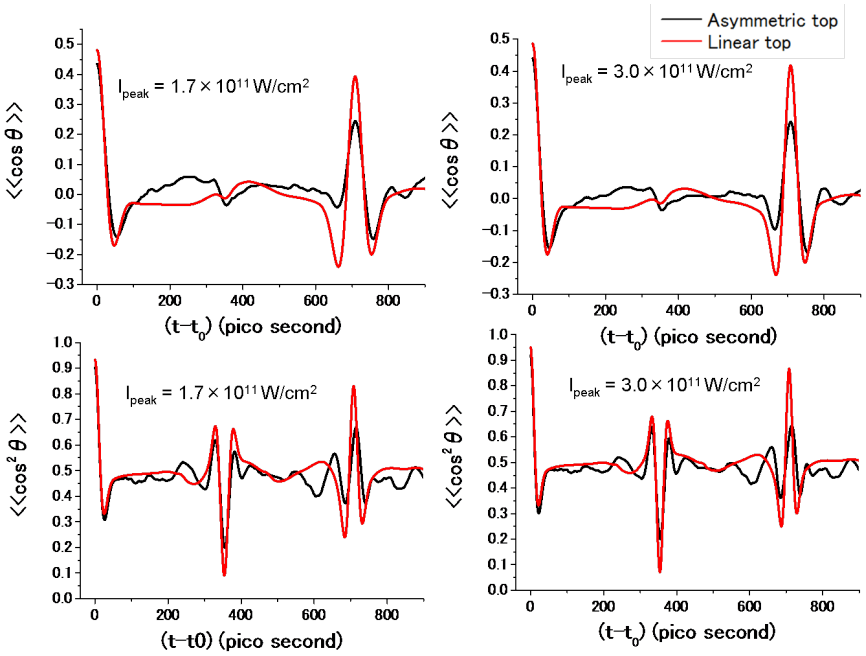

Figure 6.4: Temporal evolutions of the degrees of alignment (lower panels) and orientation (upper panels) of linear and asymmetric top molecules for the rotational temperature of 0.1 K. The electrostatic field is 2078 V/cm. The results for asymmetric top and linear molecules are shown by the black and red lines, respectively. The peak intensities of the laser field before the complete turn off are set as 1.7×10^{11}W/cm^2 (left panels) and 3.0×10^{11}W/cm^2 (right panels).

set as a mean value of those of iodobenzene molecule around C_2^x and C_2^y axes, which are denoted as B and C in the field-free Hamiltonian $A\hat{J}_x^2 + B\hat{J}_y^2 + C\hat{J}_z^2$. The rotation around the C_2^z axis is neglected.

It has been reported that the rotational revival structures of asymmetric top molecules, following the irradiation by an intense short laser pulse, differ qualitatively from those of linear molecules [42, 43]. In contrast to this, however, Fig. 6.4 and Fig. 6.5 show that the asymmetric top molecules behave like linear molecules, especially when the rotational temperature is very low (0.1 K). At around the rotational period of the imaginary linear molecule of 705 ps, not only the linear molecules but also the asymmetric top molecules experience rotational revivals. In other words, only the J-type

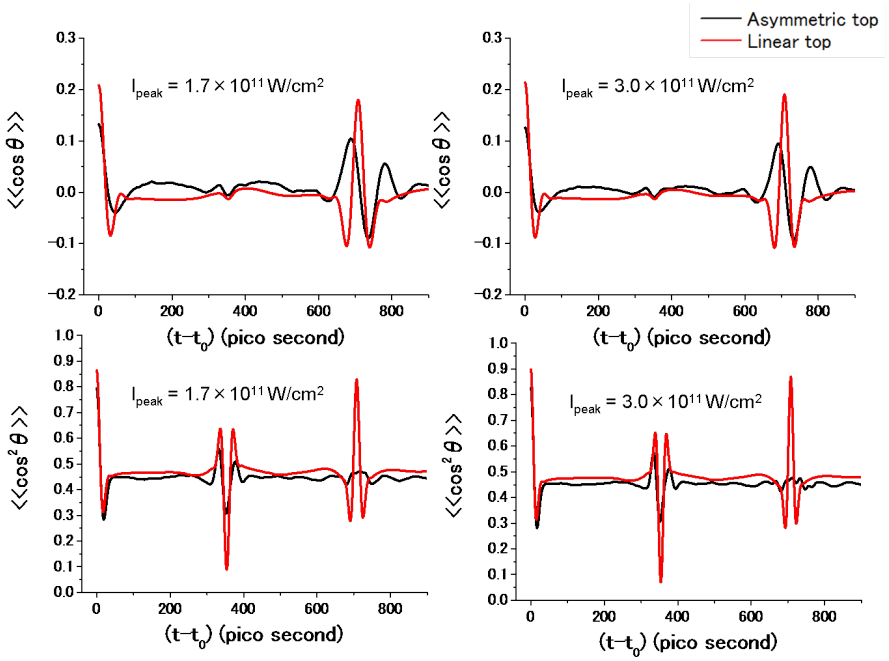

Figure 6.5: The same as in Fig. 6.5 but for the rotational temperature of 0.5 K.

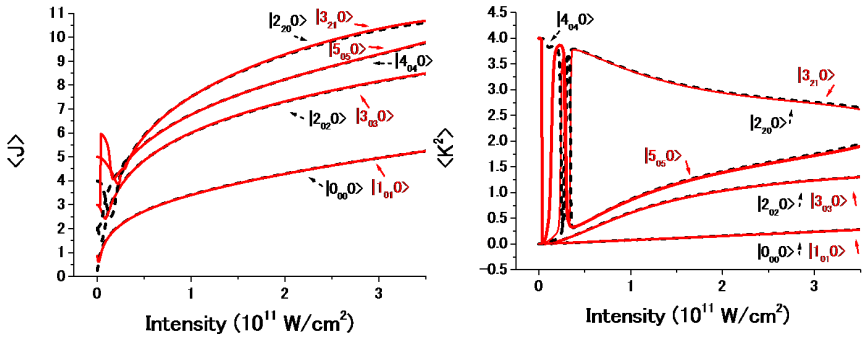

Figure 6.6: The expectation values of K^2 and J for some low lying rotational quantum states of iodobenzene molecule exposed to combined electrostatic and nonresonant laser fields in the adiabatic condition as a function of the laser intensity. The electrostatic field is 2078 V/cm. The rapid changes of the expectation values of K^2 for several states are caused when they experience avoided crossings.

revivals characterized by the period $1/[2(B+C)]$ appear after the rapid turn off of the pump pulse. This result does not seem to be with the previous study reporting that a relatively large fluence of pump pulse washes out the J-type revivals structures and causes C-type revivals instead [42].

However, the reason for the linear molecule like behavior can be clearly understood. To explain the reason for the linear molecule like behavior of the asymmetric top molecule, the expectation values of K^2 and $\hat{J}$ of the rotational wave packet of an iodobenzene molecule generated by the adiabatic interaction are shown in Fig. 6.6 as a function of the intensity of the pump pulse. Here, the quantum number J represents amplitude of total angular momentum, and the K represents the amplitude of rotation around the molecule-fixed z axis. The initial ground state denoted as $|0_{00}0>$ and some low lying quantum states are not excited to the states with higher level of K states by the adiabatic interaction with the pump pulse on the order of 10^{11} W/cm^2. Without the rotation around the C_2^z axis, the molecule acts like a linear molecule.

However, a fully adiabatic excitation is still experimentally difficult to be made, because even the irradiation by a few tens of ns pump pulse can not ensure the purely adiabatic exciatation of a large asymmetric top molecule [87].

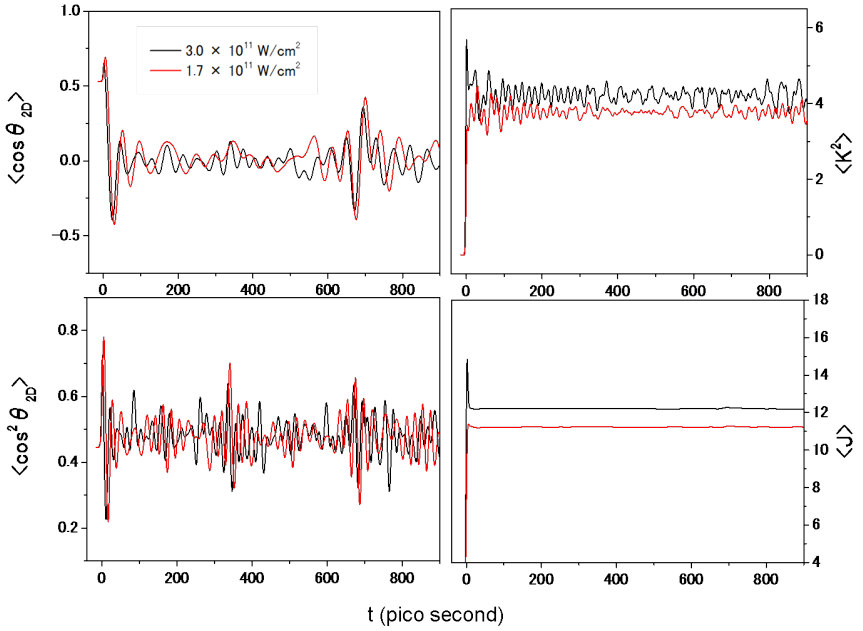

Figure 6.7: Temporal evolutions of the initial ground state of iodobenzene molecule irradiated with a short laser pulse. The molecules are in the electrostatic field of 2078 V/cm. The irradiated laser pulses, whose peak intensity are 3.0×10^{11}W/cm^2 (black) and 1.7×10^{11}W/cm^2 (red), are centered at t=0 with a FWHM of 7.05 ps.

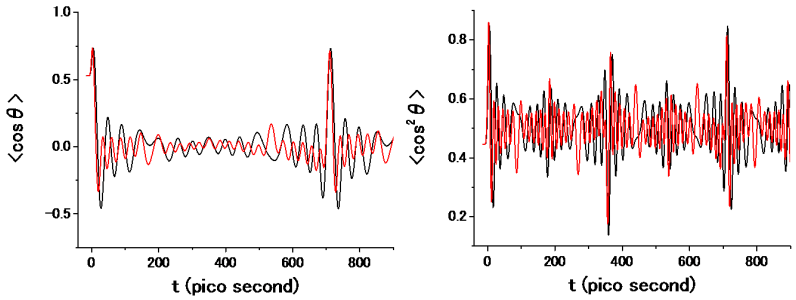

Figure 6.8: Temporal evolutions of the initial ground state of an imaginary molecule exposed to the same condition of Fig. 6.7. The irradiated laser pulses, whose peak intensity are 3.0×10^{11}W/cm^2 (black) and 1.7×10^{11}W/cm^2 (red), are centered at t=0 with a FWHM of 7.05 ps.

Before we consider nonadiabatic effect taking place on the slow rising of the laser pulse, let us demonstrate rotational dynamics of asymmetric top molecules irradiated with ultra-short laser pulse. As demonstrated in Fig. 6.7, initial low-lying quantum states can be excited to the states with high expectation values of K^2 nonadiabatically. These transitions play a crucial role for determining the characteristic rotational dynamics of asymmetric top molecules. Dynamics of the ground state of IB molecule irradiated with a short pump pulse, which are centered at $t = 0$ with a FWHM of 7.05 ps, is shown in Fig. 6.7. When the pump pulse with $3.0 \times 10^{11}\mathrm{W/cm}^2$ of peak intensity is applied, in addition to the J-type of revivals near 705 ps, the notable revival structures near 750 ps are observed for alignment $< \cos^2\theta >$. The J-type revivals become less distinct when the C-type revival appear. The expectation values of K^2 are observed to be considerably excited by nonadiabatic interactions, which we consider as a source of the characteristic revival structures qualitatively different with those of linear molecules. On the other hand, the imaginary linear molecule experience the revivals of alignment and orientation near 705 ps as shown in Fig. 9.1, irrespective of the applied laser pulse.

The results shown in Fig. 6.4 and 6.5 are those for relatively low rotational temperatures. However, even for significantly higher rotational temperature of 1K, the only J-type revivals have been observed.

6.2 Loss of adiabaticity and its effect on rotational dynamics of asymmetric top molecules

In this section, we consider nonadiabatic effect taking place on the slow rising of the laser-field. Traditionally, the interaction between molecules and non-resonant laser-pulse with a few nano second of pulse width is considered to be adiabatic. However, in recent studies [87, 32], it is reported that nonadiabatic effect on the slow rising of the laser-field is crucial for the orientation dynamics. We have employed numerical method introduced in Chapter 2 and 3 to calculate rotational dynamics of asymmetric top molecules, taking into account nonadiabatic effect on the slow rising of the laser field. (See figure 6.9)

We consider a regime where the linearly-polarized laser field and the electrostatic field are parallel to each other.

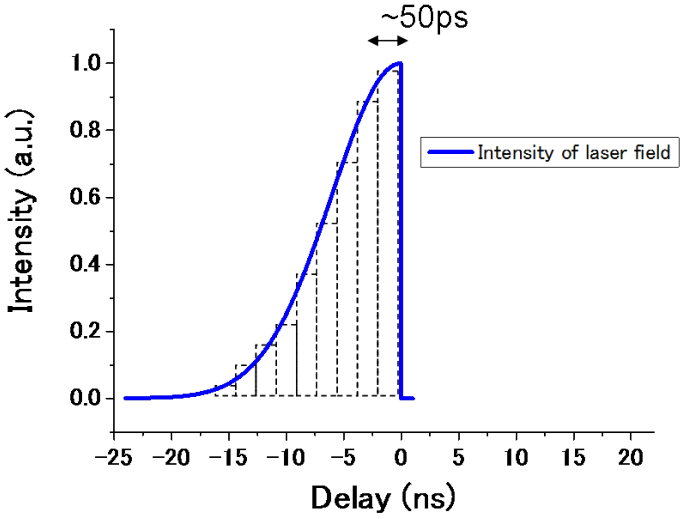

Figure 6.9: The same with Fig.3.5 Scheme of a model for numerical simulations. We accurately calculated TDSE by asumming that the laser pulse is composed by sequentially lined square shaped short laser pulses. The temporal width of square pulses are set as 50ps. See Chapter 3 to review the numerical method and the validity of this model.

6.2.1 Avoided crossings and loss of adiabaticity

We demonstrate that orientation process by a few nanoseconds of nonresonant laser pulse does not ensure pure adiabatic process of asymmetric top molecules due to presence of avoided crossings. We look to temporal evolutions of several individual rotational states exposed to a laser pulse with a slow turn on and a rapid turn off.

When we plot energy shifts of individual rotational states as a function of intensity of laser-field or electrostatic field, some plotted curves of individual states cross to each other. The crossings can be classified into avoided crossing and real crossing. When two field-dressed states satisfy different symmetry condition, the two states are independent to each other so that the two curves are really crossed. In contrast, two different states satisfying same symmetry condition experience avoided crossing. [3] Some energy curve of several low-lying quantum states are shown in Fig. 6.10. The states are exposed both electrostatic and nonresonant laser fields. Because the states have the same symmetry, avoided crossings between the states are observed. Consequently, the energy order of the initial states is preserved.

Let us show, rotational dynamics of the two lowest-lying quantum states $|0_{00}0>$ and $|1_{01}0>$shown in Fig. 6.10. The two states do not experience avoided crossings under the condition of external fields shown in the Fig. 6.10. The gap between the two curves is nearly 2500 MHz, which is mostly determined by the rotational constant of the molecule. Besides, in Fig. 6.11 we show temporal evolution of the lowest-lying quantum state $|0_{00}0>$ exposed to laser field with finite turns-on and a peak intensity of $6.0 \times 10^{10}\mathrm{W/cm}^2$. When τ, where τ is defined as half width at $1/\sqrt{e}$ maximum of laser intensity[4], is more than 500 ps , the orientation process is nearly adiabatic.

In sharply contrast to the dynamics of the ground state $|0_{00}0>$, some other states experiencing avoided crossings require still longer laser pulse for pure adiabatic processes. In energy curves shown in Fig. 6.10, we focus our attention to three states which experience three times of avoided crossings. Fig. 6.12 shows the three avoided crossings zoomed-up. Fig. 6.13 shows

[3] As a result of the avoided crossings, energy order of rotational quantum states in same symmetry condition is invariant when external field is applied adiabatically. That allows us to distinguish different quantum states, and we can correlate the eigenstates of field-dressed Hamiltonian with initial field-free states in spite of presence of crossings between quantum states.

[4] Only in the present section 6.2, we evaluate temporal width of the laser pulse with half width of at $1/\sqrt{e}$ maximum of laser intensity instead of the FWHM or HWHM.

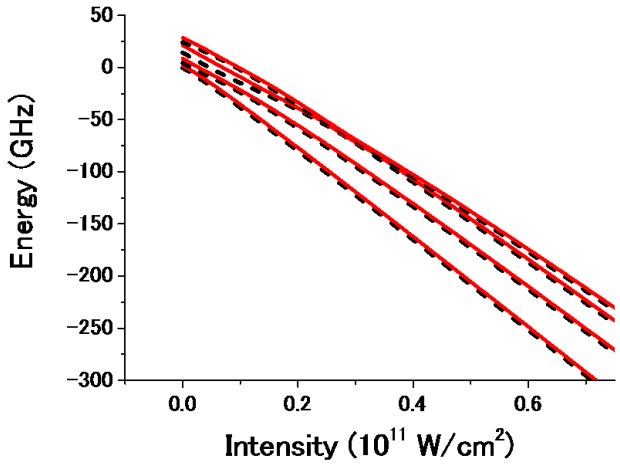

Figure 6.10: The Stark shifts of some initial rotational states exposed to both electrostatic and linearly polarized laser fields. They are plotted as a function of laser field intensity. The electrostatic field is 2078 V/cm. The lowest eight initial states, in the order of energy levels, characterized by quantum number $M = 0$ and the even parities of s and K are sown.

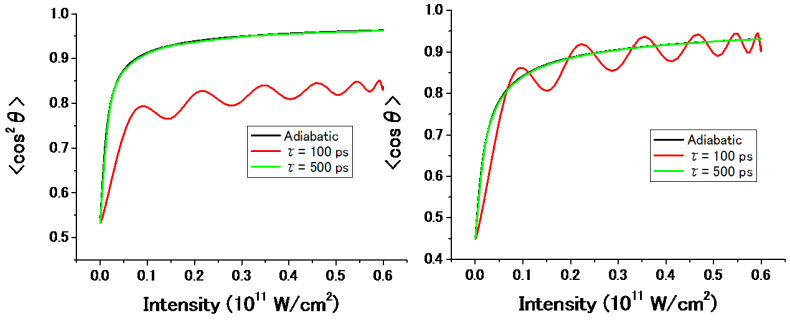

Figure 6.11: Degree of alignment (left) and orientation (right) of initial $|0_{00}0>$ state as a function of the applied intensity of laser field. 2078 V/cm of electrostatic field is applied. Two results show that τ much longer than 500 ps ensures pure adiabatic interaction, where τ is half width at $1/\sqrt{e}$ maximum of laser intensity.

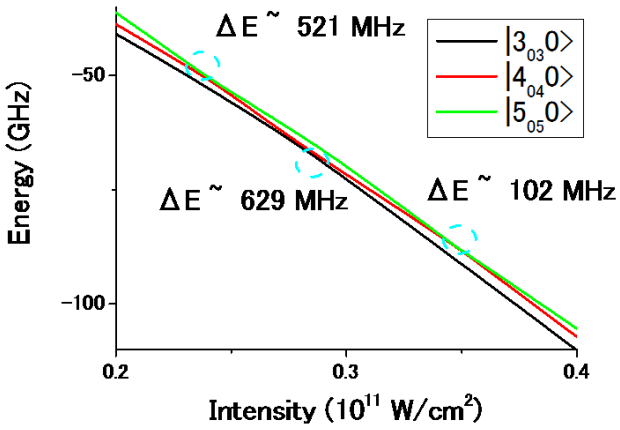

Figure 6.12: Three avoided crossings taking place among three rotational states. The states are corresponding to three field-free states represented as $|5_{05}0>$, $|4_{04}0>$, and $|3_{03}0>$, in order of energy.

temporal evolutions of the initial $|4_{04}0>$ states under irradiation of laser pulse with finite turn-ons and a peak intensity of 6.0×10^{10}W/cm^2. It is clear that the orientation and alignment processes are far from pure adiabatic process even with a very long 24 ns of laser pulse. Under the irradiation of the laser pulse with 24 ns of slow turn on, the interaction is close to adiabatic until the field-intensity is lower than 3.0×10^{10}W/cm^2. On the other hand, when the quantum state crosses the intensity region, 3.0×10^{10}W/cm^2 $\sim$ 4.0×10^{10}W/cm^2, presence of a avoided crossing with a small energy gap 102 MHz makes the interaction nonadiabatic; therefore, transition between the two quantum states becomes distinct. We note that more than 100 ns of laser pulse is required for the pure adiabatic interaction.

Let us describe rotational dynamics of single rotational quantum state exposed to a laser pulse with the 6 ns of slow turn on and the rapid turn off. Instantaneous intensity dependence of alignment and orientation are shown in Fig. 6.14 (a) and (b) respectively. Initial quantum state $|3_{03}1>$ experience an avoided crossing when the laser intensity is close to 2.3×10^{10}W/cm^2 with a energy gap of 353 MHz; then the laser field with 6 ns of slow turn on can not ensure pure adiabatic orientation. We can see that the interaction by the laser pulse is adiabatic until the laser field increase to 2.3×10^{10}W/cm^2.

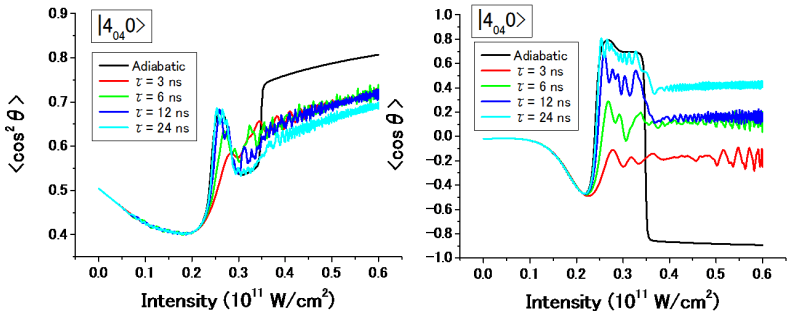

Figure 6.13: Degree of alignment (left) and orientation (right) of initial $|4_{04}0>$ state as a function of the applied intensity of laser field. 2078 V/cm of electrostatic field is applied. Two results show that τ much longer than 24 ns can not ensure pure adiabatic interaction.

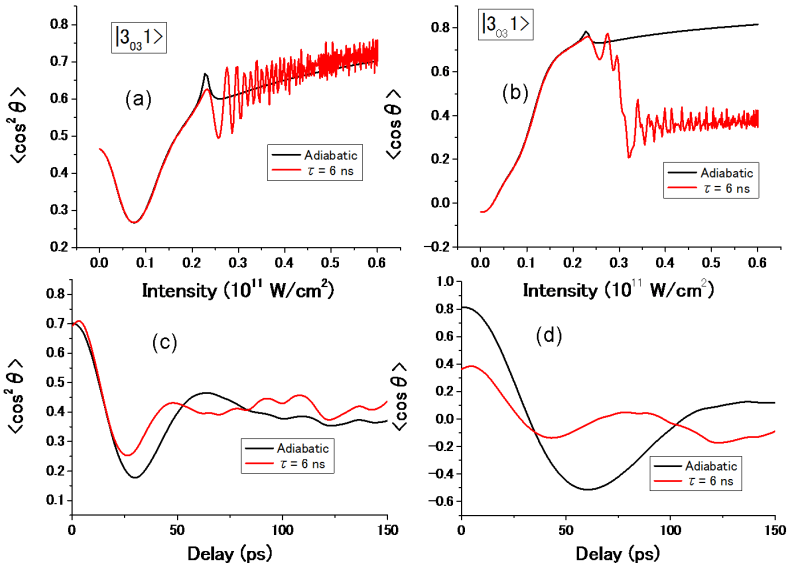

Figure 6.14: Degree of alignment (a) and orientation (b) of initial $|3_{03}1>$ state as a function of the applied instantaneous intensity of laser field. (c) and (d) show the temporal evolution of alignmet and orientation after the rapid turn off of the laser field. 2078 V/cm of electrostatic field is applied.

Fig. 6.14 (c) and (d) show temporal evolution of alignment and orientation after the rapid turn off of the laser field. The nonadiabatic transition taking place near the avoided crossing significantly affects on rotational dynamics even after the rapid turn off of the laser field. The rotational state that controlled by 6 ns of rising laser field shows "persistent" alignment and orientation after the rapid turn off of the laser field, while the oriented state by adiabatic turn on starts to decrease soon after the rapid turn off.

In conclusion of this section, loss of adiabaticity stemming from presence of a lot of avoided crossings is significant; especially, the nonadiabaticity can contributes to the persistent alignment and orientation for 5 to 10 ps after the rapid turn off of the laser field. In a given potential for molecular alignment or orientation, the best aligned or oriented quantum state is an eigenstate of the applied interaction Hamiltonian in almost of cases. Thus, wave packet generated by impure adiabatic process has a possibility to much aligned or oriented in the given intensity of external field. Therefore, the degree of alignment or orientation does not necessarily increase (decrease) following the increase (decrease) of instantaneous laser field when the interaction is not purely adiabatic. In our numerical calculation, approximately one out of ten initial quantum states has demonstrated persistent laser-field-free orientation after the rapid turn off of the laser field, while almost of quantum states experience avoided crossing during slow turn on of the laser field.

6.2.2 Rotational dynamics of molecules in thermal ensemble

Here, we show the numerically obtained result of rotational dynamics of molecules in thermal ensembles. We have shown that the orientation process by the electrostatic field and a laser field with 6 ns of rising time is far from pure adiabatic process for several individual quantum states. However, as we show in this subsection, dynamics of thermal averaged molecular samples does not show distinct nonadiabaticity.

In section 5.1, we introduce the experimental observation showing that there are significant differences between the degrees of alignment and orientation on the rising part and those on the falling part of the laser field (Fig. 5.2). This observation ensures that the process is not purely adiabatic. On the other hand, the numerical results shown Fig. 6.15 do not show the distinct asymmetry between the rising part and the falling part of the laser

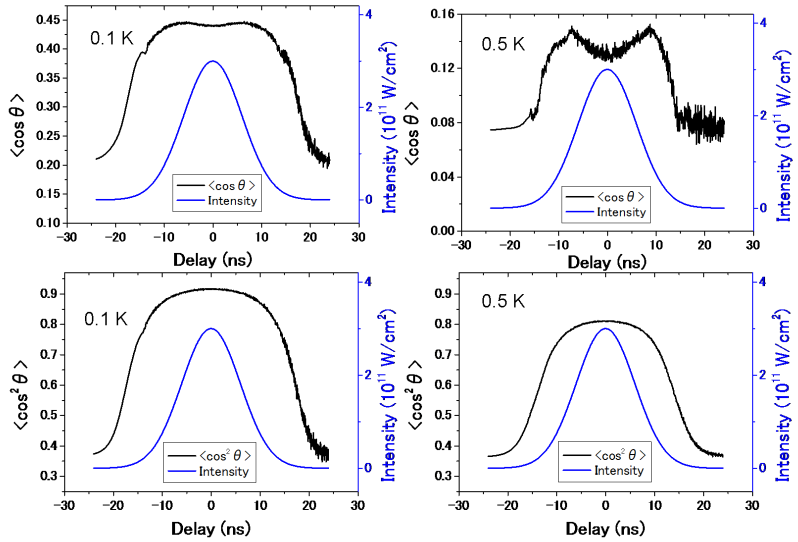

Figure 6.15: Temporal evolutions of alignment and orientation of iodobenzene molecules for two rotational temperatures of 0.1K (left) and 0.5K (right). $< \cos^2\theta >$ and $< \cos\theta >$ following the temporal variation of the applied laser field show nearly same instantaneous intensity dependences on the rising part and on the falling part.

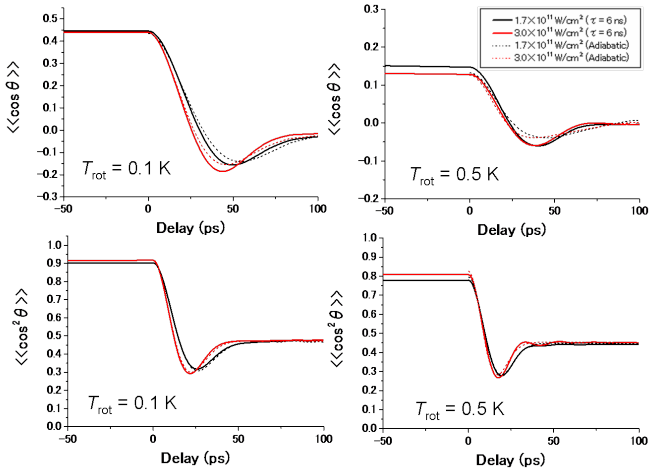

Figure 6.16: Temporal evolutions of degrees of alignment and orientation near the rapid turn-off of the applied laser field in the presence of a weak electrostatic field. The results from the two different cases does not show crucial difference.

field. We also compare numerical results of rotational dynamics for two different cases. We consider both molecules which exposed to adiabatic turn on and a rapid turn off (dotted lines in Fig. 6.16 and 6.17) and which exposed to a 6 nanosecond of turn on and a rapid turn off (real lines in Fig. 6.16 and 6.17). Revival structures and achievable degrees of orientation of molecules do not show qualitatively different behavior for the two cases.

6.2.3 Conclusion

We have found significant loss of the adiabaticity for several individual rotational quantum states. However, when we consider thermal averaged rotational dynamics of individual rotational states, the distinct gaps between pure adiabatic orientation and the impure adiabatic orientation disappear. Thus, there is discrepancy between the numerally obtained results and what we have observed from experiments; because, as we have demonstrated in Chapter 5, orientation process of asymmetric top molecules under the electrostatic field and a laser field with a 6 ns of rising time is obviously far from pure adibaticity.

We consider the discrepancy to be caused from the fact that we calculated

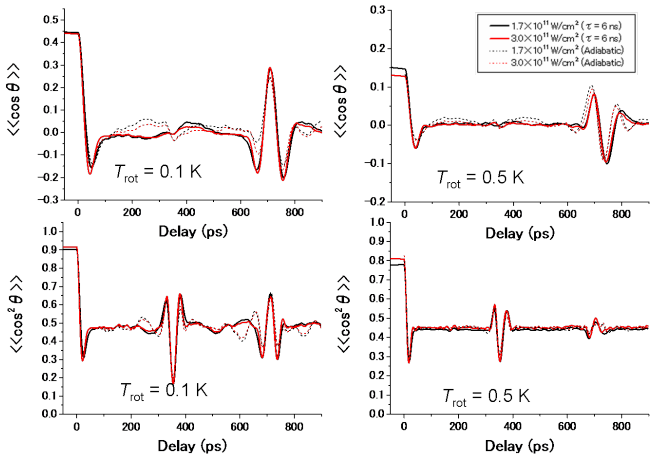

Figure 6.17: Temporal evolutions of degrees of alignment and orientation for a nano second after the rapid turn-off of the applied laser field in the presence of a weak electrostatic field. The results from the two different cases does not show crucial difference.

the rotational dynamics of molecules under the "parallel field condition" rather than "tilted field condition". In the tilted field condition, which is close to the real experimental condition, quantum number M is not preserved any more. Rotational states with different M values those are degenerated in energies in the field-free condition experience energy splitting by electrostatic field component non-parallel to the laboratory-fixed Z axis. As a result, a lot of quantum states experience extremely larger number of avoided-crossings. Thus, there must be extremely large amount of loss of adiabaticity in the tilted field condition.

However, solving the time-dependent Schrödinger equation in the tilted field condition still takes high calculation cost. In the tilted filed condition, the M is not a good quantum number, so we can not deal with states with different M values independently. Thus, size of an irreducible matrix that we need to diagonalize dramatically increases. Furthermore, the cost of calculation increases nonlinearly when the size of a matrix increases. Such computational difficulties have confined the present studies on the parallel field condition.

In near future, with a much cost effective numerical method, rotational

dynamics of asymmetric top molecules in the tilted field condition need to be solved for elucidate distinct nonadiabatic effect observed in the experiments.

Chapter 7

Results and discussions 3 : Completely field-free orientation of state-selected molecules

Combination of a fundamental and a second-harmonic laser pulses can induce a potential energy for molecular orientation, which provides an all-optical molecular orientation technique [29, 30]. Under the all-optical potential that applied adiabatically, a free-rotational state can be strongly oriented. In contrast, under an irradiation of ultra-short two-color laser pulse, a single rotational state does not show pronounced degree of orientation because of a considerable nonadiabatic transition to the oppositely oriented states. Thus, the strongest degree of orientation in the completely field-free condition can be accomplished by using a two-color laser pulse with a slow turn on and rapid turn off, provided the molecular sample includes only one rotational state.

In this section, we present experimental results and corresponding numerical simulations of completely field-free orientation of molecules. The two-color laser field with a several nanoseconds of pulse width is employed for orienting molecules without additional electrostatic field. We utilize the plasma shutter technique to rapidly turn off the laser field.

7.1 Molecular Orientation by two-color laser field

In the peak intensity of two-color nanosecond laser pulse, we have observed degrees of alignment and orientation of state-selected molecules for iodobenzene and OCS samples. Since we use a laser pulse whose pulse width is much longer than rotational period of molecule, we had expected remarkably strong orientation can be achieved [89]. However, the experimentally obtained values are much lower than that expected in the early numerical simulations.

We have numerically found that the orientation process by the two color laser field is not purely adiabatic, which is because the second harmonic laser pulse have much shorter pulse width than that of the fundamental laser pulse. That is to say, if a strong alignment without the "head versus tail" order confinement is accomplished by the one-color laser field, additionally followed external potential by the combination of the two laser fields for the "head versus tail" order confinement leads to a nonadiabatic transition between a pair of states which are oriented oppositely to each other. Even though the delayed second harmonic laser field turns on slowly compared to the rotational motion of molecule, the strongly aligned rotational state has a nearly degenerated pair state which is oriented to the opposite direction. In other word, once the doublet states are created by strong one-color laser field, it is nearly impossible to adiabatically separates them from each other.

We show a numerical result of orientation of OCS molecule (Fig. 7.1). The numerical result illustrates that the strong intensity of the fundamental laser field is not the best condition for orientation.

For making the interaction for molecular orientation to be close to the adiabatic limit, temporal delay between the two laser pulses need to be optimized so that the alignment and orientation can start to be induced simultaneously. In this study, prior to the recipe, we have optimized the intensities of the two wavelength laser pulses in order to orient the molecules as adiabatically as possible.

7.1.1 OCS molecule

We have first measured degrees of alignment and orientation without shaping the pulse by the plasma shutter. The pulse width of the fundamental laser

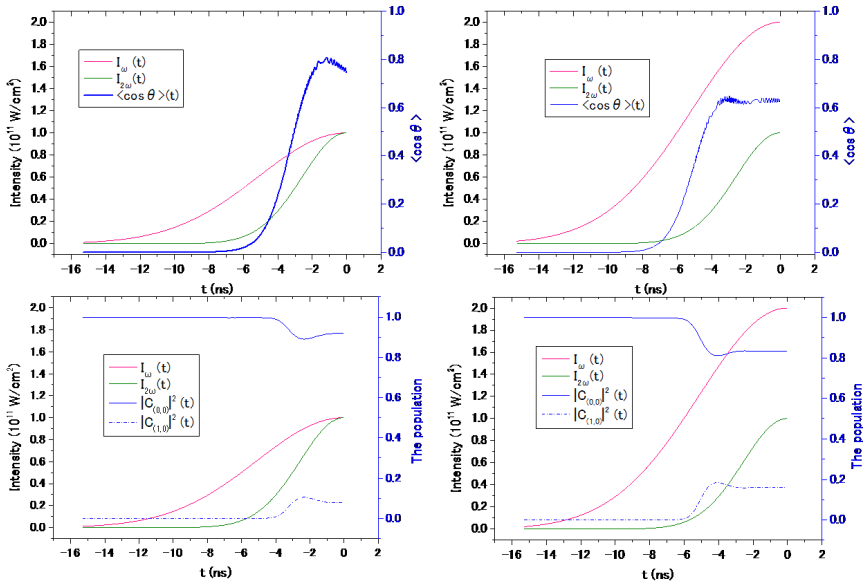

Figure 7.1: Temporal evolutions of rotational ground state of OCS molecule. The two-color laser pulse consists of the ω and 2ω pulses whose pulse widths are 6 and 3 ns respectively by HWHM. The peak intensity of ω is $1 \times 10^{11}\mathrm{W/cm}^2$ for the left panels and $2 \times 10^{11}\mathrm{W/cm}^2$ for right panels, while the peak intensity of 2ω is same for the both. $|C_{0,0}|^2$ and $|C_{1,0}|^2$ shows the squares of the coefficients for the projection of the wave function onto the adiabatic pendular state basis of field-dressed Hamiltonian. If the interaction is purely adiabatic, $|C_{0,0}|^2$ must be temporally unchanged.

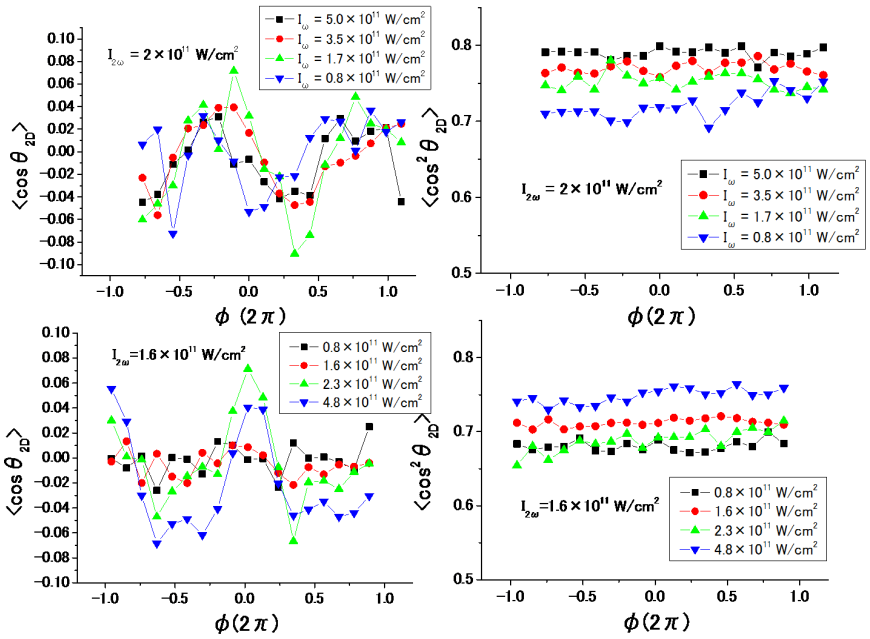

Figure 7.2: Degrees of alignment (right) orientation (left). The horizontal axises show relative phase between the ω and 2ω. In the upper and lower panels, peak intensities of the 2ω are 2.0×10^{11}W/cm^2 and 1.6×10^{11}W/cm^2, respectively.

pulse is measured as 7.7 ns and that of the second harmonics is estimated as 3.85 ns. In the experiments, we fix the energy of the 2ω pulse to be maximized as much as possible, while that of ω is adjusted with an attenuator. We use OCS molecules buffered with 50-bar of He gas, and the molecules are state-selected by the 8 kV-applied molecular deflector (Chapter 4). We irradiated the state selected molecules with the two-color pump pulse and the probe pulse. From the obtained two-dimensional images by the velocity-map imaging spectrometer, we estimated the degrees of orientation $< \cos\theta_{2\mathrm{D}} >$ and alignment $< \cos^2\theta_{2\mathrm{D}} >$.

Fig. 7.2 shows result of the measurement. Degrees of alignment increase with the intensity of the applied laser fields. In contrast, the degree of orientation decrease when the intensity of the fundamental laser field is too strong. For the best orientation we need to apply an appropriate intensity of the fundamental laser pulse when the intensity of the second harmonics is

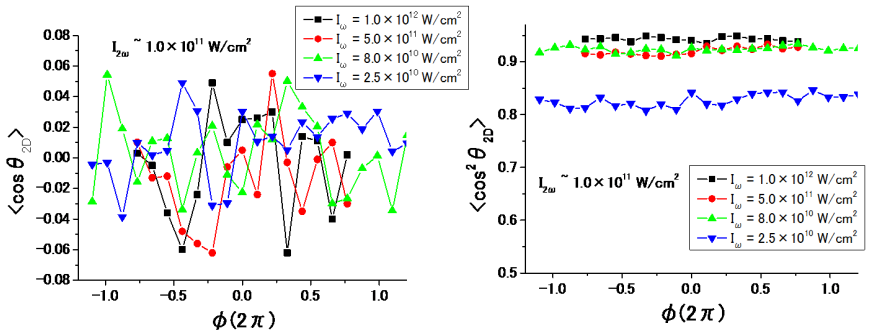

Figure 7.3: Degrees of alignment (right) orientation (left). The horizontal axises show relative phase between the ω and the 2ω. The peak intensities of the 2ω is 1.0×10^{11}W/cm^2.

fixed. This experimental result is consistent with the numerically obtained prediction.

7.1.2 Iodobenzene molecule

The two-color orientation experiment have also been performed with iodobenzene molecules buffered with 60-bar of He gas and state-selected by 7 kV-applied molecular deflector.

We show the results in Fig. 7.3. While higher degrees of alignment are obtained, the obtained degrees of orientation are smaller than the result obtained for the OCS molecules. Also, the modulation depending on the change of the relative phase between the two wavelength is not clear. As shown in Fig. 7.4 (a), we plot the result of the orientation with a sine curve to conclude which intensity of the ω is the best for the orientation in the present experimental condition. Figure 7.4 (b) shows the amplitudes of the fitted sine curves as a function of the intensity of ω. From the graph shown in Fig. 7.4 (b), we can conclude that the best orientation is achieved when the strongest intensity of ω is applied.

The weak orientation obtained with the iodobenzene sample probably comes from several reasons. First of all, compared to the OCS molecule, the iodobenzene has a longer rotational period so that the orientation process seems to be far from pure adiabatic interaction. Secondly, there are still many initial rotational-states in the state-selected iodobezene molecular

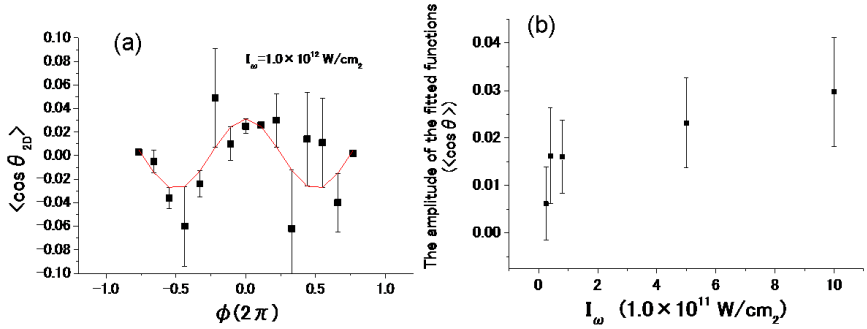

Figure 7.4: (a) : The degrees of orientation when intensity of the ω 1.0×10^{12}W/cm^2 in Fig. 7.3 is fitted by a sine curve. (b) : Amplitudes of other fitted since curves as a function of the intensity of the ω.

sample. Practically, isolating only one quantum state of a large asymmetric top molecule like iodobenzene is virtually impossible, while it is possible with small linear molecule such as OCS molecule. Thirdly, the intensity of the 2ω pulse is lower than that in the experiment with the OCS sample, which is because the 2ω pulse was focused loosely to the iodobenzene molecules.

7.2 Completely field-free orientation of OCS molecules

After we have observed the orientation of state-selected OCS molecules by a two-color laser pulse, the plasma shutter is employed to rapidly turn off the second half of the pump pulse.

However, we have found a possibility of that the circulating liquid jet-sheet for the plasma generation and the vapor around the jet-sheet generated by the plasma shutter operation make the relative phase between the ω and the 2ω unstable temporally. To confirm this, measurement same with the Fig. 7.2 is conducted when the plasma shutter is operating. 11ps before the time of rapid truncation, we have probed the orientation of molecules.

From recorded images of the S^+ fragment ions, we plot the degrees of alignment and orientation as a function of the relative phase. Fig. 7.5 (a) and (b) show the degrees of alignment and orientation, respectively. We accumulated data for two minutes for one image. Fig. 7.5 (c) shows result

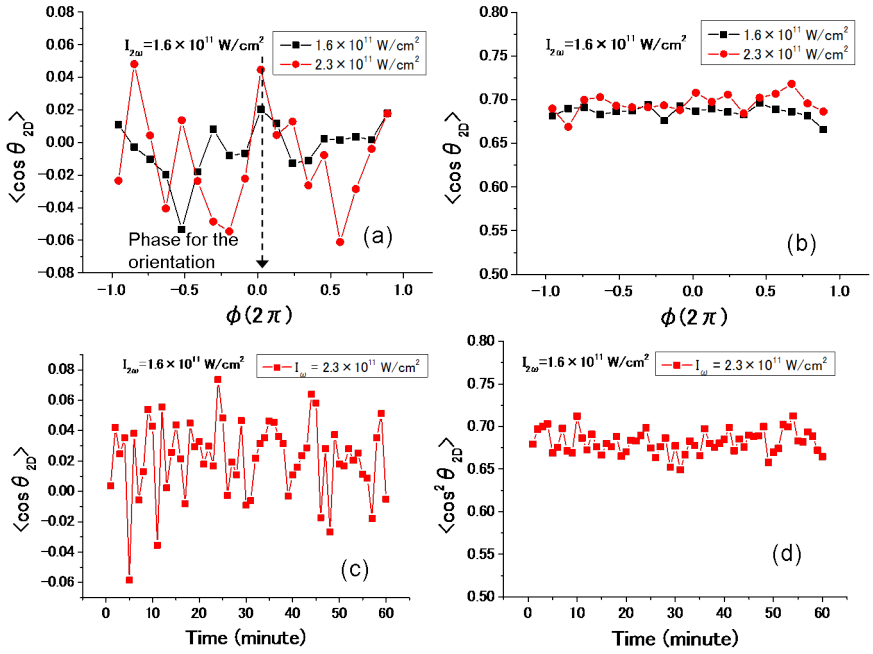

Figure 7.5: The upper panels show the relative phase dependence of the degrees of orientation (left) and alignment (right) when the plasma shutter is operating. The lower panels show the degrees of orientation (left) and alignment (right) obtained repeatedly when the relative phase is fixed to value pointed by the black arrow in the upper-left panel.

of orientations that repeatedly measured, when the relative phase is fixed to the value arrowed in the Fig. 7.5 (a) and the probe pulse is applied to the oriented molecules 11 ps before the rapid turn off as well. As we can see from Fig. 7.5 (c) and (d), the obtained molecular orientation is temporally unstable because of the plasma shutter operation, while the obtained degrees of alignment do not fluctuate.

Then, we have observed the time evolutions of the degrees of alignment and orientation (Fig. 7.6). The degrees of alignment show quite clear modulation, while the modulation of the orientation is covered by a severe fluctuation. In spite of the serious fluctuation of the phase, the averaged value of the orientation is kept positive in Fig.7.5 (c) and Fig.7.6 (a). That means, at least, it is not a fault that field-free orientation is achieved.

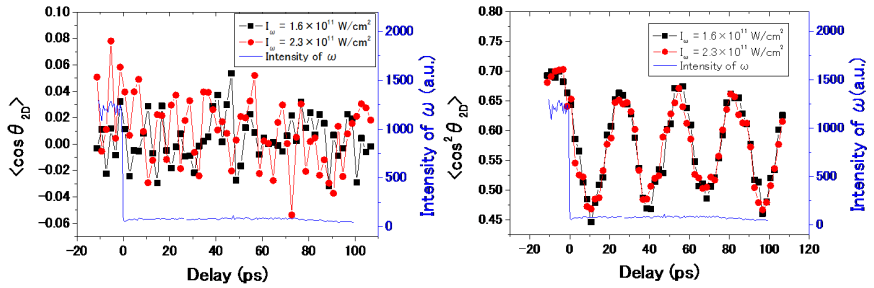

Figure 7.6: Temporal evolution of degrees of orientation (left) and alignment (right) applied to the two-color laser pulse with a slow turn on and the rapid turn-off. After the rapid turn off at $t = 0$, the alignment shows clear modulation, while the orientation is covered by severe fluctuation.

We have performed numerical simulation to compare it's result with the obtained experimental result. The pulse widths of the ω and the 2ω are 7.7 and 3.85 ns respectively, and residual laser field after the rapid turn off is neglected. We take into account the non-adiabatic effect on the slow rising of the laser field with the numerical method explained in Chapter 3.

We could estimate the applied intensity of the laser field and the population of initial rotational states from the temporal evolutions of the alignment since the modulation in the experimental data is quite clear. We have numerically found that the experimentally observed modulation of alignment illustrates two important facts. First, in the experiment, most of the state-selected molecules used this time are in their rotational ground state. In Chapter 4, we have described that the state-selected molecules used in the present experiment are mostly composed by $|0,0>$ and $|1,1>$ states, while the ratio between the two states is not reliable. On the other hand, the experimentally observed modulation have been reproduced only from the ground state $|0,0>$ in the calculation, whereas $|1,1>$ state have shown different revival pattern as it is show in the lower panel of Fig. 7.7. Furthermore, we have reproduced the revival structure of the ground state with much lower laser intensities than that we have estimated in the experiment. The stronger intensities applied to molecules diminish the alignment peak that appear at 27 ps and 54ps (Fig. 7.7).

This discrepancy of the laser intensity between the experiment and the calculation must come from the finite volume of the probe laser pulse. In

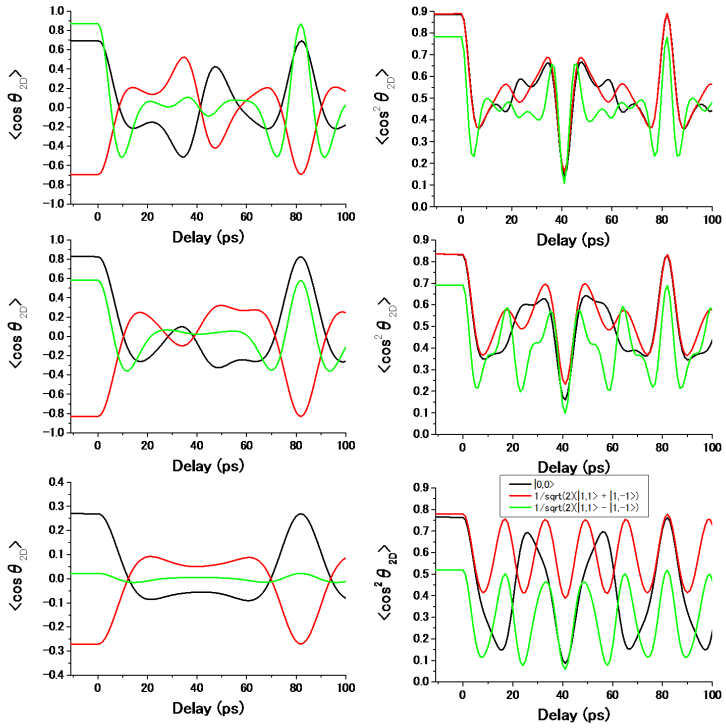

Figure 7.7: Numerical results of temporal evolutions of alignment and orientation after the rapid turn off the two-color laser field at $t = 0$. The black line represents the initial ground state $|0, 0>$, while the red and green represent the $|1, 1> + |1, -1>$ and $|1, 1> - |1, -1>$ states respectively. The upper panels show result when the peak intensity of ω is $2.3 \times 10^{11}\mathrm{W/cm}^2$ and the 2ω is $1.6 \times 10^{11}\mathrm{W/cm}^2$. The middle and lower panels show result with half and quarter intensity of the field intensities are applied with the same ratio ω to 2ω.

our experiment of two-color laser field, the radius of the focused probe pulse is not small enough compared to that of pump pulses. Even though optimizing the contrast of spatial radius of the laser pulses is very important to preferentially probe the molecules exposed to the strongest pump fields, we could not perform the experiment in the ideal condition this time. That was because the focusing positions of the $\omega$and the 2ω laser pulses are significantly displaced to each other and their spatial shapes have not been ideally controlled.

With the rotational wave function that reproduces the revival structure of alignment (the right panels in 7.7), the degrees of orientation is calculated as well, which are shown in the left panels of Fig. 7.7. Considering the rotational period of the OCS molecule, at least, we will be able to achieve field-free orientation just after the rapid turn off and at 81ps after the turn off, if the relative phase between the ω and 2ω pulses is temporally and spatially controlled better. Also, further strong intensities of the pump pulses can give rise to a remarkably strong degree of orientation ($< \cos\theta > \sim 0.9$).

Chapter 8

Summay and outlook

8.1 Laser-field-free orientation of state-selected asymmetric top molecules

With all available techniques successfully combined, we have demonstrated laser-field-free orientation of state-selected asymmetric top molecules with very high degrees of orientation. (1) In order to achieve high degrees of orientation, rotationally cold molecules are prepared by a high-pressure pulsed valve. In order to achieve even higher degrees of orientation, molecules in lower-lying rotational states are selected by deflecting a molecular beam with a molecular deflector. (2) Since rotational states are closely distributed in their energies of asymmetric top molecules, it is virtually impossible to prepare a single rotational state even with a molecular deflector. For those molecules not in a single rotational state but in some lower-lying rotational states, some of which are oriented one way and the others are oriented the other way, it is of crucial importance to create molecular orientation adiabatically so that the rotational states in the molecules can be bound more on the deeper potential wall than the shallower one and the highest possible degrees of orientation can be achieved. (3) In order to achieve laser-field-free orientation, the pump laser pulse is rapidly turned off at its peak intensity by the plasma shutter technique. Then the laser-field-free molecular orientation is realized just after the rapid turn off of the pump pulse.

Even though our development of the orientation technique have been motivated by the strong contribution of adiabatic process to the achieved degree of orientation, we have found that the orientation process is not purely adi-

abatic and the nonadibatic effect plays an important role. From the experimentally obtained data, we have shown that the asymmetric top molecules can be strongly oriented in the laser-field-free condition with 5-10 ps of long duration. Such a long period of laser-field-free orientation has been observed for the first time. This, in fact, illustrates an important role played by nonadiabatic effect taking place on the slow turn on of laser field.

According to recently reported studies including our numerical study shown in Chapter 6, pure adiabatic orientation of large asymmetric top molecular sample such as iodobenzene is practically impossible. However, our orientation technique based on laser pulse with a slow turn on and a rapid turn off give rise to a remarkably strong degree of orientation compared to other methods, and also can make the molecules to be kept oriented in the laser-field-free orientation for 5-10 ps.

Our orientation technique can open up new opportunity to explore many experimental researches on large asymmetric top molecules. A lot of studies of field-free molecular alignment and orientation have been restricted on the molecules with simpler structures and samples of oriented asymmetric top molecules are mainly created in the presence of laser-field. Therefore, we can expect that our orientation technique can fuel the progress of diverse research area with asymmetric top molecules such as photoelectron angular distribution, stereodynamic control of chemical reactions, dissociation of molecules, electron diffraction, or high-harmonic generation.

8.2 Numerical study on rotational spectrum and dynamics of asymmetric top molecules

Not only the small linear molecules but also more large molecules, which are often asymmetric top molecules, have been active subjects of research. The experimental studies on asymmetric top molecules have been accompanied by theoretical efforts to understand and estimate their unique rotational dynamics. In Chapter 6, we have focused our attention to the rotational dynamics of iodobezene molecules exposed to a combination of an electrostatic and a nonresonant laser field with a slow turn on and a rapid turn off.

We have numerically shown that the prolate asymmetric top molecules like iodobenzene behave like linear molecules when they are exposed to the combined fields, provided the molecular sample is in a low initial rotational

temperature. Prolate asymmetric top molecule's rotational motion around molecule fixed z-axis is represented by relatively large rotational constant. Therefore, the rotation around the z-axis is not highly being excited in a low rotational temperature. The rotational motion around the z-axis is kept frozen under a slowly applied external field. Thus, the cold iodobenzene molecules irradiated with a laser pulse with a slow turn on and a rapid turn off behave like linear molecules.

However, when a short laser pulse is irradiated to prolate asymmetric top molecules, the rotation around molecule fixed z-axis is considerably excited. This is a big difference of asymmetric top molecules and symmetric top molecules, which make the rotational dynamics of asymmetric top molecules are qualitatively different with those of symmetric and linear molecules.

In addition, we have numerically reproduced the appearance of "persistent laser-field-free orientation". That is also a characteristic behavior of asymmetric top molecules. To take into account nonadiabatic effect that exists on the slow rising of laser field, we have solved time-dependent Shrödinger equation describing rotational motion of asymmetric top molecules. It have been challenging subject to solve the time-dependent Shrödinger equation for asymmetric top molecules over a few nanosecond. In this time, we have developed a numerical method, based on time-dependent unitary transformation, to calculate rotational motions of large molecules very effectively.

We have confirmed that orientation process with the 6 nanosecond of turn on is still far from adiabatic interaction for many rotational states. We have shown that even more than 50 nanosecond of laser pulse can not ensure pure adiabatic interaction. In a given potential for molecular alignment or orientation, the best aligned or oriented quantum state is an eigenstate of the applied interaction Hamiltonian in almost of cases. Thus, wave packet generated by impure adiabatic process has a possibility to much aligned or oriented in the given intensity of external field. Thus, the degree of alignment or orientation does not necessarily increase (decrease) following the increase (decrease) of instantaneous laser field when the interaction is not purely adiabatic.

The "persistent orientation" have been reproduced numerically for several individual rotational quantum states among those have experienced avoided crossings. The nonadiabatic interactions on the slow turn on of the laser field have contributed to the "persistent laser-field-free orientation" after the rapid turn off of the laser field.

However, thermally averaged degrees of alignment and orientation are

almost the same with the results obtained by assuming that interaction on the slow turn on is adiabatic. This is because we have restricted our attention on the "parallel field" condition. If we consider further nonadiabatic effect existing in the "crossed field condition," there are probably extremely remarkable nonadiabatic behaviors [86].

8.3 Completely field-free orientation of molecules

Field-free orientation of molecules is one of the most attracting fields of research. We have oriented OCS molecules in the field-free condition by using both state-selection technique and plasma shutter technique. Degree of orientation that we can obtain from a single rotational state is maximized when the orientation potential is applied adiabatically. And ground state of OCS molecule can be selected by using molecular deflector, while large asymmetric top molecule like iodobenzene molecule state-selected by our method still include amount of rotational states. Thus, in principle, we could achieve the highest degree of orientation of small molecules with our approach.

We have utilized the two-color laser pulse with a slow turn on and a rapid turn off to orient state-selected OCS molecules in the field-free condition. Considering underlying physics associated with molecular orientation, our experimental approach provides an opportunity to achieve the possible strongest molecular orientation. In principal, degree of orientation $< \cos\theta >$ can be over 0.9 with our approach. We can complete our purpose if we overcome several technical issues that we have recognized this time.

First, we need to make the orientation process on the slow rising of the laser field to be close to adiabatic as much as possible. We have found numerically and experimentally that interaction by the two-color laser pulse is not adiabatic for molecular orientation due to the different pulse widths of the ω and 2ω; once rotational state strongly aligned only by the ω is created, they can not be adiabatically oriented by the additionally applied 2ω. We have optimized intensities of the ω and 2ω in order to make the alignment and orientation processes take place simultaneously as much as possible.

Secondly, we need to apply much strong intensities of pump pulses. From observed modulation of the temporal evolution of the degree of alignment, we have shown that the rotational ground state is successfully selected by the molecular deflector and that the degree of orientation can be further in-

creased by stronger laser field. This time, the achieved maximum degree of orientation is $\sim$0.08 in $< \cos\theta_{2\mathrm{D}} >$. As we numerically have found, the degree of orientation can be significantly increased with stronger pump pulses. Extremely high degree of orientation $< \cos\theta_{2\mathrm{D}} > \sim$0.9 can be expected in the near future.

Also, we have found that the plasma shutter operation influences the relative phase between the ω and the 2ω, that makes the achieved degrees of orientation temporally unstable. This issue is the most challenging and important subject for using the oriented molecular sample to other experimental researches. The effect of the plasma shutter on the relative phase can be minimized if the rapidly truncated quantity of laser pulses is reduced. However, since we need to increase total intensity of the pump pulse in the future, other solution is required. Therefore, we have been preparing a feedback system for stabilizing the relative phase between the ω and 2ω.

Chapter 9

Appendix

9.1 Matrix elements of Hamiltonians

We summarize all non-zero elements of the Hamiltonian matrices used for our calculations.

9.1.1 Linear molecule

Rigid rotor Hamiltonian

The rigid rotor Hamiltonian of linear molecule, $H_{\rm rot} \equiv B\hat{J}^2$, have non-zero diagonal elements of

$$< J, M|H_{\rm rot}|J, M >= BJ(J+1). \tag{9.1}$$

DC Stark Hamiltonian

The interaction Hamiltonian of the permanent dipole with electrostatic field, $E_{\rm static}\mu\cos\theta$, have off-diagonal elements expressed by

$$\begin{aligned} &< J, M|\cos\theta|J+1, M > \\ &= \sqrt{\frac{(J+1+M)(J+1-M)}{(2J+1)(2J+3)}} \end{aligned} \tag{9.2}$$

AC Stark Hamiltonian

The Hamiltonian of interaction between a nonresonant laser field and the induced dipole moment, $-\frac{I}{2c\epsilon}((\alpha_{\parallel}-\alpha_{\perp})\cos^2\theta)$, have non-zero matrix elements described below.

$$\begin{aligned} &< J, M|\cos^2\theta|J, M > \\ &= \frac{1}{3} + \frac{2(2J+1)(J(J+1)-3M^2)}{3(2J+1)(2J+3)(2J-1)} \end{aligned} \tag{9.3}$$

$$\begin{aligned} &< J, M|\cos^2\theta|J+2, M > \\ &= \sqrt{\frac{((J+1)^2-M^2)((J+2)^2-M^2)}{(2J+1)(2J+3)^2(2J+5)}} \end{aligned} \tag{9.4}$$

Hamiltonian for interaction of hyperpolarizability

Nonresonant two-color laser field give rise to interaction of hyperpolarizablilty given by,

9.1.2 Asymmetric top molecule

Rigid Rotor Hamiltonian

The nonzero matrix elements for the field-free Hamiltonian of asymmetric top molecule are

$$\begin{aligned} &< J, K, M|H_{\rm rot}|J, K, M >= \\ &\frac{1}{2}(B+C)[J(J+1)-K^2] + AK^2 \end{aligned} \tag{9.5}$$

$$\begin{aligned} &< J, K, M|H_{\rm rot}|J, K+2, M >= \\ &\frac{1}{4}(B-C)\sqrt{(J(J+1)-K(K+1))}\times \\ &\sqrt{J(J+1)-(K+1)(K+2)} \end{aligned} \tag{9.6}$$

DC Stark Hamiltonian

The interaction Hamiltonian of the permanent dipole with electrostatic field, $E_{\text{static}}\mu\cos\theta$, have matrix elements expressed by

$$\begin{aligned} &< J,K,M|\cos\theta|J,K,M > \\ &\qquad = \frac{MK}{J(J+1)} \end{aligned} \tag{9.7}$$

$$\begin{aligned} &< J,K,M|\cos\theta|J+1,K,M > \\ &= \sqrt{\frac{((J+1)^2-M^2)((J+1)^2-K^2)}{(2J+3)(2J+1)(J+1)^2}} \end{aligned} \tag{9.8}$$

AC Stark Hamiltonian

The interaction between a linearly polarized non-resonant laser field and the induced dipole is $-\frac{I}{2c\epsilon}(\alpha^{zx}\cos^2\theta + \alpha^{yx}\sin^2\theta\sin^2\chi)$, whose nonzero matrix elements are summarized below.

$$\begin{aligned} &< J,K,M|\cos^2\theta|J,K,M > \\ &= \frac{[3M^2-J(J+1)][3K^2-J(J+1)]}{3J(J+1)(2J-1)(2J+3)} + \frac{1}{3} \end{aligned} \tag{9.9}$$

$$\begin{aligned} &< J+1,K,M|\cos^2\theta|J,K,M > \\ &= \frac{2MK\sqrt{[(J+1)^2-M^2][(J+1)^2-K^2]}}{9J(J+1)(J+2)\sqrt{(2J+3)(2J+1)}} \end{aligned} \tag{9.10}$$

$$\begin{aligned} &< J+2,K,M|\cos^2\theta|J,K,M > \\ &= \sqrt{[(J+2)^2-K^2][(J+1)^2-K^2]}\times \\ &\frac{\sqrt{[(J+2)^2-M^2][(J+1)^2-M^2]}}{9(J+1)(J+2)(2J+3)\sqrt{(2J+1)(2J+5)}} \end{aligned} \tag{9.11}$$

$$< J, K+2, M|\sin^2\theta\sin^2\chi|J, K, M > = \frac{1}{\sqrt{3}}[3M^2 - J(J+1)] \times \frac{\sqrt{[J^2-(K+1)^2](J-K)(J+K+2)}}{2J(J+1)(2J+3)(2J-1)} \tag{9.12}$$

$$< J+1, K, M|\sin^2\theta\sin^2\chi|J, K+2, M > = \frac{1}{\sqrt{3}}M\sqrt{[(J+1)^2-M^2]} \times \frac{\sqrt{[(J-K)^2-1](J-K)(J+K+2)}}{2J(J+1)(J+2)\sqrt{(2J+1)(2J+3)}} \tag{9.13}$$

$$< J+2, K, M|\sin^2\theta\sin^2\chi|J, K+2, M > = \frac{1}{\sqrt{3}}M\sqrt{[(J+2)^2-M^2][(J+1)^2-M^2]} \times \frac{\sqrt{[(J-K)^2-1](J-K)(J-K+2)}}{4J(J+1)(2J+3)\sqrt{(2J+1)(2J+5)}} \tag{9.14}$$

9.2 Effect of the residual laser field

We explore effects of the residual fields on the rotational dynamics of molecules numerically. We assume that molecules are oriented with a pure adiabatic process by a slow turn on of the laser field, and the laser field are turned off rapidly. As explored in Chapter 5 and 6, nonadiabatic effect plays crucial roles in determining the rotational dynamics of asymmetric top molecules. Thus, to more clearly investigate the effect of residual laser field on the rotational dynamics, we focus our attention on the case of a small linear molecule. However, things we elucidate in this section are general for other asymmetric top molecules. We explore time evolution of OCS molecules exposed to both continuous 800 V/cm of electric field and the shaped pulse. We assume conditions where residual laser field components are exaggerated than real experimental conditions; we consider conditions where up to 5 percent of a fixed peak intensity of 2×10^{12} W/cm^2 is kept remaining after the rapid turn off.

Fig. 9.1 shows that the revivals of alignment and orientation show up at the times characterized by the rotational period of the molecule, which is similar to the rotational dynamics induced by short laser pulse [34, 36]. However, constantly remainning finite laser field after the rapid truncation makes the rotational wave packet dynamics different from those pumped by the shaped pulse without any residual laser field after the rapid turn off. The effect by the residual field is more distinct for the sample with lower initial rotational temperatures and for the higher residual field components. For example, when 5 percent of laser field remains, revivals of alignment and orientation at the rotational period of the molecule 82ps can not be observed anymore . In principle, linear molecules must show distinct revival peaks when there is no residual field remaining.

In the previous experiments using plasma shutter [36, 65], the power (Watt) of residual fields are assumed to be less than 5 percent of the peak power of the shaped pulse as a result of the cross-correlation measurement. However, the intensity of the residual laser field is much lower than 5 percent of the peak intensity since the plasma shutter not only truncates the second half of the laser pulse but also dramatically modify the focusability of the residual laser field [36]. [1] Moreover, it has been confirmed from our numerical simulations that the time interval between the rapid turn off and the first

[1] It is important to estimate the remaining field intensity if the controlled molecular sample by the plasma shutter technique is applied to other experimental researches. The

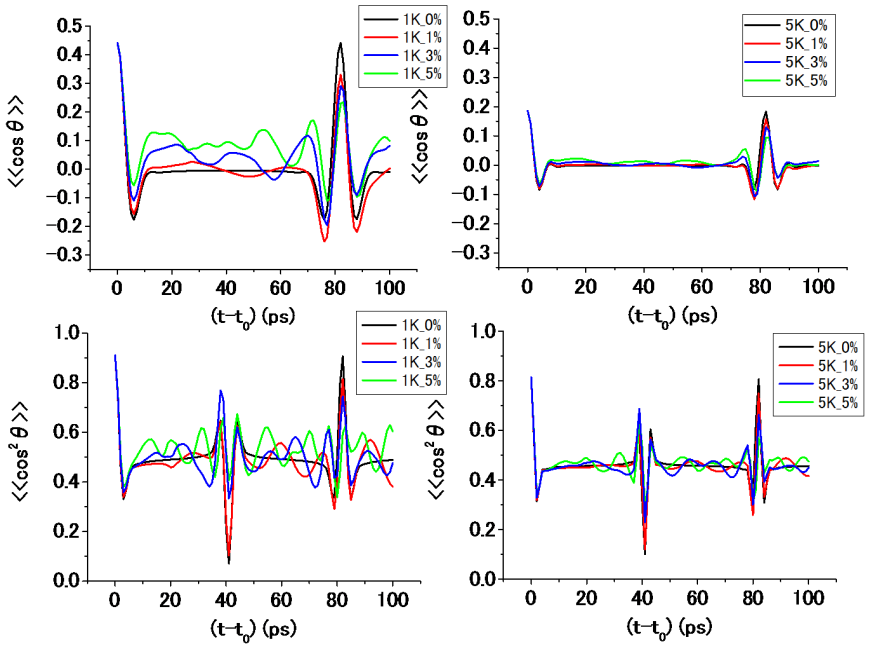

Figure 9.1: Temporal evolutions of alignment and orientation of OCS molecules for two rotational temperatures of 1K (left) and 5K (right). Degrees of alignment and orientation are thermal averaged by considering Boltzmann distributions. The results with different residual field components after the rapid turn off are shown in each panel.

local minimum of the temporal evolutions of alignment and orientation are independent to the remaining field intensity. The time interval, the dephasing time, is determined by only the wave-packet property before the rapid turn off. This characteristic has been found from an asymmetric top molecule too. This numerical observation makes sure that the experimental result showing persistent laser-field-free alignment and orientation for 5-10ps is caused from other effects rather than that of the residential field [65]. As we notice in Chapter 5 and 6, we have thought that nonadiabatic interaction on the rising part of the laser field can cause the persistent laser-field-free alignment and orientation.

present numerical simulation, based on the comparison with experimental result, can serve us a precise way for estimating the actual intensity (W/cm^2) of the residual field applied to the molecules.

Bibliography

[1] K. H. Kramer and R.B.Bernstein, J. Chem. Phys. **42**, 767 (1965).

[2] P. R. Brooks and E. M. Jones, J. Chem. Phys. **45**, 3449 (1966).

[3] B. Friedrich and D. Herschbach, Nature (London), **353**, 412 (1991).

[4] R. C. Estler and R. N. Zare, J. Am. Chem. Soc. **100**, 1323 (1978).

[5] M. J. Weida and C. S. Parmenterm, J. Chem. Phys. **107**, 7138 (1997).

[6] B. Friedrich and D. Herschbach, Phys. Rev. Lett. **74**, 4623 (1995).

[7] B. Friedrich and D. Herschbach, J. Phys. Chem. **99**, 15686 (1995).

[8] T. Seideman, J. Chem. Phys. **103**, 6487 (1995).

[9] H. Sakai, C. P. Safvan, J. J. Larsen, K. M. hilligsoq, K. Hald, and H. Stapelfeldt, J. Chem. Phys. **110**, 10235 (1999).

[10] J.J. Larsen, H. Sakai, C. P. Safvan, I. Wendt-Larsen, and H. Stapelfeldt, J. Chem. Phys. **111**, 7774 (1999).

[11] T. Seideman, Phys. Rev. Lett. **83**, 4971 (1999).

[12] Z. C. Yan and T. Seideman, J. Chem. Phys. **111**, 4113 (1999).

[13] C. M. Dion, A. Keller, and O. Atabek, Phys. Rev. A **59**, 1382 (1999).

[14] J. Ortigoso, M. Rodriguez, M. Gupta, and B. Friedrich, J. Chem. Phys. **110**, 3870 (1999).

[15] F. Rosca-pruna, and M. J. J. Vrakking, Phys. Rev. Lett. **87**, 153902 (2001).

[16] Niels E. Hehriksen, Chem. Phys. Lett., **312**, 196 (1999).

[17] T. Suzuki, S. Minemoto, T. Kanai, and H. Sakai, Phys. Rev. Lett. **92**, 133005 (2004).

[18] J. Itatani et al., Nature (London) **432**, 867 (2004).

[19] G. Vozzi, M. Negro, F. Calegari, G. Sansone, M. Nisoli, S. De Silvestri and S. Stagira, Nat. Phys. **7**, 822 (2011).

[20] T. Kanai, S. Minemoto, and H. Sakai, Nature (London) **435**, 470 (2005).

[21] T. Kanai, S. Minemoto, and H. Sakai, Phys. Rev. Lett. **98**, 053002 (2007).

[22] K. Kato, S. Minemoto, and H. Sakai, Phys. Rev. A **84**, 021403(R) (2011).

[23] Y. Sakemi, K. Kato, S. Minemoto, and H. Sakai, Phys. Rev. A **85**, 051801(R) (2012).

[24] B. Friedrich and D. Herschbach, J. Chem. Phys. **111**, 6157 (1999).

[25] B. Friedrich and D. Herschbach, J. Phys. Chem. A **103**, 10280 (1999).

[26] H. Sakai, S. Minemoto, H. Nanjo, H. Tanji, and T. Suzuki, Phys. Rev. Lett. **90**, 083001 (2003).

[27] S. Minemoto, H. Nanjo, H. Taji, T. Suzuki, and H. Sakai, J. Chem. Phys. **118**, 4052 (2003).

[28] H. Tanji, S. Minemoto, and H. Sakai, Phys. Rev. A **72**, 063401 (2005).

[29] T. Kanai and H. Sakai, J. Chem. Phys. **115**, 5492 (2001).

[30] K. Oda, M. Hita, S. Minemoto, and H. Sakai, Phys. Rev. Lett. **104**, 213901 (2010).

[31] Y. Sugawara, A. Goban, S. Minemoto, and H. Sakai, Phys. Rev. A **77**, 031403(R) (2008).

[32] J. H. Nielsen, P. Simesen, C. Z. Bisgaad, H. Stapelfeldt, F. Filsinger, B. Friedrih, G. Meijer and J. Kupper Phys. Chem. Chem. Phys. **13**, 18971 (2011).

[33] J. J. Omiste, and R. González-Ferez, Phys. Rev. A **88**, 033416 (2013).

[34] T. Seideman, J. Chem. Phys. **115**, 5965 (2001).

[35] J. G. Underwood et al., Phys. Rev. Lett. **90**, 223001 (2003).

[36] A. Goban, S. Minemoto, and H. Sakai, Phys. Rev. Lett. **101**, 013001 (2008).

[37] O. Ghafur, A. Rouzee, A. Gijsbertsen, W. K. Siu, S. Stolte, and M. J. J. Vrakking, Nature. Phys. **5**, 289 (2009).

[38] L. Holmegaard, J. H. Nielsen, I. Nevo, H. Stapelfeldt, F. Filsinger, J. Kupper, and G. Meijer Phys. Rev. Lett. **102**, 023001 (2009).

[39] F. Filsinger, J. Kupper, G. Meijer, L. Holmegaard, J. H. Nielsen, I. Nevo, J. L. Hansen, and H. Stapelfeldt, J. Chem. Phys. **131**, 064309 (2009).

[40] C. C. Shu, K. J. Yuan, W. H. Hu, and S. L. Cong, J. Chem. Phys. **132**, 244311 (2010).

[41] S. Fleischer, Y. Zhou, R. W. Field, and K. A. Nelson, Phys. Rev. Lett. **107**, 163603 (2011).

[42] M. D. Poulsen, E. Péronne, H. Stapelfeldt, C. Z. Bisgaard, S. S. Viftrup , E. Hamilton and T. Seideman J. Chem. Phys. **121**, 783 (2004).

[43] L. Holmegaard, S. S. Viftrup, V. Kumarappan, C. Z. Bisgaard, H. Stapelfeldt, E. Hamilton, and T. Seideman, Phys. Rev. A **75**, 051403(R) (2007).

[44] K. F. Lee, D. M. Villeneuve, P. B. Corkum, A. Stolow, and J. G. Underwood Phys. Rev. Lett. **97**, 173001 (2006).

[45] M. Artamonov and T. Seideman, J. Chem. Phys. **128**, 154313 (2008).

[46] M. Artamonov and T. Seideman, Phys. Rev. A, **82**, 023413 (2010).

[47] S. S. Viftrup, V. Kumarappan, S. Trippel, H. S.E. Hamilton, and T. Seideman, Phys. Rev. Lett. **99**, 143602 (2007).

[48] S. S. Viftrup, V. Kumarappan, L. Holmegaard, C. Z. Bisgaard, H. Stapelfeldt, M. Artamonov, E. Hamilton, and T. Seideman, Phys. Rev. A **79**, 023404 (2009).

[49] D. T. Moore, L. Oudejans, and R. E. Miller, J. Chem. Phys. **110**, 197 (1999).

[50] L. Holmegaard, J. L. Hansen, L. Kalhoj, S. S. Kragh, H. Stapelfeldt, F. Filsinger, J. Köpper, G. Meijer, D. Dimitrovski, M. Abu-samha, C. P. J. Martiny, and L. Madsen, Nat. Phys. **6**, 428 (2010).

[51] J. L. Hansen, L. Holmegaard, L. Kalhoj, S. L. Kragh, H. Stapelfeldt, F. Filsinger, G. Meijer, J. Köpper, D. Dimitrovski, M. Abu-samha, C. P. J. Martiny, and L. B. Madsen, Phys. Rev. A **83**, 023406 (2011).

[52] S. Zhang, C. Lu, T. Jia, Z. Wang, and Z. Sun, Phys. Rev. A **83**, 043410 (2011).

[53] R. González-Férez and P. Schmelcher, Phys. Rev. A **69**, 023402 (2004).

[54] R. González-Férez and P. Schmelcher, Phys. Rev. A **71**, 033416 (2005).

[55] S. De, I. Znakovskaya, D. Ray, F. Anis, Nora G. Johnson, I. A. Bocharova, m. Magrakvelidze, B. D. Esry, C. L. Cocke, I. V. Litvinyuk, and M. F. Kling, Phys. Rev. Lett. **103**, 153002 (2009).

[56] C. M. Dion, A. Keller, and O. Atabek, Eur. Phys. J. D **14**, 249 (2001).

[57] K.-L. Yeh, M. C. Hoffmann, J. Hebling, and K. A. Nelson, Appl Phys. Lett. **90**, 171121 (2007).

[58] X. Ren, V. Makhija, H. Li, M. F. Kling, and V. Kumarappan, Phys. Rev. A **90**, 013419 (2014).

[59] P. M. Kraus, D. Baykusheva, and H. J. Wörner, Phys. Rev. Lett. **113**, 023001 (2014).

[60] K. Kitano, N. Ishii, N. Kanda, Y. Matsumoto, T. Kanai, M. Kuwata-Gonokami, J. Itatani, Phys. Rev. A **88**, 061405(R) (2013).

[61] D. Rösch, S. Willitsch, Y. P. Chang, J. Küpper J. Chem. Phys. **140**, 124202 (2014).

[62] M. S. de Vries, V. I. Srdanov, C. P. Hanrahan, and R. M. Martin, J. Chem. Phys. **78**, 5582 (1983).

[63] B. C. Stuart, M. D. Feit, S. Herman, A. M. Rubenchik, B. W. Shore, and M. D. Perry , Phys. Rev. B **53**, 1749 (1996).

[64] L. N. Gaier, M. Lein, M. I. Stockman, P. L. Knight, P. B. Corkum, M. Y. Kvanov and G. L. Yudin J. Phys. B : At. Mol. Opt. Phys. **37**, L57 (2004).

[65] J. H. Mun, D. Takei, S. Minemoto, and H. Sakai, Phys. Rev. A **89**, 051402(R) (2014).

[66] J. H. Mun, Master's thesis (2012).

[67] X. M. Tong, Z. X. Zhao, and C. C. Lin, Phys. Rev. A **66**, 033402 (2002).

[68] I. V. Litvinyuk, K. F. Lee, P. W. Dooley, D. M. Rayner, D. M. Villeneuve, and P. B. Corkum, Phys. Rev. Lett. **90**, 233003 (2003).

[69] P. W. Dooley, I. V. Litvinyuk, Kevin. F. Lee, D. M. Rayner, M. Spanner, D. M. Villeneuve, and P. B. Corkum, Phys. Rev, A **68**, 023406 (2003).

[70] V. Kumarappan, L. Holmegaard, C. martiny, C. B. Madsen, T. K. Kjeldsen, S. S. Viftrup, L. B. Madsen, and H. Stapelfeldt, Phys. Rev. Lett. **100**, 093006 (2008).

[71] D. Zeidler, A. Staudte, A. B. Bardon, D. M. Villeneuve, R. Dörner, and P. B. Corkum, Phys. Rev. Lett. **95**, 203003 (2005).

[72] O. Gessner, A. M. D. Lee, J. P. Shaffer, H. Reisler, S. V. Levchenko, A. I. Krylov, J. G. Underwood, H. Shi, A. L. L. East, D. M. Wardlaw, E. T. H. Chrysostom, C. C. Hayden, and A. Stolow, Science **311**, 219 (2006).

[73] R. Baumfalk, N. H. Nahler, and U. Buck, J. Chem. Phys. **114**. 4755 (2001).

[74] M. Suzuki, Master's thesis (2011).

[75] T. Hoshino, Mster's thesis (2011).

[76] R. N. Zare, “ANGULAR MOMENTUM” (1988).

[77] G. Scoles, “Atomic and Molecular Beam Methods” (1988).

[78] K. Shobatake, and H. Shinohara, J. Spectroscopic. Soc. Japan **39**, 187 (1990).

[79] F. Filsinger, Doctoral Thesis, Fritz-Haber-Institut der Max-Planck-Cesellschaft in Berlin, Germany (2010).

[80] I. I. Rabi, Nature, **123**, 163 (1929).

[81] I. I. Rabi, J. M. B. Kellogg, and J. R. Zacharias, Phys. Rev. **46**, 157 (1934).

[82] M. E. Lusty and M. H. Dunn, Appl. Phys. B **44**, 193 (1987).

[83] A. T. J. B. Eppink and D. H. Parker, Rev. Sci. Instrum. **68**, 3477 (1997).

[84] D. H. Parker and A. T. J. B. Eppink, J. Chem. Phys. **107**, 2357 (1997).

[85] V. Kumarappan, C. Z. Bisgaard, S. S. Viftrup, L. holmegaard and H. Stapelfeldt, J. Chem. Phys. **125**, 194309 (2006).

[86] J. J. Omiste, R. Gonzalez-Ferez, and P. Schmelcher, J. Chem. Phys. **135**, 064310 (2011).

[87] J. J. Omiste et al., Phys. Chem. Chem. Phys. **13**, 18815 (2011).

[88] M. Härtelt and B. Friedrich, J. Chem. Phys. **128**, 224313 (2008).

[89] M. Muramatsu, M. Hita, S. Minemoto, and H. Sakai, Phys. Rev. A **79**, 011403(R) (2009).